

AN ABSTRACT OF THE THESIS OF

KENNETH EDWARD SPENCER for the DOCTOR OF PHILOSOPHY
(Name) (Degree)

in ELECTRICAL ENGINEERING presented on May 10, 1968
(Major) (Date)

Title: A SIGNAL-PROCESSED ANTENNA SYSTEM AND THE
SIMULATION OF THE EFFECTS OF BALANCED-MIXER
FREQUENCY CONVERSION

Abstract approved:

Gerald C. Alexander

In this paper a signal-processed antenna and receiver system is proposed and analyzed. In addition, a simulation of the balanced-mixer portion of the processing system is made on a hybrid computer to find the bandwidth limitations for the total system. The system utilizes both the amplitude and phase information of a one-dimensional antenna array as compared to only amplitude information for normal antenna systems.

The proposed processing system is analyzed by using a simplified model for the balanced-mixer portion of the processor. The analysis is done both for a processor with a CW local oscillator and for one with a pulsed local oscillator. The analysis shows that, in addition to the normal amplitude factors in the processor output signal and in the effective electric field pattern, a phase-dependent amplitude

factor is obtained.

It is shown that, by a method of phase manipulation, this phase-dependent term is made to depend only on the characteristics of the antenna array, the displacement of a reference antenna from the center of the antenna array and a pattern control shift. The method of phase manipulation uses the processed signal from the reference antenna to adjust the phase of the antenna array signal at the receiver. The pattern control phase shift is used to put a null or maximum in the direction of the pattern maximum for simple amplitude detection. The analysis indicates that the phase manipulated term in the effective pattern can be used to improve the pattern over that for simple amplitude detection. The pattern improvement consists of at most a sidelobe reduction of 5.3 db or beamwidth reduction by a factor of two. The bandwidth limitations of the information signals carried on the receiver input signal for reproduction of the information is found to be similar to other detection systems.

In the simulation of the balanced-mixer portion of the processing system, the balanced-mixer transmission lines are considered to be lossless and free of dispersion. Also, the junctions are considered to be lossless and free of energy storage. The simulation results indicate that the simulation on the hybrid computer gives a very representative model for the balanced-mixer operation. From the simulation results, it is shown that the bandwidth for pulsed input

signals to hold normal beam-pointing accuracies is in the range of 2-9% of the local oscillator frequency. The useable bandwidth range of the processor for a CW input signal is found to be about 17%. Also, it is found that the simplified, balanced-mixer model should be used only for a representative analysis for a 10% bandwidth. In addition, the simplified model should not be used alone for pulsed input signals when the phase information is important.

Copyright 1968

KENNETH EDWARD SPENCER

A Signal-Processed Antenna System and the Simulation of
the Effects of Balanced-Mixer Frequency Conversion

by

Kenneth Edward Spencer

A THESIS

submitted to

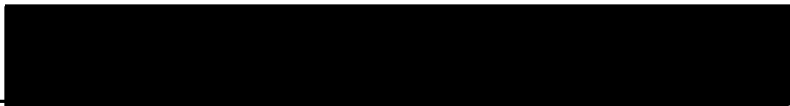
Oregon State University

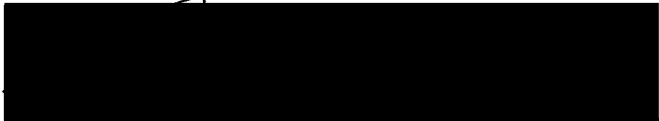
in partial fulfillment of
the requirements for the
degree of


Doctor of Philosophy

June 1968

APPROVED:


Associate Professor of Electrical Engineering
in charge of major


Head of Department of Electrical and
Electronics Engineering


Dean of Graduate School 0

Date thesis is presented May 10, 1968

Typed by Clover Redfern for Kenneth Edward Spencer

ACKNOWLEDGMENT

I am deeply indebted to my major professor, Gerald C. Alexander, for the many hours of discussion of this thesis topic and for his comments on the thesis text.

Credit is also due Professor Leonard J. Weber for his comments on the text and Professor John L. Saugen for his help with the hybrid computer. Moreover I would like to thank the National Aeronautics and Space Administration for their financial aid in the form of a traineeship.

TABLE OF CONTENTS

Chapter	Page
I. INTRODUCTION	1
II. RECEIVES SIGNAL AND EFFECTIVE ELECTRIC FIELD PATTERN FOR A ONE-DIMENSIONAL ARRAY	6
Reception of a CW Signal	6
Reception of a Pulsed Signal	9
III. ANALYSIS OF THE PROCESSING SYSTEM USING A SIMPLIFIED BALANCED-MIXER MODEL	15
System Description	15
Balanced-Mixer Features	17
The Simplified, Balanced-Mixer Model	18
Output for CW Local Oscillator and Pulsed, Received Signals	20
Output for CW Local Oscillator and CW, Received Signals	26
Output for Pulsed Local Oscillator and Pulsed, Received Signals	28
Output for Pulsed Local Oscillator and CW, Received Signals	32
IV. PHASE MANIPULATION FOR IMPROVEMENT OF THE FIELD PATTERN	34
General Case	34
CW Local Oscillator Signal System	38
Pulsed Local Oscillator Signal System	40
V. USES OF THE PHASE MANIPULATED TERM IN THE FIELD PATTERN	42
Beamwidth Minimization	43
Sidelobe Level Minimization	45
Radar Applications	46
VI. LIMITATIONS OF PHASE MANIPULATION AND OF THE SIGNAL PROCESSOR AS INDICATED BY THE SIMPLIFIED, BALANCED-MIXER MODEL	49
Method of Phase Manipulation	49
Signal Processor	53

Chapter	Page
VII. SIMULATION OF A LOSSLESS STRIP-LINE, HYBRID-RING, BALANCED-MIXER FREQUENCY CONVERTER UTILIZING AN EXTENDED MODEL	54
An Extended Model	54
The Simulation Study	60
Simulation Results	66
Circuit Design	66
IF Signal Characteristics as a Function of the IF Frequency	77
Validity of the Simulation	81
VIII. CALCULATION OF THE BANDWIDTH LIMITATIONS FROM THE SIMULATION RESULTS FOR THE EXTENDED, BALANCED-MIXER MODEL	86
CW Local Oscillator System	86
Pulsed Local Oscillator System	99
IX. ACCURACY AND LIMITATIONS OF THE SIMPLIFIED, BALANCED-MIXER MODEL	102
X. SUMMARY AND CONCLUSION	105
BIBLIOGRAPHY	109
APPENDIX	110
Appendix I	110
Appendix II	114
Appendix III	124
Appendix IV	140

LIST OF FIGURES

Figure	Page
1. Block diagram of a signal-processed antenna system.	2
2. An n-identical element, one-dimensional array.	7
3. Amplitude-detected, normalized, electric field patterns for a one-dimensional antenna array with n-identical elements.	10
4. Pulse envelope and frequency spectrum envelope of a typical symmetrical transmitted pulse.	12
5. Block diagram of the processing portion of a signal-processed antenna system.	16
6. Center strip of a strip-line, hybrid-ring, balanced-mixer frequency converter.	19
7. The processor output signal for different input signals and types of processing.	27
8. Processed effective electric field patterns for a one-dimensional antenna array.	37
9. Partial realization of the hybrid-ring, balanced-mixer, extended model.	56
10. Microwave diode and IF input equivalent circuits.	57
11. Analog computer circuit diagram for the simulation of the microwave diode and IF input equivalent circuits on the EAI 690 hybrid computer.	63
12. Digital circuit diagram for the analog computer in the simulation of a hybrid-ring, balanced-mixer frequency converter.	64
13. Revised IF junction of the realization of the hybrid-ring, balanced-mixer, extended model.	70
14. A typical analog recording of various scaled voltages during a simulated balanced-mixer operation.	71

Figure		Page
15.	The variation of the power-normalized IF signal amplitude as a function of the line lengths between the diodes and the hybrid ring or the IF terminal.	72
16.	The variation of the power-normalized IF signal amplitude as a function of the local oscillator input power.	75
17.	The variation of the power-normalized IF signal amplitude as a function of the IF input impedance and the characteristic impedance of the hybrid-ring circuit.	76
18.	Final design for the center strip of the strip-line, hybrid-ring, balanced-mixer frequency converter.	78
19.	The phase difference between the IF signal and the beat signal of the input signals and the IF signal amplitude as a function of the normalized frequency difference between the input signals.	79
20.	The absolute value of the slope of the phase difference curve of Figure 19 as a function of the normalized frequency difference between the input signals.	80
21.	Phase difference between the IF signal and the beat signal of the input signals as a function of the normalized frequency difference between the input signals for various delays in the input lines.	82
22.	Nonlinear portion of the phase difference curve of Figure 19 as taken from Figure 20 as a function of the normalized frequency difference between the input signals.	92
23.	The magnitude of the IF carrier signal phase change for variation of the pulse position between 0.15 (pulse maximum) points versus the normalized bandwidth for various values of the normalized frequency difference between the input signal carrier frequency and the center frequency of the IF input signal amplitude distribution.	93

24. The magnitude of the IF carrier signal phase change for variation of the pulse position between 0.33 (pulse maximum) points versus the normalized bandwidth for various values of the normalized frequency difference between the input signal carrier frequency and the center frequency of the IF input signal amplitude distribution. 94
25. Comparison of the power-normalized IF input signal amplitude as a function of the normalized frequency difference between the input signals for different design frequencies. 98

LIST OF TABLES

Table		Page
1.	Distribution of maximums and nulls for $f(\psi_0)$ and $\cos ((n+p-1)\psi_0/2)$ for minimum beamwidth and slight change in the sidelobe levels.	45
2.	Bandwidth limitations of the received input signal and of the information carried on the receiver input signal as indicated by the analysis for the signal processor.	53

A SIGNAL-PROCESSED ANTENNA SYSTEM AND THE SIMULATION OF THE EFFECTS OF BALANCED-MIXER FREQUENCY CONVERSION

I. INTRODUCTION

Antenna array systems are used in certain applications for the following reasons:

1. The directivity of the pattern of the antenna array and the maximum received signal can be increased by increasing the number of antenna array elements (4).
2. The antenna beam pointing direction can be changed by varying linearly along the array the effective transmission line lengths from the antenna elements to the receiver (4).

In present and future applications, these effective transmission line lengths are and will be varied by the use of electronically controlled phase shifters. Normal antenna-array-and-receiver systems utilize only the amplitude of the total received signal and completely disregard the phase information when using amplitude detection.

Although other papers have explored signal-processed antenna systems in general (5), specific signal-processed antenna systems have not been explored in detail. This thesis will propose and be concerned with a signal-processed antenna system that uses the phase information of the total received signal in addition to that of the amplitude. The system block diagram considered is given in Figure 1.

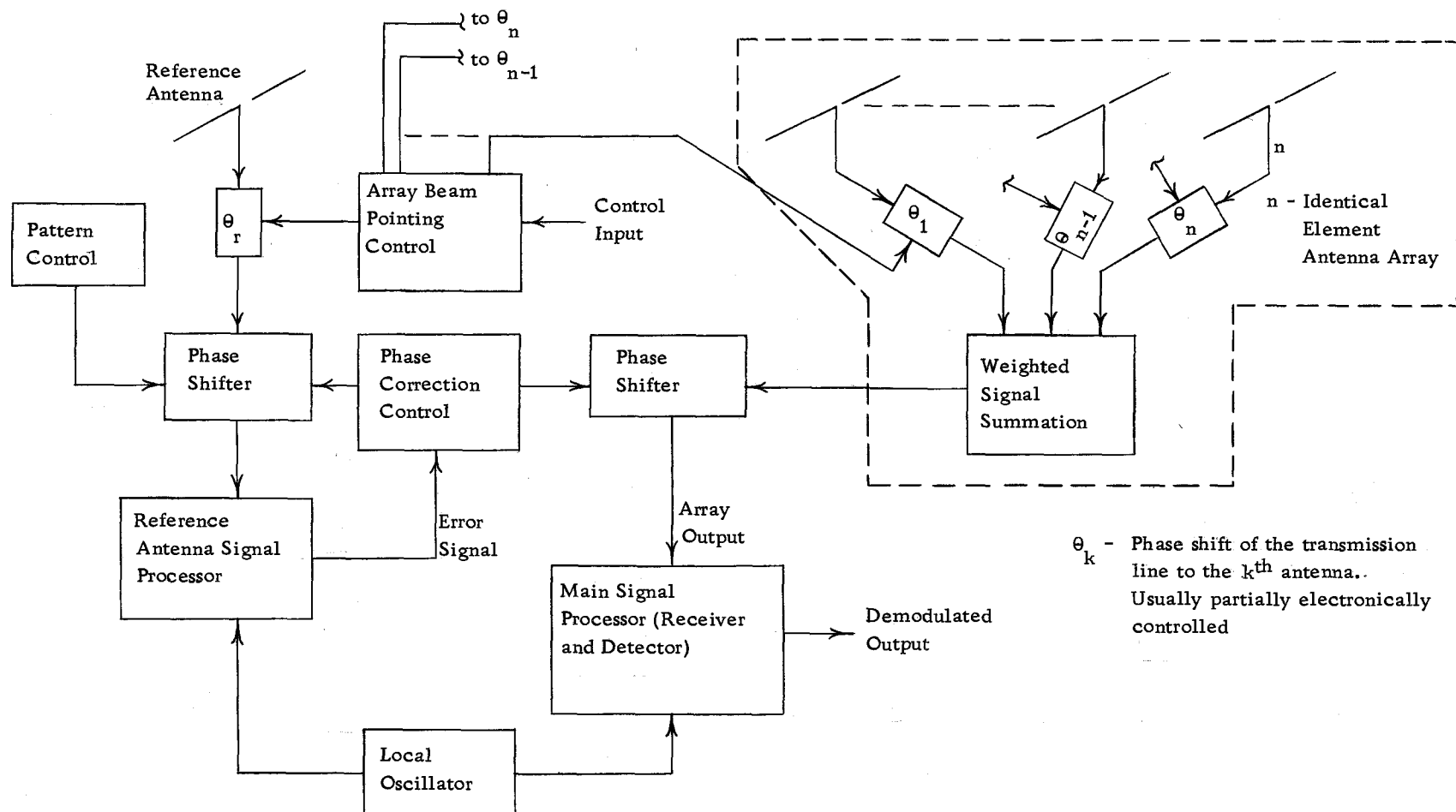


Figure 1. Block diagram of a signal-processed antenna system.

The signal processors are phase-and-amplitude detectors and use balanced-mixer frequency converters. Their outputs are a function of the received input signal and $\cos \gamma$, where γ is the phase difference between the received and local oscillator input signals.

The system uses the reference antenna signal to adjust the phase of the received signal input to the main processor so that γ depends only on the characteristics of the main antenna array and a pattern-control phase shift. The pattern-control phase shift is used to adjust the $\cos \gamma$ term so that a maximum, null, or intermediate level signal is obtained for reception from the direction of the beam maximum of the antenna array. For the pattern-control phase shift set for maximum signal level, the placement of the reference antenna with respect to the antenna array can be used to improve the effective electric field pattern over that of the normal array pattern. The pattern improvement can be a reduction of the beamwidth by a factor of two or a reduction in the sidelobe level.

Although additional electronic complexity would be required, the use of this signal-processed system should be economically and technically considered in future antenna systems. The substantial reduction in the number of array elements, electronically controlled phase shifters, summing networks and transmission lines should make the system very attractive.

As background and basis for the development of the thesis, the

received signal and the electric field pattern for a one-dimensional array and an analysis of the processing system using a simplified, balanced-mixer model will be presented. Then a method of phase manipulation of the input signal from the array to obtain the desired amplitude factor in the effective pattern of the array and uses of the phase-manipulated amplitude term will be investigated. Also the limitations of the method of phase manipulation and of the signal processor as indicated by the simplified, balanced-mixer model will be considered. Then an extended, balanced-mixer model, its simulation and the simulation results will be investigated. The remainder of the thesis will consider the bandwidth limitations and the limitations for use of the simplified, balanced-mixer model as derived from the simulation results.

In addition to the properties stated earlier for this system on Figure 1, the analysis of the processing system and of the method of phase manipulation will show some limitations. One of these limitations is, as for other comparable detection systems, that for reproduction of the information the information signals must be carried only in a narrow bandwidth. Another limitation is that phase error maximums of 1.125° in tracking radar applications and 11.25° in normal communication applications must be maintained in order that beamwidth requirements can be met.

Moreover, the thesis will show that a hybrid-ring balanced

mixer can be simulated on the hybrid computer in scaled real time. From the simulation data, a balanced-mixer design will be determined. Using this design, calculations based on the simulation data will indicate that, to meet the phase error limitations, the maximum bandwidth for a pulsed received signal is limited to approximately nine percent of the local oscillator frequency. However, for the processing system with a CW (continuous wave) local oscillator signal, this maximum bandwidth would also require an IF (intermediate frequency) amplifier passband down to dc, which is not practical. For a practical IF amplifier passband for the processing system with a CW local oscillator, the maximum, pulsed, received-signal bandwidth is approximately two percent. Moreover, the simulation data will show that the greatest frequency dependence of the IF input signal of this balanced mixer is due to the mixer circuitry at the IF frequency. For a CW input signal the only restriction in bandwidth would be due to an insertion loss requirement. The simulation data will show that the simplified, balanced-mixer model gives a representative analysis of the balanced mixer for a CW input signal for a ten percent bandwidth range of the difference frequency of the received input frequency and the local oscillator frequency. For pulsed signals the simplified, balanced-mixer model should not be used as the only model if the phase information is important.

II. RECEIVED SIGNAL AND EFFECTIVE ELECTRIC FIELD PATTERN FOR A ONE-DIMENSIONAL ARRAY

In this section, as background for the remainder of the thesis, the receiver input signal from a one-dimensional antenna array in both the CW and pulsed cases will be given. Also, for conventional amplitude detection of the received signal, the effective electric field pattern for each case will be developed.

Reception of a CW Signal

For an n -identical element, one-dimensional array with the geometry defined in Figure 2, the receiver input signal from an effective CW source located at a distance R from the center of the array is (4), for $R \gg nd$,

$$V_R = \frac{V_0 h(\omega_s) g(\theta, \phi) L_e}{R \lambda} R_e (e^{j(\omega_s t + \alpha_{s0})} \sum_{u=(1-n)/2}^{u=(n-1)/2} A_u e^{ju\psi_0(\theta)})$$

where the terms are as defined in the symbol state, Appendix I.

In this thesis, the antenna element electric field pattern, $g(\theta, \phi)$, will be considered to have negligible effect on the receiver input signal and the antenna array pattern and will be set equal to one. This will be done for the following reasons:

1. In normal cases, the variation of $g(\theta, \phi)$ with angle is

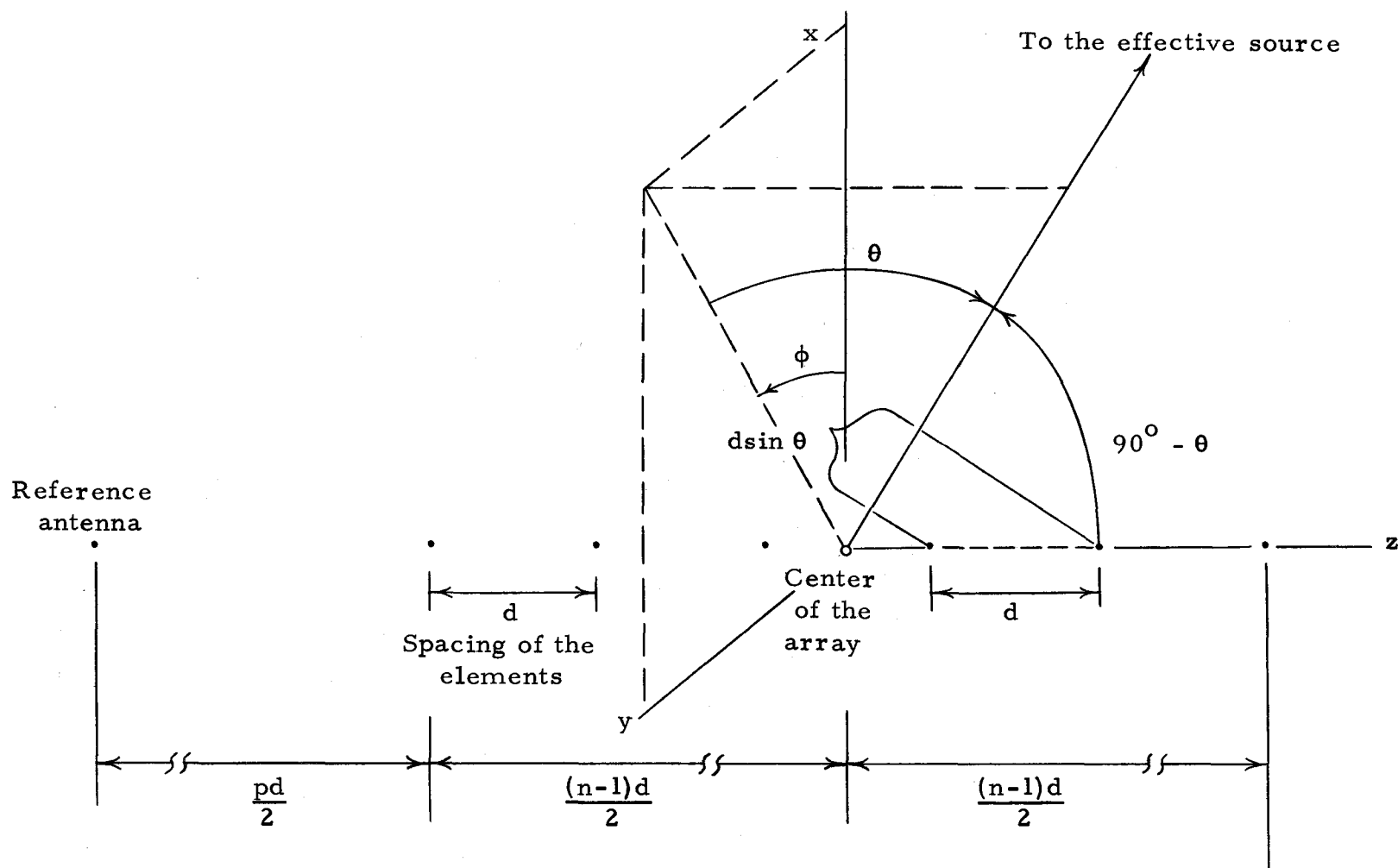


Figure 2. An n -identical element, one-dimensional array.

much slower than that of the resulting pattern of the array.

2. It will be assumed that the main-beam angle of the array pattern is within the half-power angles of the antenna-element pattern.

For cases in which $g(\theta, \phi)$ cannot be neglected, all receiver input signals and electric field patterns in this thesis should be multiplied by $g(\theta, \phi)$. Also, A_u will be restricted to being symmetrical in u around the center of the array, which, in general, is a normal distribution for an antenna array whose main-beam pointing-angle range is centered around $\theta = 0$ of Figure 2 (4).

The preceding restrictions result in the sum,

$$f(\psi_0) = \sum_{u=(1-n)/2}^{u=(n-1)/2} A_u e^{ju\psi_0(\theta)} \quad (2-1)$$

being real. Therefore, the CW received signal reduces to,

$$V_R = \frac{V_0 L_e h(\omega_s) f(\psi_0)}{R\lambda} \cos(\omega_s t + a_{s0}) \quad (2-2)$$

For amplitude detection of this signal, only the factor multiplying the $\cos(\omega_s t + a_{s0})$ term remains in the demodulated output signal. The normalized electric field pattern is defined to be the ratio of the electric field at any angle to the maximum electric field. Then,

since the output voltage is considered to be directly proportional to the electric field, the normalized electric field pattern for amplitude detection of the received signal is,

$$A_{el} = \frac{f(\psi_0)}{f(0)} \quad (2-3)$$

A_{el} is plotted versus ψ_0 in Figure 3 for A_u equal to a constant and for $n = 10$ and $n = 20$. For later reference in the thesis, the effect of increasing the number of antenna elements by a factor of two on the pattern beamwidth and sidelobe level should be noted.

Reception of a Pulsed Signal

Let us consider a pulsed signal whose pulse shape at the effective source is assumed to be symmetrical about the pulse center, or of the form

$$V_T = \left[V_0 + \sum_{m=1}^q 2V_m \cos m\omega_2 t \right] \cos(\omega_s t + \gamma_2) \quad (2-4)$$

$$= \sum_{m=-q}^{m=q} V_m \cos((\omega_s + m\omega_2)t + \gamma_2)$$

where $f_2 = \omega_2 / 2\pi$ is the pulse repetition frequency. Then the output signal of the one-dimensional antenna array of n -identical

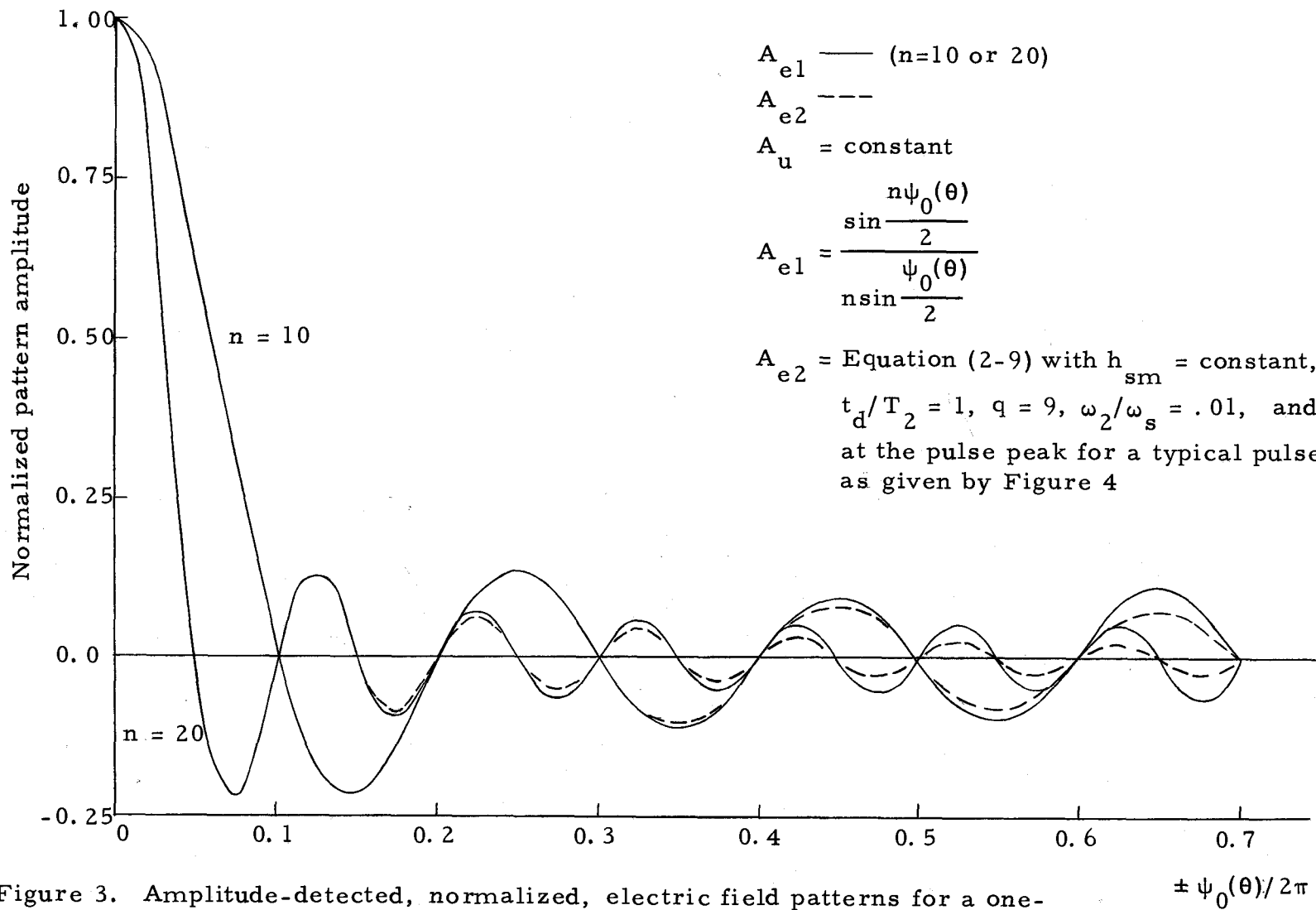


Figure 3. Amplitude-detected, normalized, electric field patterns for a one-dimensional antenna array with n -identical elements.

elements is

$$V_{RP} = \sum_{m=-q}^{m=q} \frac{V_m L_e f(\psi_m) h(\omega_s + m\omega_2)}{R\lambda} \cos((\omega_s + m\omega_2)t + a_{sm}) \quad (2-5)$$

where the terms are defined in the symbol table, Appendix I.

If β is linear in ω ,

$$\psi_m = \frac{(\omega_s + m\omega_2)\psi_0(\theta)}{\omega_s} \quad (2-6)$$

and the resulting median phase of the m^{th} frequency component of the input signal at the receiver is given by

$$a_{sm} = \gamma_0(\omega_s + m\omega_2) - \gamma_1(\omega_s + m\omega_2) - (\omega_s + m\omega_2) \left(\frac{R}{c} + \frac{\beta_s \ell_0}{\omega_s} \right) \quad (2-7)$$

Figure 4 gives the pulse envelope and the frequency spectrum envelope of a typical symmetrical transmitted pulse (11).

With originally symmetric pulsed signals at transmission, when the frequency bandwidth is less than $1/4$ of the carrier frequency ($|q\omega_2| < \omega_s/8$), the following assumptions are made in the literature (2, 4, 8):

$$f(t) = \frac{A}{2} \left(1 + \cos \frac{\pi t}{t_d}\right) \cos \omega_s t \quad \text{during the pulse}$$

$$= \sum_{m=-q}^{m=q} V_m \cos (\omega_s + m\omega_2)t$$

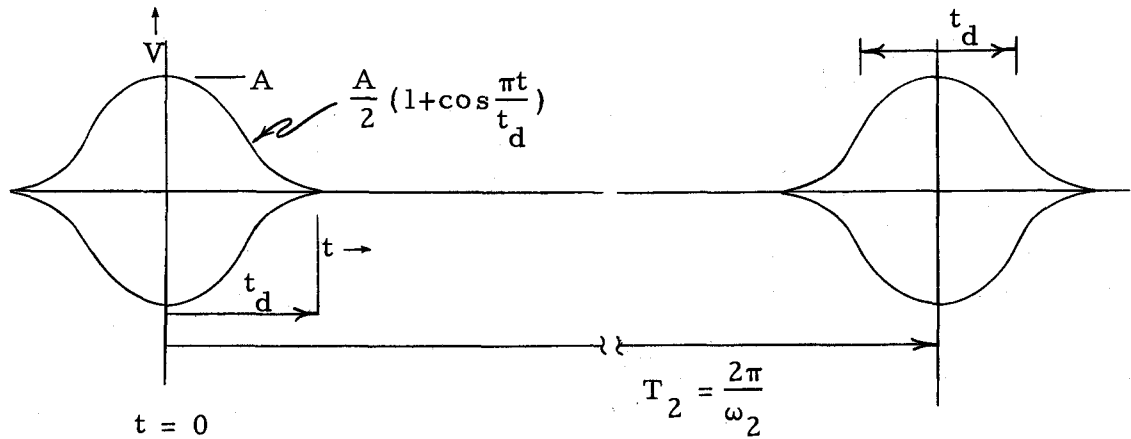
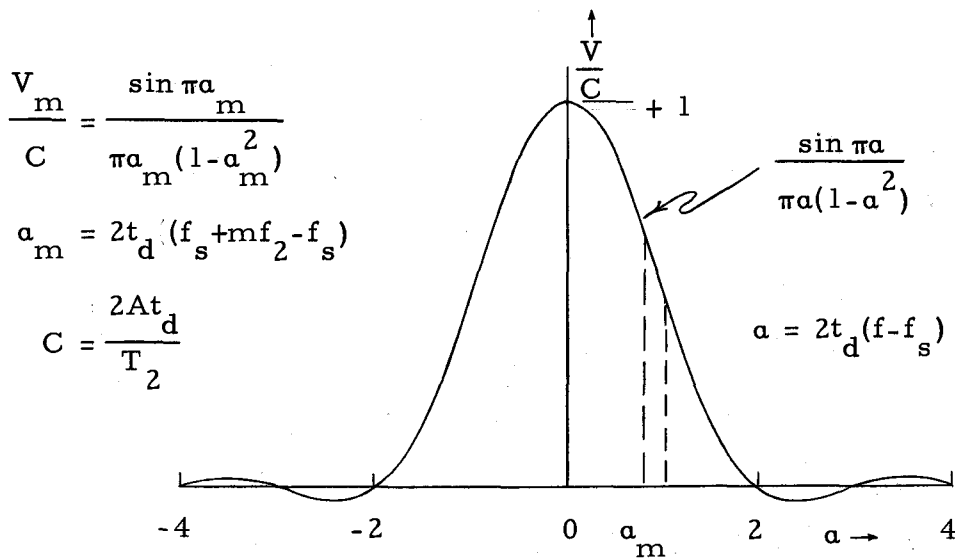
(a) Pulse envelope of $f(t)$ (b) Frequency spectrum envelope for $f(t)$

Figure 4. Pulse envelope and frequency spectrum envelope of a typical symmetrical transmitted pulse.

$$L_e/\lambda \approx \text{constant}$$

$$\beta = \text{term linear in } \omega$$

$$\gamma_0(\omega_s + m\omega_2) = (\text{constant}) + (\text{term linear in } m)$$

$$\gamma_1(\omega_s + m\omega_2) = (\text{constant}) + (\text{term linear in } m)$$

$$h_{sm} \gg h_{am}$$

where

h_{sm} = symmetrical part of loss factor, $h(\omega_s + m\omega_2)$, with m around $m = 0$ ($\omega = \omega_s$).

h_{am} = antisymmetrical part of loss factor, $h(\omega_s + m\omega_2)$, with m around $m = 0$ ($\omega = \omega_s$).

For these conditions, the signal at the receiver input is

$$V_{RP} \approx \frac{L_e}{R\lambda} \left[\sum_{m=-q}^{m=q} V_m h_{sm} f(\psi_m) \cos(m\omega_2 t + a_{sm} - a_{s0}) \right] \cos(\omega_s t + a_{s0}) \quad (2-8)$$

The normalized electric field pattern for amplitude detection of this pulsed, received signal is, for normalization at the pulse peak,

$$A_{e2} = \frac{\sum_{m=-q}^{m=q} V_m h_{sm} f(\psi_m) \cos(m\omega_2 t + a_{sm} - a_{s0})}{f(0) \sum_{m=-q}^{m=q} V_m h_{sm}} \quad (2-9)$$

A_{e2} is time dependent, meaning the antenna pattern changes during the pulse. The time dependence of A_{e2} , as the pulse amplitude goes from pulse peak to zero, would generally be to reduce the main beam amplitude and to cause the sidelobe levels to vary with respect to the main beam amplitude. Near the pulse peak and for small ψ_0 , A_{e2} reduces to A_{e1} . In Figure 3, A_{e2} is plotted at the pulse peak as a function of ψ_0 when A_u and h_{sm} are constant, for the typical pulse of Figure 4 with $t_d/T_2 = 0.1$, $q = 9$ and $\omega_2/\omega_s = 0.01$, and when $n = 10$ or 20 .

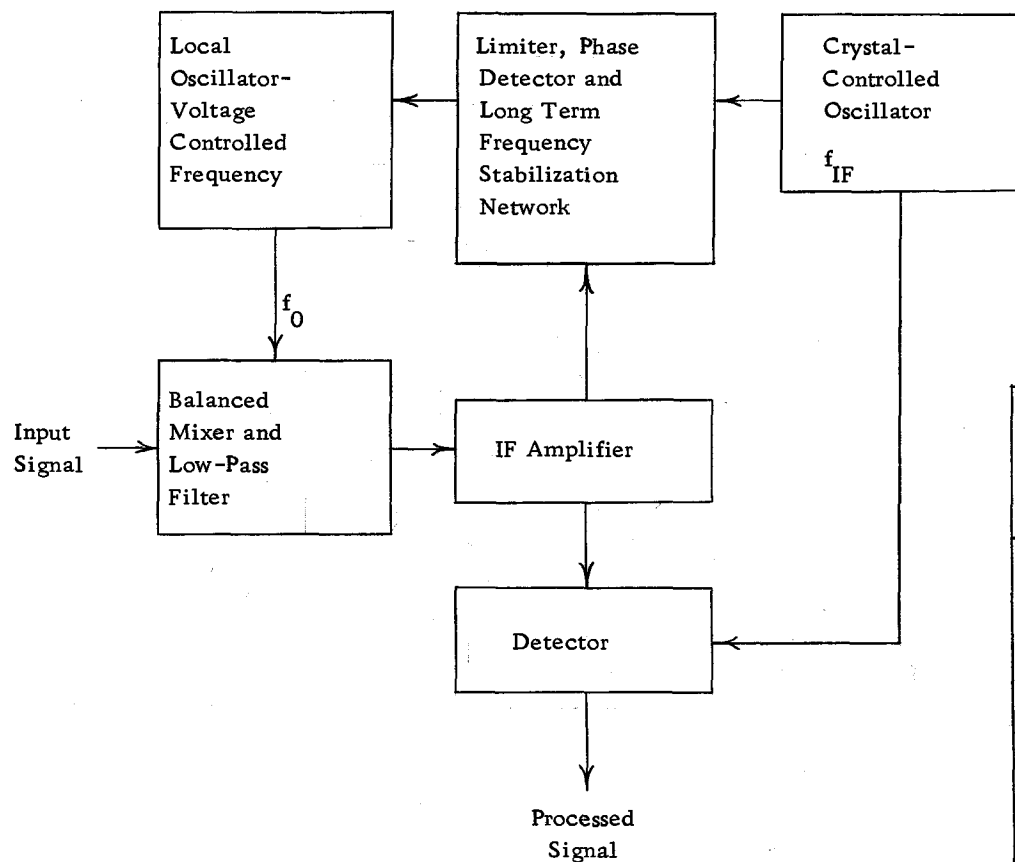
Figure 3 indicates that the main effect on the pattern of this pulsed signal is to reduce the level of the sidelobes from their values for a CW signal as ψ_0 increases.

III. ANALYSIS OF THE PROCESSING SYSTEM USING A SIMPLIFIED BALANCED-MIXER MODEL

System Description

In this section, the signal processors which are used in the signal-processed antenna system of Figure 1 will be analyzed. The analysis will show that the processor output signal contains a $\cos \gamma$ term in addition to the amplitude of the received input signal, where γ is the phase difference between the received carrier and the local oscillator signals. In the first part of this section, a simplified, balanced-mixer model will be introduced which will make it possible to mathematically analyze the balanced-mixer portion of the processor. Then, the signal processor will be analyzed for the following signal inputs: CW local oscillator and pulsed, received input signals; CW local oscillator and CW, received input signals; pulsed local oscillator and pulsed, received input signals; and pulsed local oscillator and CW, received input signals. Because it is the part of the processor that originally detects the amplitude and phase information, the emphasis in the analysis will be placed on the balanced-mixer, frequency down-converter.

The block diagram of the signal processor is given in Figure 5 along with a table of required component characteristics. The voltage-controlled local oscillator can be a low frequency oscillator with a



Characteristics		
	CW L. O.	Pulsed L. O., frequency = f_0 , repetition frequency = f_1
Input signal frequency	Carrier = f_s	Carrier = f_0 , pulse repetition = f_1
Amplifier	Wide band-width, center frequency = $ f_0 - f_s $	Narrow band-width, center frequency = f_1
Detector	Amplitude and phase	Amplitude
Crystal controlled oscillator	Required, $f_{IF} = f_0 - f_s $	Not required

Figure 5. Block diagram of the processing portion of a signal-processed antenna system.

harmonic generator, which is the state of the art, or a high frequency oscillator.

Balanced-Mixer Features

A balanced mixer utilizes two separate mixer units driven by the local oscillator signal such that at the IF input the IF signal is independent of the local oscillator signal amplitude, but is dependent on the received input signal (16). Since the mixers are driven by the local oscillator signal, the IF signal will depend on the instantaneous phase difference between the received and local oscillator signals. Only the balanced-mixer, frequency down-converter will be considered in this thesis for the following main reasons:

1. Although there are other frequency down-converters, they have a large additive portion in the IF signal which is dependent on local oscillator signal amplitude and which is not phase dependent (1, 6).
2. Since the balanced mixer suppresses, in the IF signal, any component due to the local oscillator signal, it also suppresses local oscillator noise without resorting to frequency-selective circuits, which are required by other types of mixers (1, 6).
3. The balanced mixer has large isolation between the received-input port and the local oscillator signal. Other

types of mixers have, unless filtered, half the local oscillator power transmitted out this port.

A typical hybrid balanced mixer of the TEM mode type is shown schematically in Figure 6. The design frequency, f_0 , of the balanced mixer is the frequency at which the line lengths are as shown in Figure 6. The design frequency is usually identical with the local oscillator frequency in order to maintain the isolation of the IF and the received-signal input ports from the undesirable effects of the local oscillator signal (6).

The Simplified, Balanced-Mixer Model

Although a simplified, balanced-mixer model will be used in the analysis of the processor, an extended model will be used later in the thesis to place restrictions on the results of this analysis.

For a simplified model of the balanced mixer of Figure 6, the normal assumptions for ideal mixers will be made (1, 6).

1. The signals transmitted from the inputs of the balanced mixer to the diodes have the same magnitude transmission properties and the phase shifts are linear with frequency for all frequencies within $f_0/8$ of the design frequency, f_0 (7).
2. The effect of the reflected signals which are propagating away from the diodes towards the hybrid ring on the IF

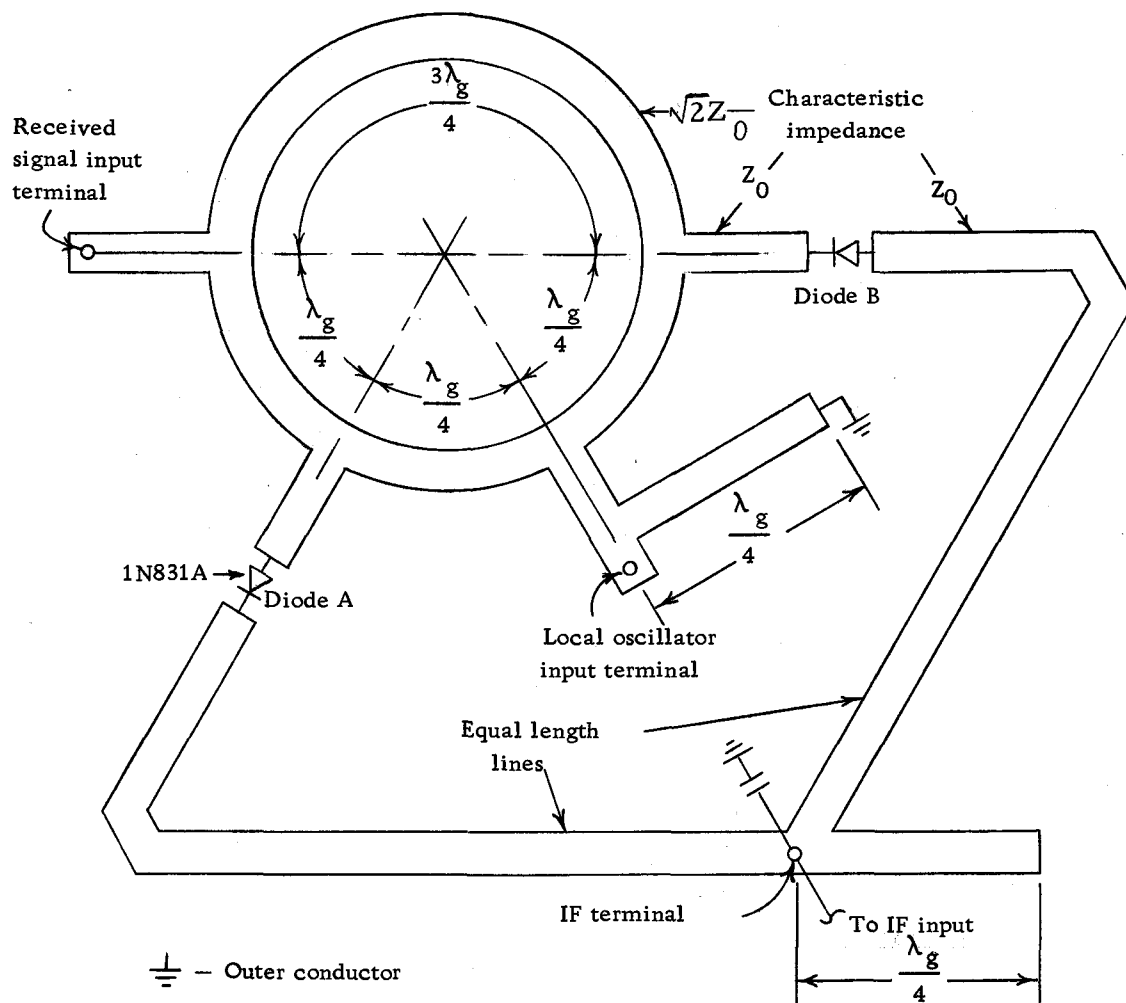


Figure 6. Center strip of a strip-line, hybrid-ring, balanced-mixer frequency converter.

signal are considered to be negligible.

3. The lengths of the lines between the hybrid ring and the diodes, and the diodes and the IF input are negligible.
4. Signals of all frequencies greater than, or on the order of, the magnitude of the design frequency are shorted at the IF input.
5. The local oscillator signal voltage is much larger than the received signal voltage.
6. A good approximation to the diode crystal behavior under condition 5 is that it acts as a half-wave rectifier that has a signal magnitude in its output which is directly proportional to the received input signal magnitude (1).

In general the stripline hybrid ring used in the balanced mixer of Figure 6 is a fairly narrow bandwidth device. The actual device will have narrower bandwidth restrictions than the ones imposed in this analysis for the simplified model.

Output for CW Local Oscillator and Pulsed, Received Signals

The pulsed, received signal case will be developed first since the CW, received signal case can be obtained directly from it. The block diagram is given in Figure 5 for the processing portion of the signal-processed antenna system. The following paragraphs develop,

for a pulsed input signal, an analysis of this processing system starting from the balanced mixer through the final detector with the emphasis on the balanced-mixer portion. It will be shown that the balanced-mixer output signal to the IF is given by

$$A(t) \cos \theta(t)$$

where $A(t)$ is the pulse envelope amplitude of the input carrier signal and $\theta(t)$ is the instantaneous phase difference between the input carrier signal and the local oscillator signal.

When a CW local oscillator signal voltage of

$$f_r(t) = H_0 \cos\left[\omega_0\left(t + \frac{\pi}{2\omega_0}\right) + a_{r0}\right] \quad (3-1)$$

and a pulsed input signal voltage of

$$f_s(t) = \sum_{m=-q}^{m=q} B_m \cos\left[(\omega_s + m\omega_2)\left(t + \frac{\pi}{2\omega_0}\right) + a_{sm}\right] \quad (3-2)$$

are applied to the junctions of the input arms of the balanced mixer shown in Figure 6, the incident voltages at the diodes A and B respectively are, using assumptions 1, 2, and 3,

$$f_{DA}(t) = 2^{-1/2} (f_r(t - \frac{\pi}{2\omega_0}) + f_s(t - \frac{\pi}{2\omega_0})) \quad (3-3)$$

and

$$f_{DB}(t) = 2^{-1/2} (f_r(t - \frac{\pi}{2\omega_0}) + f_s(t - \frac{3\pi}{2\omega_0})) \quad (3-4)$$

where the symbols are defined in the symbol table, Appendix I.

Equations (3-1) and (3-2) are defined such that the phase reference for the balanced mixer is at diode A.

Expanding the pulsed input signal at time $(t - \pi/2\omega_0)$ results in

$$\begin{aligned} f_s(t - \frac{\pi}{2\omega_0}) &= \cos(\omega_s t + a_{s0}) \sum_{m=-q}^{m=q} B_m \cos(m\omega_2 t + a_{sm} - a_{s0}) \\ &\quad - \sin(\omega_s t + a_{s0}) \sum_{m=-q}^{m=q} B_m \sin(m\omega_2 t + a_{sm} - a_{s0}) \end{aligned} \quad (3-5)$$

Let

$$B_m = B_{ms} + B_{ma}$$

where

B_{ms} = symmetrical part of B_m around $m = 0$, or $\omega = \omega_s$

B_{ma} = antisymmetrical part of B_m around $m = 0$, or $\omega = \omega_s$.

From Figure 4, it can be seen that B_{ma} is zero at the source for a symmetrical pulse shape. However, since the attenuation in media is

usually antisymmetrical in frequency around the center frequency,

B_{ma} is nonzero at the receiver. In normal applications, that is for distances less than interplanetary communications, $B_{ma} \ll B_{ms}$ (2, 8). Thus, under these conditions and since $\sin(m\omega_2 t + a_{sm} - a_{s0})$ is antisymmetrical in m for media with linear phase propagation,

$$\sum_{m=-q}^{m=q} B_m \sin(m\omega_2 t + a_{sm} - a_{s0}) \approx 0.$$

With this simplification, Equation (3-5) becomes

$$\begin{aligned} f_s(t - \frac{\pi}{2\omega_0}) &\approx A(t) [\cos(\theta(t) + \omega_0(t) + a_{r0})] \\ &\approx A(t) [\cos\theta(t)\cos(\omega_0 t + a_{r0}) - \sin\theta(t)\sin(\omega_0 t + a_{r0})] \end{aligned}$$

where

$$A(t) = \sum_{m=-q}^{m=q} B_{ms} \cos(m\omega_2 t + a_{sm} - a_{s0})$$

= pulse envelope amplitude of the input signal

and

$$\theta(t) = (\omega_s - \omega_0)t + a_{s0} - a_{r0} = (\omega_s - \omega_0)t + \gamma$$

= instantaneous phase difference between the
input carrier signal and the local oscillator
signal

The voltage across diode A is of the same polarity as the incident signal but that across diode B is of opposite polarity. If diode A is conducting at time t , diode B is at the same stage of conduction at time $(t+\pi/\omega_0)$. The incident signals of diode A at time t and diode B at time $(t+\pi/\omega_0)$, respectively, are

$$f_{DA}(t) \approx (A(t)\cos\theta(t)+H_0) \left[\frac{1+\phi_1^2(t)}{2} \right]^{1/2} \cos(\omega_0 t + \alpha_{r0} - \phi_1(t))$$

and

$$f_{DB}(t+\frac{\pi}{\omega_0}) \approx (A(t)\cos\theta(t)-H_0) \left[\frac{1+\phi_2^2(t)}{2} \right]^{1/2} \cos(\omega_0 t + \alpha_{r0} - \phi_2(t))$$

where

$$\phi_1(t) = \frac{A(t)\sin\theta(t)}{H_0 + A(t)\cos\theta(t)}$$

and

$$\phi_2(t) = \frac{A(t)\sin\theta(t)}{H_0 - A(t)\cos\theta(t)}$$

Under assumption 5, $\phi_1(t)$ and $\phi_2(t)$ are small. Letting

$$x = A(t) \cos \theta(t)$$

$$y = A(t) \sin \theta(t)$$

and for the approximation $(1+u^2)^{1/2} \approx 1 + u^2/2$

$$\begin{aligned}
 (x \pm H_0) \left(1 + \frac{y^2}{(H_0 \pm x)^2} \right)^{1/2} &\approx x \pm H_0 \pm \frac{y^2}{2(H_0 \pm x)} \\
 &\approx x \pm H_0 - \frac{y^2(x \mp H_0)}{2(H_0^2 - x^2)}
 \end{aligned}$$

Using assumptions 4, 5, and 6, the contributions of the diodes to the IF input signal is, for $|\omega_s - \omega_0| < \omega_0$,

$$\begin{aligned}
 V_{IF_i} &\approx \frac{1}{\pi} [(\text{amplitude of } \cos(\omega_0 t + a_{r0} - \phi_1(t)) \text{ in } f_{DA}(t)) \\
 &\quad + (\text{amplitude of } \cos(\omega_0 t + a_{r0} - \phi_2(t)) \text{ in } f_{DB}(t + \frac{\pi}{\omega_0}))] \\
 &\approx \frac{2^{1/2}}{2\pi} \left[x + H_0 - \frac{y^2(x - H_0)}{2(H_0^2 - x^2)} + x - H_0 - \frac{y^2(x + H_0)}{2(H_0^2 - x^2)} \right] \\
 &\approx \frac{2^{1/2} A(t)}{\pi} \left[1 - \frac{A^2(t) \sin^2 \theta(t)}{2(H_0^2 - A^2(t) \cos^2 \theta(t))} \right] \cos \theta(t)
 \end{aligned}$$

Since by assumption 5 $A(t) \ll H_0$, the IF input signal becomes,

$$V_{IF_i} \approx \frac{2^{1/2}}{\pi} \cos[(\omega_s - \omega_0)t + a_{s0} - a_{r0}] \sum_{m=-q}^{m=q} B_{ms} \cos(m\omega_2 t + a_{sm} - a_{s0}) \quad (3-6)$$

For the processing system in Figure 5, after amplification of the IF input signal of Equation (3-6) and after amplitude and phase

detection with the oscillator signal, $\cos[(\omega_s - \omega_0)t]$, the output signal is (1)

$$V \approx K_1 \cos(a_{s0} - a_{r0}) \sum_{m=-q}^{m=q} B_{ms} \cos(m\omega_2 t + a_{sm} - a_{s0}) \quad (3-7)$$

where K_1 is a constant and, as in the usual amplitude detection system, $q\omega_2 \ll |\omega_s - \omega_0|$ (8). The output signal amplitude is thereby only a function of the input signal pulse-envelope amplitude and an amplitude term which depends on the phase difference between the input carrier frequency signal and the local oscillator signal. The processor output signal, Equation (3-7), and the typical pulse envelope for the input signal of Equation (3-2) are plotted in Figure 7.

In the output signal, the frequency-component-amplitude term, B_{ms} , may be a function of time. Similar to other amplitude detection schemes, in order to obtain all information, its frequency is limited to frequencies less than f_2 , the repetition frequency of the input signal, and less than $|f_s - f_0|$, the absolute value of the difference between the input carrier frequency and the local oscillator frequency (8).

Output for CW Local Oscillator and CW, Received Signals

With a CW signal instead of a pulsed input signal, the analysis

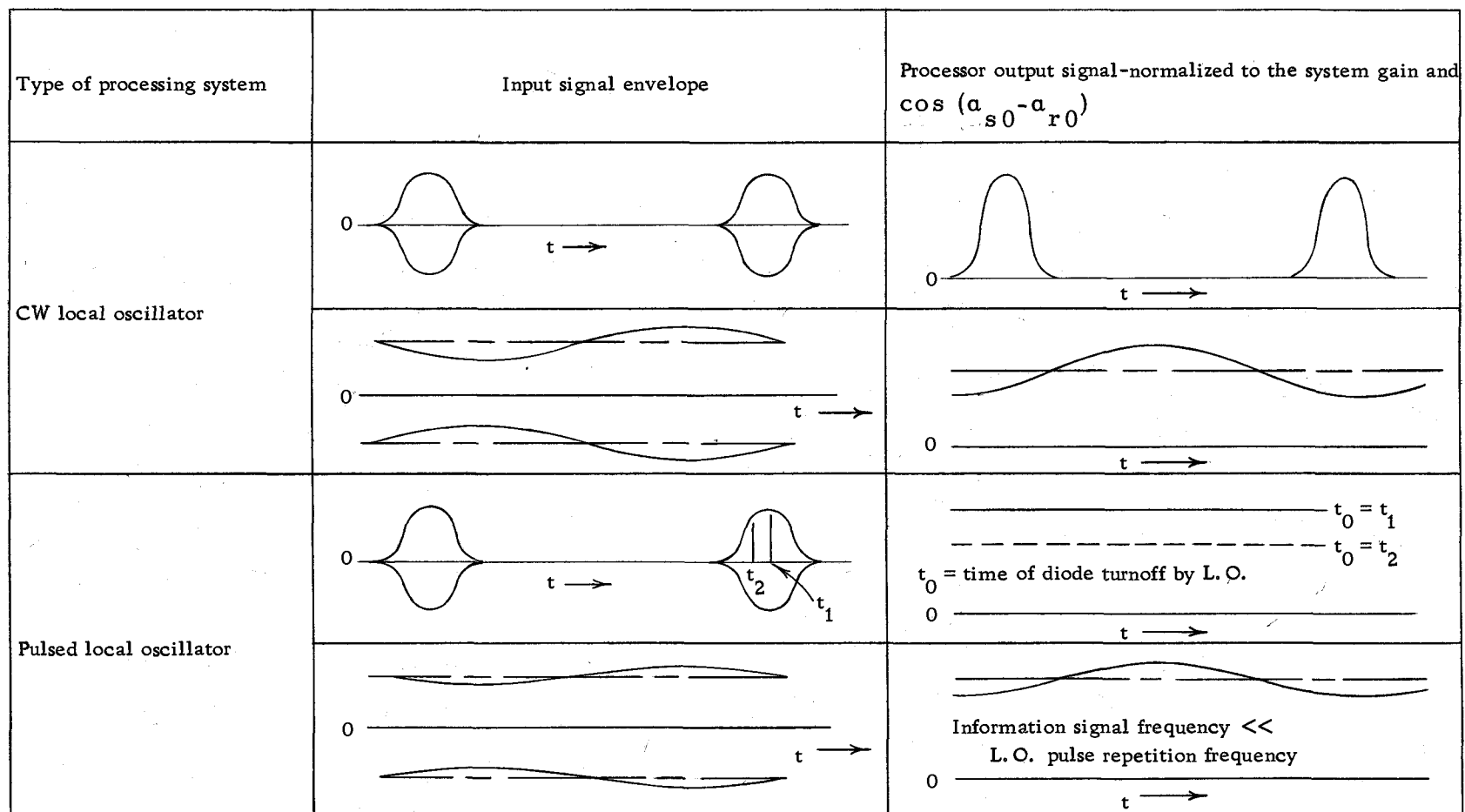


Figure 7. The processor output signal for different input signals and types of processing.

would follow approximately the same steps as in the preceding section except q would be zero. Therefore, for CW input and local oscillator signals, Equation (3-7) for the output of the processing system in Figure 6 becomes (1)

$$V \approx K_1 B_0 \cos (a_{s0} - a_{r0}) \quad (3-8)$$

where K_1 is a constant and where the other terms are defined in the symbol table, Appendix I. Again the processor output signal is only a function of the input amplitude and an amplitude term which depends on the phase difference between the input signal and the local oscillator signal. The processor output signal of Equation (3-8) and the input signal amplitude are plotted in Figure 7.

In the output signal, the input amplitude, B_0 , may be a function of time. Similar to other amplitude detection schemes, in order to obtain all information, its frequency range is limited to frequencies less than $|f_s - f_0|$, the absolute value of the difference between the input frequency and the local oscillator frequency (8).

Output for Pulsed Local Oscillator and Pulsed, Received Signals

The block diagram for the processing portion of a signal-processed antenna system is given in Figure 5. The following paragraphs develop, for the pulsed input signal of Equation (3-2), an

analysis of this processing system starting from the balanced mixer and going through the final detector.

For a pulsed, local oscillator signal voltage of

$$f_r(t) = \sum_{i=-v}^{i=v} H_i \cos[(\omega_0 + i\omega_1)(t + \frac{\pi}{2\omega_0}) + \alpha_{ri}] \quad (3-9)$$

where the terms are defined in the symbol table, Appendix I, the incident voltages at the inputs to diodes A and B, respectively, are again given by Equations (3-3) and (3-4).

Let

$$H_i = H_{is} + H_{ia}$$

where

H_{is} = symmetrical part of H_i around $i = 0$, or $\omega = \omega_0$

H_{ia} = antisymmetrical part of H_i around $i = 0$, or $\omega = \omega_0$

Then, assuming the local oscillator pulse was originally symmetrical and for normal applications, $H_{ia} \ll H_{is}$ (2, 8). Since the sine term is antisymmetrical in i for media with linear phase propagation,

$$\sum_{i=-v}^{i=v} H_i \sin(i\omega_1 t + \alpha_{ri} - \alpha_{r0}) \approx 0$$

For the conditions of the preceding equation and following the

same steps as were done for the pulsed, received input signal, the local oscillator signal at the diodes reduced to

$$f_r(t - \frac{\pi}{2\omega_0}) \approx \left[\sum_{i=-v}^{i=v} H_{is} \cos(i\omega_1 t + a_{ri} - a_{r0}) \right] \cos(\omega_0 t + a_{r0}) \quad (3-10)$$

Hence the local oscillator signal has a pulse envelope for the $\cos(\omega_0 t + a_{r0})$ term for this case as compared to a constant envelope for the CW local oscillator signal case.

Because the diodes are not ideal, they only rectify during the portion of time when the envelope of the local oscillator signal is greater than some cutoff voltage, assuming a weak received input signal (11, p. 8-11). Normally the local oscillator signal is either pulsed at a high duty rate, v small, which can be approximated by the CW case, or at a low duty rate, v large (8). The low duty rate case is analyzed in this section.

For short-pulse operation of the balanced mixer, the input signal and the local oscillator signal must have the same repetition frequency and the same carrier frequency. The short-pulsed local oscillator processing system is essentially a sampled data system. In a sample data system, the pulse repetition frequency determines the theoretical maximum bandwidth for reproduction of information signals.

With a bandpass IF amplifier of bandwidth, $\delta f_{IF} \leq f_1/2$, the processed signal for the processing system in Figure 5 is (11, p. 12-20)

$$V \approx K_2 \cos(a_{s0} - a_{r0}) \sum_{m=-q}^{m=q} B_{ms}(t) \cos(m\omega_1 t_0 + a_{sm} - a_{s0}) \quad (3-11)$$

where K_2 is a constant and t_0 is the time of diode turnoff. t_0 is approximately given by

$$t_0 \approx -\frac{a_{r0}}{\omega_0} + \frac{t_d}{2} \quad (3-12)$$

where $(-a_{r0}/\omega_0)$ is the time when the symmetric, pulsed, local oscillator signal is at its center and t_d is the pulse width of the local-oscillator-signal pulse between half-voltage points.

Equation (3-11) is just a constant times the IF input signal for the processing system with a CW local oscillator, Equation (3-7), sampled at each time of diode turnoff. As for the CW local oscillator signal case, the processor output signal is a function only of the input signal pulse amplitude and an amplitude term which depends on the phase difference between the input and local oscillator carrier frequency signals. The processor output signal of Equation (3-11), and the typical pulse envelope for the input signal of Equation (3-2) are plotted in Figure 7.

As for the CW local oscillator signal case and for other amplitude detection schemes, the frequency-component amplitude term, B_{ms} , may be a function of time; but its frequency is limited by the frequency bandwidth of the IF, δf_{IF} .

Output for Pulsed Local Oscillator and CW,
Received Signals

For a CW input signal instead of a pulsed input signal, the analysis would follow approximately the same steps as in the preceding section except q would be zero. Thus, for CW input and pulsed, local oscillator signals, Equation (3-11) for the output of the processing system in Figure 5 becomes

$$V \approx K_2 B_0 \cos (a_{s0} - a_{r0}) \quad (3-13)$$

Again the output signal is only a function of the input signal amplitude and an amplitude term, $\cos (a_{s0} - a_{r0})$, which depends on the phase difference between the input signal and the local oscillator, center-frequency signal. The processor output signal represented by Equation (3-13) and the input signal amplitude are plotted in Figure 7.

As for the pulsed local oscillator and pulsed, received signal case and for other amplitude detection schemes, the input amplitude term, B_0 , may be a function of time, but its frequency is limited by the frequency bandwidth of the IF, δf_{IF} . This processor output-

signal Equation, (3-13), is identical, except for a constant factor, to the output signal Equation, (3-8), for the processing system shown in Figure 5 for CW input and CW local oscillator signals.

IV. PHASE MANIPULATION FOR IMPROVEMENT OF THE FIELD PATTERN

In this section, a method of manipulation of the phase term γ in the processor output signal by the use of the signal of a reference antenna displaced an integral number of element half-spacings away from the array will be presented for the general case for the receiver input and local oscillator signals. Then, it will be applied to the specific types of processing system for a CW or a pulsed local oscillator signal with a CW or a pulsed input signal. The actual improvement in the effective electric field pattern will be given in the next section.

General Case

Let us apply the processing system of section III to the receiver input signal of the array as given in section II. Moreover, in the array of Figures 1 and 2, let ℓ_0 be the effective, median length of the transmission lines from the array elements to the balanced-mixer input junction plus a length equivalent to the length between the junction and diode A. Note that the effect of ℓ_0 can be changed by means of the main-line phase shifters shown in Figure 1. Then, assuming the simplified model of the balanced mixer gives a correct analysis, the phase-dependent factor in the final processed signal of the array, Equation (3-7), (3-8), (3-11), or (3-13), is

$$\cos (a_{s0} - a_{r0}) = \cos \gamma \quad (4-1)$$

Now let a reference antenna with the same phase shift properties as the array elements be placed $(p+n-1)d/2$ to the left of the center of the array as shown in Figure 2 and let the effective length of its transmission line to diode A of the reference system processor be $[\ell_0 - (n+p-1)\ell_1/2 - \phi_0/\beta_s]$ where ϕ_0 is the pattern control phase shift. Then the phase of the carrier frequency signal at the balanced mixer of the reference system processor is

$$a_{s0R} = a_{s0} - \frac{(n+p-1)\psi_0(\theta)}{2} + \phi_0$$

The phase-dependent factor of the reference-system-processor output signal becomes

$$\cos (a_{s0} - \frac{(n+p-1)\psi_0(\theta)}{2} + \phi_0 - a_{r0}) \quad (4-2)$$

Now, changing the phases in the reference antenna line and in the input line to the main processor equally (phase change = $\beta_s \delta \ell_0$) so that Equation (4-2) becomes zero results in

$$a_{s0} = a_{r0} + \frac{(n+p-1)\psi_0(\theta)}{2} - \phi_0 - \frac{(2b+1)\pi}{2} \quad (4-3)$$

where $b = 0, \pm 1, \pm 2, \pm 3, \text{ etc.}$

In the processed received signal of Equation (3-7), (3-8), (3-11), or (3-13) with the input amplitude as given by the receiver input signal of the array, Equation (2-2) or (2-8), let the constant factors be denoted by K_3 and let the ψ_0 -, m -, and q -dependent factors be denoted by $F(\psi_0, m, q)$, where $F_0(0, m, q)$ is the maximum obtained with the variation of ψ_0 and t . Then for a_{s0} as given in Equation (4-3), the processed received signal of the array is given by

$$\begin{aligned} G(\psi_0, m, q) &= K_3 F(\psi_0, m, q) \cos \left(\frac{(n+p-1)\psi_0}{2} - \phi_0 - \frac{(2b+1)\pi}{2} \right) \\ &= (-1)^b D_3 F(\psi_0, m, q) \sin \left(\frac{(n+p-1)\psi_0}{2} - \phi_0 \right) \end{aligned} \quad (4-4)$$

and the effective electric field pattern, for normalization by

$(-1)^b K_3 F_0(0, m, q)$, is

$$A_{e3} = \frac{F(\psi_0, m, q) \sin \left(\frac{(n+p-1)\psi_0}{2} - \phi_0 \right)}{F_0(0, m, q)} \quad (4-5)$$

This pattern is plotted as a function of $\psi_0(\theta)$ in Figure 8 for $n = 10$, $p = 1$, for various values of the pattern control phase shift, ϕ_0 , and for $F(\psi_0, m, q) = f(\psi_0)$, Equation (2-1) with $A_u = 1$. For $\phi_0 = 0$, it is characterized by a null at $\psi_0 = 0$ and a maximum amplitude very close on either side of $\psi_0 = 0$. For $\phi_0 = -\pi/2$, A_{e3} has a maximum at $\psi_0 = 0$.

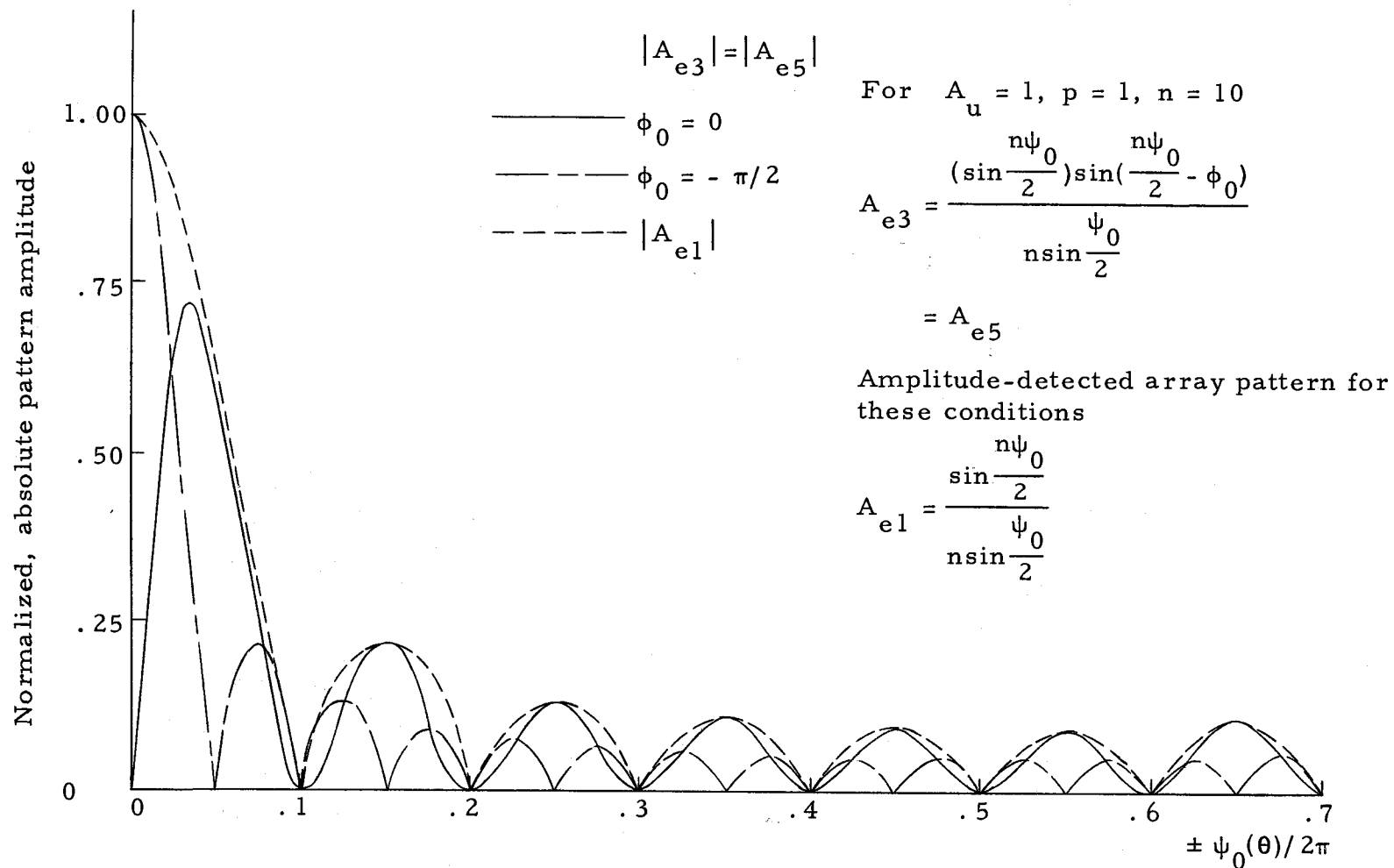


Figure 8. Processed effective electric field patterns for a one-dimensional antenna array.

By using the processed signal from a reference antenna to adjust a common phase shift in the transmission lines of the antenna array and the reference antenna, the effective electric field pattern for the system of Figure 1, with the processors as shown in Figure 5, has an amplitude term, $\sin[(n+p-1)\psi_0/2 - \phi_0]$, multiplying the normal pattern for amplitude detection.

CW Local Oscillator Signal System

For the processing system of Figure 5 with a CW local oscillator signal and under the conditions given in the first paragraph of the general case, the processed signal of Equation (3-7) becomes for a pulsed input signal to the array

$$V \approx \frac{K_1 L_e}{R\lambda} \cos(a_{s0} - a_{r0}) \sum_{m=-q}^{m=q} V_m h_{sm} f(\psi_m) \cos(m\omega_2 t + a_{sm} - a_{s0})$$

Therefore $F(\psi_0, m, q)$ and $F_0(0, m, q)$ are given respectively by

$$F(\psi_0, m, q) = \sum_{m=-q}^{m=q} V_m h_{sm} f(\psi_m) \cos(m\omega_2 t + a_{sm} - a_{s0})$$

and

$$F_0(0, m, q) = f(0) \left(\sum_{m=-q}^{m=q} V_m h_{sm} \right)$$

Hence Equation (4-5) becomes for a pulsed input signal and a CW local oscillator signal

$$A_{e4} = \frac{\left(\sum_{m=-q}^{m=q} V_m h_{sm} f(\psi_m) \cos(m\omega_2 t + a_{sm} - a_{s0}) \right) \sin\left(\frac{(n+p-1)\psi_0}{2} - \phi_0\right)}{f(0) \left(\sum_{m=-q}^{m=q} V_m h_{sm} \right)}$$

$$= A_{e2} \sin\left(\frac{(n+p-1)\psi_0}{2} - \phi_0\right) \quad (4-6)$$

where A_{e2} is given by Equation (2-9).

With a CW input signal, which is the pulsed input signal with $q = 0$, the effective electric field pattern, or Equation (4-6), becomes

$$A_{e5} = \frac{f(\psi_0) \sin\left(\frac{(n+p-1)\psi_0}{2} - \phi_0\right)}{f(0)} = A_{e1} \sin\left(\frac{(n+p-1)\psi_0}{2} - \phi_0\right) \quad (4-7)$$

where A_{e1} is given by Equation (2-3).

Thus by this method of using the processed received signal from a reference antenna to adjust a common phase shift of the antenna array and the reference antenna, the effective normalized electric field patterns for the CW and pulsed received signals are found to have an amplitude term, $\sin((n+p-1)\psi_0/2 - \phi_0)$, multiplying the usual

patterns for amplitude detection.

Pulsed Local Oscillator Signal System

For a pulsed local oscillator signal as given by Equation (3-9), it was shown in section III for the processing system of Figure 5 that the final processed signal had the same form as for the CW local-oscillator-signal case except that $t = t_0$ where t_0 was the time of diode turnoff. Therefore, the effective normalized electric field pattern for pulsed local oscillator and receiver input signals is, from Equation (4-6),

$$A_{e6} = \frac{\left[\sum_{m=-q}^{m=q} V_m h_{sm} f(\psi_m) \cos(m\omega_2 t_0 + a_{sm} - a_{s0}) \right] \sin\left(\frac{(n+p-1)\psi_0}{2} - \phi_0\right)}{f(0) \left(\sum_{m=-q}^{m=q} V_m h_{sm} \right)} \quad (4-8)$$

which is the same as Equation (4-6) near the peak of the pulses.

With a CW receiver input signal and a pulsed local oscillator signal, the normalized effective electric field pattern is identical to that for the CW local oscillator and receiver input signals case or Equation (4-7).

As for the CW local-oscillator-signal case, this method of using the processed receiver input signal from a reference antenna to adjust

a common phase shift of the antenna array and the reference antenna yields effective, normalized, electric field patterns for the CW and pulsed receiver input signals which have an amplitude term, $\sin (n+p-1)\psi_0/2-\phi_0$), multiplying the usual patterns for amplitude detection.

V. USES OF THE PHASE MANIPULATED TERM IN THE FIELD PATTERN

This section will give uses of the phase-manipulated term in the effective electric field pattern for the system of Figure 1 and will indicate the improvements of the pattern over that for the normal array pattern for amplitude detection. The minimization of beamwidth and sidelobes and radar applications will be discussed.

For different input signals and for the different processors of Figure 5, all the phase-manipulated, effective array patterns, as given in the preceding section, reduce to that for a CW receiver-input signal, Equation (4-7) or

$$A_{e5} = \frac{f(\psi_0) \sin\left(\frac{(n+p-1)\psi_0}{2} - \phi_0\right)}{2} = A_{e1} \sin\left(\frac{(n+p-1)\psi_0}{2} - \phi_0\right) \quad (5-1)$$

where $f(\psi_0)$ is defined by Equation (2-1).

Due to the time or diode turnoff time dependence of the patterns for pulsed input signals, the pattern given by Equation (5-1) is true for pulsed input signals only when the processed signal is near maximum amplitude as a function of t or t_0 and when $\psi_0(\theta)$ is small. However, since all the processed patterns of the preceding section do reduce under some conditions to the pattern of Equation (5-1), only it will be considered here.

In the first two parts of this section, only the case, where $\phi_0 = -\pi/2$, will be considered; because it produces a maximum in the direction of the beam pointing-angle for the amplitude-detected array pattern, A_{e1} . Thus, for $\phi_0 = -\pi/2$, Equation (5-1) becomes

$$A_{e5} \Big|_{\phi_0 = -\frac{\pi}{2}} = A_{e1} \cos \left(\frac{(n+p-1)\psi_0}{2} \right) \quad (5-2)$$

Beamwidth Minimization

Let us assume that $\cos((n+p-1)\psi_0/2)$ rather than A_{e1} controls the beamwidth. Then the half power point is at $\psi_0 = \pm \pi/2(n+p-1)$ and $\psi_{BW} \approx \pi/(n+p-1)$ where ψ_{BW} is the beamwidth in ψ_0 between half power points.

When each antenna element had equal weighting, A_{e1} , the amplitude-detected pattern, is (4)

$$A_{e1} = \frac{f(\psi_0)}{f(0)} = \frac{\sin(\frac{n\psi_0}{2})}{n \sin(\frac{\psi_0}{2})} \quad (5-3)$$

This condition of equal weighting of the signals from the antenna elements produces minimum beamwidth for A_{e1} (4). This pattern is plotted versus ψ_0 in Figure 3 for $n = 10$ and $n = 20$ and in

Figure 8 for $n = 10$. A_{e1} has a half-power point at $\psi_0 \approx \pi/1.11n$ and for $\psi_0 = \pi/2n$ it has a value of 0.9. Therefore, for $(n+p-1) > n$, $\cos((n+p-1)\psi_0/2)$ controls the beamwidth and $\psi_{BW} \approx \pi/(n+p-1)$.

For the case where p , the number of element half-spacings that the reference antenna is placed away from the end element of the antenna array (see Figure 2), is equal to one and the antenna elements have equal weighting, Equation (5-2) becomes

$$A_{e5} \Big|_{\phi_0 = -\frac{\pi}{2}} = \frac{\sin(\frac{n\psi_0}{2}) \cos(\frac{n\psi_0}{2})}{n \sin(\frac{\psi_0}{2})} = \frac{\sin(\frac{2n\psi_0}{2})}{2n \sin(\frac{\psi_0}{2})} \quad (5-4)$$

which is an effective doubling of the number of elements in the array from the case for amplitude detection as given by Equation (5-3). However, the processing does not increase the received signal amplitude by a factor of two as would occur for an array with twice the number of elements. Equation (5-4) is plotted in Figure 8 for $n = 10$, and in Figure 3 as A_{e1} with $n = 10$ and $n = 20$, corresponding respectively to A_{e5} with $n = 5$ and $n = 10$.

For minimum beamwidth and to keep the sidelobe levels from increasing, the nulls and maximums of $f(\psi_0)$ should be maximums and nulls of $\cos((n+p-1)\psi_0/2)$ respectively for all except the first two as shown in Table 1.

Table 1. Distribution of maximums and nulls for $f(\psi_0)$ and $\cos((n+p-1)\psi_0/2)$ for minimum beam-width and slight change in the sidelobe levels.

	$\psi_0=0$	$ \psi_0 =C_1$	$ \psi_0 =C_2$	$ \psi_0 =C_3$
$f(\psi_0)$	maximum	---	null	maximum
$\cos((n+p-1)\psi_0/2)$	maximum	null	maximum	null

C_1, C_2 and C_3 are constants and $0 < C_1 < C_2 < C_3$

Sidelobe Level Minimization

When $p < 0$, A_{e1} determines the beamwidth of the pattern of Equation (5-2). Therefore, the $\cos((n+p-1)\psi_0/2)$ term can be used to reduce the sidelobe levels by making the term small when A_{e1} is at its largest sidelobes.

As an example let us take the case for equal weighting of the antenna elements. The sidelobes of Equation (5-3) are located at $\psi_0 = \pm(2m+3)\pi/n$ for $m = 0, 1$, etc. and the value at the sidelobes is (4)

$$S_m = \frac{1}{n \sin\left(\frac{(2m+3)\pi}{2n}\right)}$$

With n large, the magnitudes of the first and second sidelobes are respectively $2/3\pi$ and $2/5\pi$. Now the value of $\cos((n+p-1)\psi_0/2)$ at the sidelobes is given by

$$P_m = \cos \left(\frac{(n+p-1)(2m+3)\pi}{2n} \right) = (-1)^m \sin \left(\frac{(p-1)(2m+3)\pi}{2n} \right)$$

Letting $|P_0/P_1| = |S_1/S_0|$, then the first two sidelobes of the pattern of Equation (5-2) become equal and lower than the first two sidelobes of A_{e1} . Making this calculation results in $p - 1 \approx -0.545n$ and a maximum sidelobe level of 0.115 for the pattern of Equation (5-2), which is 5.3 db less than for A_{e1} .

Radar Applications

With the pattern control phase shift, ϕ_0 , equal to zero, the pattern given by Equation (5-1) has a null for $\psi_0 = 0$ with a maximum close by on either side. This can be seen from Figure 8 where A_{e5} is plotted for $n = 10$, $p = 1$, A_{e1} given by Equation (5-3) and for $\phi_0 = 0$ and $-\pi/2$. This type of pattern can be used in tracking radar to follow a target by keeping its signal in the null between the two maximums of the pattern. Since $\psi_0(\theta) = k_s d \sin \theta - \beta_s \ell_1$, this is done for a variation in θ by varying ℓ_1 while also maintaining the validity of Equation (4-3).

In order to find other benefits of the system of Figure 1, let the manipulated phase α_{s0} as given in Equation (4-3) be equated to α_{s0} as defined in the symbol table, Appendix I, or

$$a_{r0} + \frac{(n+p-1)\psi_0(\theta)}{2} - \phi_0 - \frac{(2b+1)\pi}{2} = \gamma_0(\omega_s) - \gamma_1(\omega_s) - \beta_s \ell_0 - k_s R$$

Considering $\gamma_0(\omega_s)$, $\gamma_1(\omega_s)$ and ϕ_0 to be constant, denoting $\gamma_0(\omega_s) - \gamma_1(\omega_s)$ by a constant K_4 , and $\phi_0 + (2b+1)\pi/2$ by K_5 , and substituting for $\psi_0(\theta)$, gives for γ or $a_{s0} - a_{r0}$

$$\gamma = \left(\frac{n+p-1}{2}\right)(k_s d \sin \theta - \beta_s \ell_1) - K_5 = K_4 - \beta_s \ell_0 - k_s R - a_{r0}$$

Solving for $\beta_s \ell_0$ gives

$$\beta_s \ell_0 = \left(\frac{n+p-1}{2}\right)(\beta_s \ell_1 - k_s d \sin \theta) + K_4 + K_5 - k_s R - a_{r0} \quad (5-5)$$

Therefore, for any change in ℓ_1 , R , θ , and a_{r0} , the system of Figure 1, in order to maintain the desired pattern and Equation (4-3), must make the following hold true;

$$\beta_s \ell_0 = \left(\frac{n+p-1}{2}\right)(\beta_s \delta \ell_1 - k_s d \delta \theta \cos \theta) - k_s \delta R - \delta a_{r0} \quad (5-6)$$

where $\delta \theta$ is small. For this condition with $\delta R = \delta \theta = 0$, varying ℓ_1 scans the processed received signal of the array through the amplitude pattern given by Equation (5-1) for different values of ψ_0 . For instance, if $\psi_0 \neq 0$ (center of the pattern not pointing toward the object), ℓ_1 could be varied until Equation (5-1) with $\phi_0 = 0$ gives a null between two large maximum amplitudes, and hence

$$\psi_0 = 0.$$

Let

$$\delta l_0 = \delta l_0' + \delta l_0''$$

and

$$\delta l_0' = \frac{(n+p-1)\delta l_1}{2}$$

Then, if in order to maintain Equation (4-3), an additional change in $\beta_s l_0$ is required, it is given by

$$\beta_s \delta l_0'' = -k_s \left(\delta R + \frac{(n+p-1)d\delta\theta \cos\theta}{2} \right) - \delta a_{r0}$$

If $\delta\theta$ is known from the pattern, say by the use of Equation (5-1) with $\phi_0 = 0$, and assuming δa_{r0} is small, zero, or known, then δR can be determined. $\delta R + ((n+p-1)d\delta\theta \cos\theta)/2$ is the change in the distance to the transmitting object from the reference antenna, and δR is the change in the distance to the transmitting object from the center of the array. From δR , and $\delta\theta$, the distance the object moves can be determined. Thus, if $\delta l_0''/\delta t$ is known, the speed of the object can be determined.

It can also be seen from Equation (5-6), that if the system maintains the validity of this equation, it corrects any phase error due to a change in the local oscillator signal phase a_{r0} .

VI. LIMITATIONS OF PHASE MANIPULATION AND OF THE SIGNAL PROCESSOR AS INDICATED BY THE SIMPLIFIED, BALANCED-MIXER MODEL

In this section, the limitations of the method of phase manipulation and the bandwidth limitations of the signal processor for pulsed input signals and for information signals will be given. These limitations will be based on the analysis of the processor of Figure 5, which utilized a simplified, balanced-mixer model.

In a later section, on the basis of the simulation results for an extended, balanced-mixer model, further restrictions will be placed on the bandwidth of the signal processor for pulsed input signals and on the IF frequency for CW input signals. However, no additional restrictions will be placed on the information signal since, as in other amplitude detection schemes, it is limited by the type of processor and not the characteristics of the down converter.

Method of Phase Manipulation

One limitation of the method of phase manipulation given in section IV is that the received signal of the reference antenna may be too weak to be detected by its balanced mixer. One method of counteracting this is to amplify the signal from the reference antenna before sending it to the balanced-mixer processor. A second way is to have the reference antenna be an array thereby resulting in increased

received signal for the reference antenna.

A second limitation is that of multiple signals. For multiple signals of different strengths received by the reference antenna, this method of phase manipulation would find the phase null for Equation (4-2) for the sum of the signals instead of just one and therefore would not obtain the proper pattern. A method to eliminate this is again to use an array for the reference antenna to give some directionality. In radar applications another method is to use pulsed local oscillator and receiver input signals so that the detected receiver signal is that reflected from an object in a small range of distances around a distance specified by the delay of the local oscillator signal pulse. Then by varying the delay of the local oscillator signal pulse, all distances can be checked. Also in radar applications, if instead of a pulsed local oscillator signal a CW local oscillator signal is used, then there are IF signal processing methods that can be used to range gate the pulsed received signal and to vary the range gate position (8).

Another possible limitation is the tolerance that is required in obtaining a phase null for the reference antenna signal as given in Equation (4-2). This tolerance can be found from the term

$$a_{s0} - a_{r0} = \frac{(n+p-1)(\psi_0 + \psi_e)}{2}$$

where $\psi_0 = k_s d(\sin \theta - \sin \theta_m)$, $\psi_e = k_s d(\sin(\theta_e + \theta) - \sin \theta)$, θ is the

received signal direction angle, θ_m is the angle of the beam maximum, and θ_e is the error angle in θ . Letting α_e be the error angle of $\alpha_{s0} - \alpha_{r0}$ so that

$$\alpha_e = \frac{(n+p-1)\psi_e}{2} \approx \frac{(n+p-1)k_s d \theta_e \cos \theta_r}{2}$$

Therefore, the maximum error angle is given by

$$\alpha_{em} = \frac{(n+p-1)\psi_{em}}{2} \approx \frac{(n+p-1)k_s d \theta_e}{2}$$

A typical value for ψ_{em} in tracking radar applications is (8)

$$\psi_{em} = 0.025\psi_{BW}$$

and in normal communications applications is (8)

$$\psi_{em} = 0.25\psi_{BW}$$

where ψ_{BW} is the beamwidth of ψ_0 of the array pattern. Let us use the value of ψ_{BW} given by the array effective pattern, Equation (5-3), for equal weighting of the antenna elements and for $p = 1$.

This case gives minimum beamwidth for the array effective pattern, while retaining the same sidelobe level as for the amplitude detected

pattern, Equation (5-2). Hence $\psi_{BW} = \pi/2n$. Therefore, for

$p = 1$ and in order to maintain the desired angle accuracy for an

array of twice the number of elements, the maximum phase angle error allowed for phase nulling is for tracking radar applications

$$\alpha_{em} \approx 0.0625 \pi \approx 1.125^\circ \quad (6-1)$$

and for normal communications applications is

$$\alpha_{em} \approx 0.625 \pi \approx 11.25^\circ \quad (6-2)$$

Therefore, the error in $\beta_s \ell_0$ must remain in magnitude less than Equation (6-1) or (6-2). Also, if there is any other nonconstant error in the phase term, $\alpha_{s0} - \alpha_{r0}$, its sum with the error of $\beta_s \ell_0$ must remain in magnitude less than Equation (6-1) or (6-2).

In the method of phase manipulation of section IV, the reference antenna signal is used to set $\beta_s \ell_0$. Therefore any phase error due to the processing system will be included in $\beta_s \ell_0$, and thus this type of phase error will effectively be cancelled out for the processed array received signal. The general array pattern, assuming no other errors, would then be given by Equation (4-5). This is true if the measurements are done under the same conditions such as carrier frequency and pulse shape. However, in the worst case such as a different carrier frequency and pulse shape, the phase error due to the processing system can be counted as a phase error in $\beta_s \ell_0$, while ideally there would not be any phase error due to the processing system.

In a later section, for the simulation results of the extended model of the balanced mixer, this phase angle error limitation of Equation (6-1) or (6-2) will require a further restriction in the frequency bandwidth of the system for a pulsed input signal.

Signal Processor

As analyzed in section III of this thesis for a simplified, balanced-mixer model, the limitations in bandwidth for the system of Figure 1 with the signal processor of Figure 5 are given in Table 2 with the terms as defined in the symbol table, Appendix I. The $f_0/8$ limitation is a limitation which was placed on the simplified, balanced-mixer model because of the characteristics of the hybrid ring.

Table 2. Bandwidth limitations of the received input signal and of the information carried on the receiver input signal as indicated by the analysis for the signal processor.

	CW local oscillator	Pulsed local oscillator
Pulsed received input signal	$ f_s \pm qf_2 - f_0 < f_0/8$ with $qf_2 < f_0/8$	$qf_2 = qf_1 < f_0/8$
CW received input signal	$ f_s - f_0 < f_0/8$	$qf_1 < f_0/8$
Information on the input signal	$f_I \ll f_s - f_0 , f_I < f_2$	$f_I < \delta f_{IF} \leq f_1/2$

VII. SIMULATION OF A LOSSLESS STRIP-LINE, HYBRID-RING, BALANCED-MIXER FREQUENCY CONVERTER UTILIZING AN EXTENDED MODEL

This simulation study was undertaken to show the accuracy and bandwidth limitations of the processor of Figure 5 in its use in the signal-processed antenna system of Figure 1. It was also undertaken to show the accuracy of and limitations for the use of the simplified, balanced-mixer model of section III.

In this section, an extended model of the hybrid-ring, balanced-mixer frequency converter will be given for use in a simulation study of the mixer, and will be followed by the simulation study and the simulation results. The simulation results will show the validity of the simulation and the behavior of the hybrid-ring, balanced mixer as modeled.

In the next two sections, the simulation results will be used to show the bandwidth limitations of the processor for unmodulated CW and constant peak pulsed input signals and the accuracy and limitations of the simplified, balanced-mixer model.

An Extended Model

The extended mathematical model will account for all physical characteristics of the hybrid-ring, balanced mixer of Figure 6 with the following exceptions:

1. The strip transmission line is considered lossless.
2. The junctions between line sections are lossless and free of energy storage.
3. The propagation in the transmission lines is considered non-dispersive.

The computer realization of the model will be based on the set of equations for the power-normalized, traveling-wave amplitudes and will utilize the scattering coefficients of the junctions. The following equivalent replacements will be made:

1. Energy propagation in the transmission lines will be replaced by time delays.
2. The junctions will be replaced by weighted summations based on the scattering coefficients.
3. The diodes and the IF input circuit will be replaced by their equivalent circuits.

Figure 9 gives the extended model equivalent of the equations for the hybrid-ring, balanced mixer except for the diode and IF input circuits. An analysis of the relationship between the traveling-wave amplitudes at the strip-line junctions of the balanced mixer of Figure 6 is made in Appendix II. This analysis gives the equivalent, weighted summations of Figure 9 for the junctions of the balanced mixer. Figure 10 gives the equivalent circuits for the mixer diodes and the IF input circuit including the capacitance to the outer conductor at the

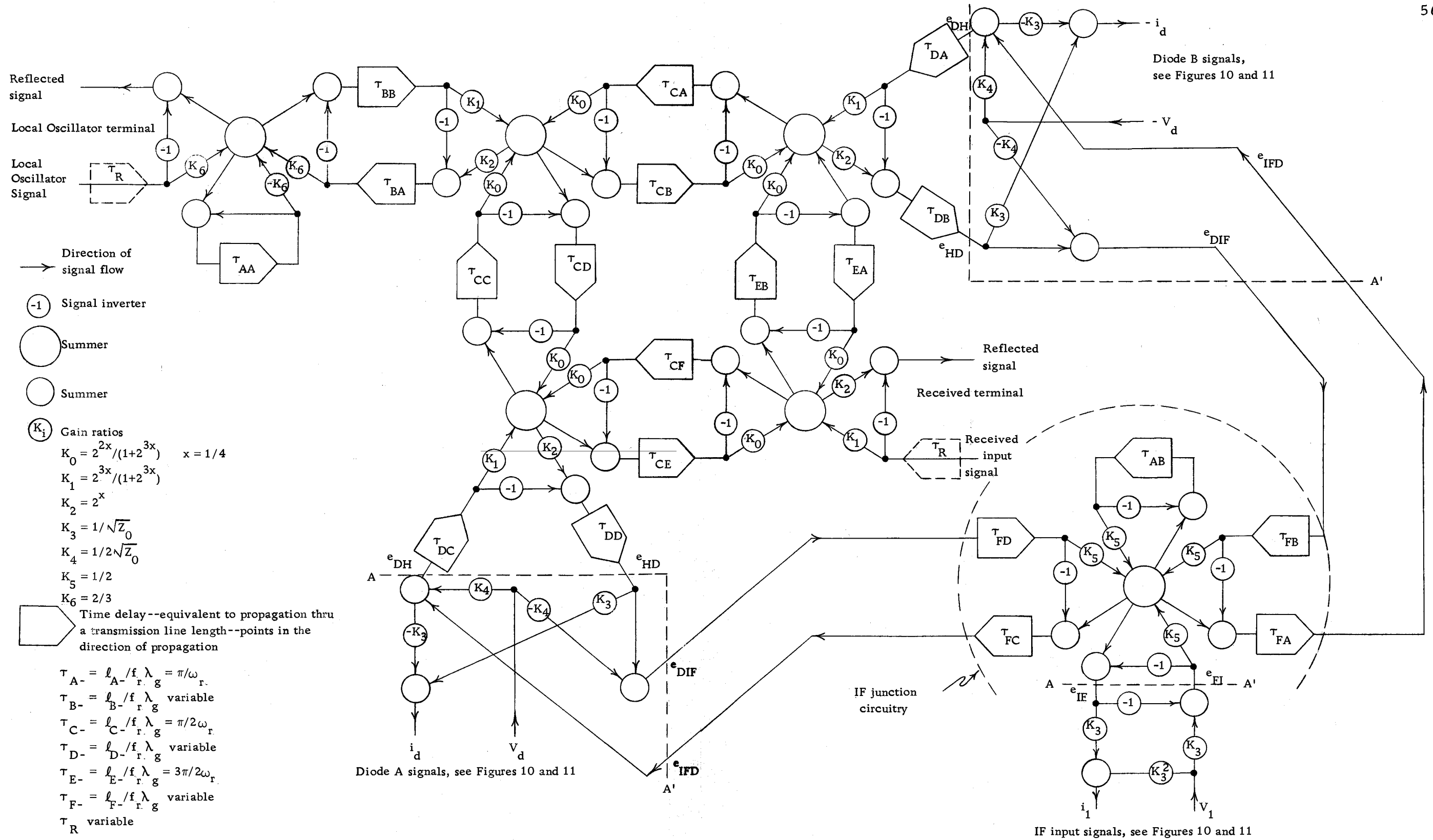


Figure 9. Partial realization of the hybrid-ring, balanced-mixer, extended model.

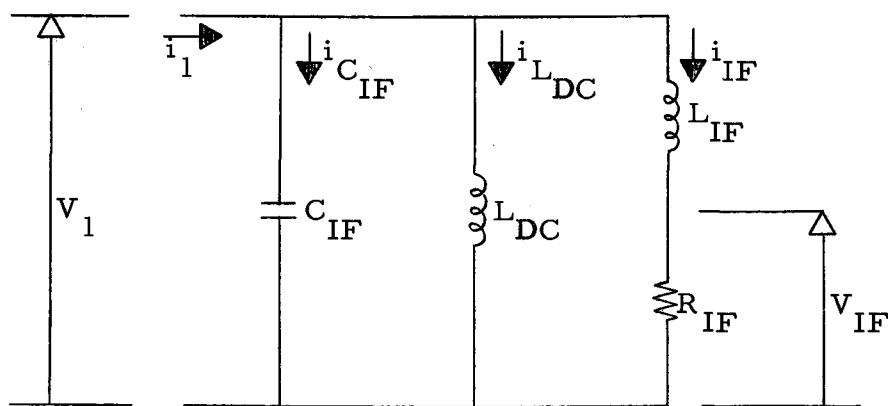
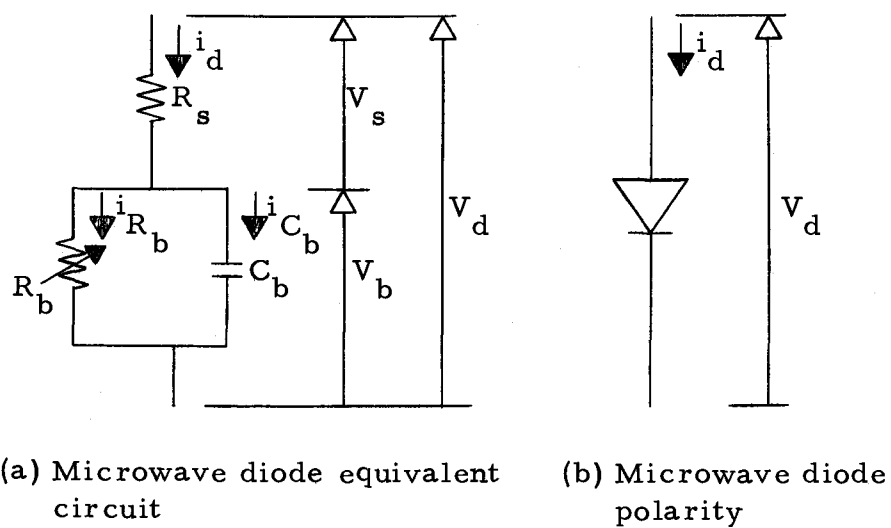


Figure 10. Microwave diode and IF input equivalent circuits.

IF terminal in Figure 6 (6, 10).

In the equivalent circuit of the mixer diode, Figure 10a, R_s is the ohmic spreading resistance of the diode, and R_b and C_b are the barrier resistance and the barrier capacitance of the diode respectively. The barrier resistance is a function of the applied voltage (10). Since the barrier width is a function of the applied voltage, the barrier capacitance is a function of the applied voltage (10). Even though the barrier capacitance is variable with applied reverse bias voltage, conventional practice is to consider it to be constant (10). Therefore the barrier capacitance will be held constant in this work.

The mixer diode has a d. c. current-voltage relationship given by (10)

$$i_d = a(e^{\frac{b(V_d - i_d R_s)}{V_T}} - 1)$$

where i_d is the current into the diode, V_d is the voltage across the diode, R_s is the spreading resistance and a and b are constants. The voltage across the barrier is given by

$$V_b = V_d - i_d R_s = V_d - V_s$$

Now let us choose a typical microwave mixer diode the 1N831A, an S-band diode. For this diode, the d. c. current-voltage relationship is given by (11)

$$i_d = 5.2(10^{-6})(e^{21.6(V_d - 12.1i_d)} - 1) \text{ amperes}$$

Thus the spreading resistance, R_s , is 12.1 ohms and the total current through the barrier resistance, R_b , is given by

$$i_{R_b} = 5.2(10^{-6})(e^{21.6V_b} - 1) \quad (7-1)$$

where V_b is the total voltage across the barrier. For the 1N831A mixer diode, the barrier capacitance was assumed to be 0.25 pf, which is a typical value for an S-band diode (10)

In the IF input equivalent circuit, Figure 10c, R_{IF} is the input resistance. The inductance, L_{DC} is intended to be a d.c. short to ground, but a very high impedance at the IF frequency and above. The inductance, L_{IF} , is a very low impedance at the IF frequency, but a high impedance at the local oscillator signal frequency or higher. The reason that this inductance was needed in the simulation will be discussed in the simulation results. Capacitance, C_{IF} , is also a high impedance at the IF frequency, but is a very low impedance at the local oscillator signal frequency or higher. In addition to capacitance C_{IF} , a quarter wavelength open stub at the local oscillator signal frequency is placed in parallel at the IF terminal to form an effective short at the local oscillator signal frequency and odd harmonics of it.

Since in the simulation study the IF frequency will be varied to find the frequency bandwidth of the hybrid-ring balanced mixer, the IF input equivalent circuit was designed to have an impedance of approximately R_{IF} over the IF frequency range of 0.001 to 0.125 of the local oscillator frequency. This range was used, because the assumed useable bandwidth of the simplified, balanced-mixer model was given by $|f-f_0|/f_0 < 0.125$. The design resulted in the following values for the components of the IF equivalent circuit,

$$L_{DC} = 0.075 \text{ mh}$$

$$C_{IF} = 0.25 \text{ pf}$$

$$L_{IF} = 1.8 \text{ nh}$$

The Simulation Study

The simulation study of the hybrid-ring, balanced-mixer frequency converter was made on an Electronic Associates, Inc. 690 hybrid computer in the Engineering Simulation Laboratory at Oregon State University. The properties and available functions for this computer at this facility are given in Appendix III. The simulation study almost used the entire capabilities of the computer.

The portion of the simulation of the hybrid-ring balanced mixer that was done on the digital part of the hybrid computer is the portion of the realization of the extended model up to the terminals marked

A-A' in Figure 9. The digital program was so designed that one cycle of the digital operating program represented one degree at the local oscillator signal frequency. In a way to minimize a computation cycle, the local oscillator and input signals were generated on the digital computer. The local oscillator signal was generated by table lookup, while the input signal was generated from the formula for the sine of two angles where one angle is small or

$$\sin(\theta + \delta\theta) = \cos \delta\theta \sin \theta + \cos \theta \sin \delta\theta \approx \sin \theta + \delta\theta \cos \theta$$

in which the $\sin \theta$ and $\cos \theta$ terms were generated by table lookup. The transmission line lengths were simulated by storage of the input data over a number of computation cycles; since the propagation through a length of lossless transmission line is equivalent to a time delay. The digital program was designed to take equal time in any path through the operating program. The program was written in assembly language; since, at the time of the simulation study, Fortran could not be used for this computer at the Oregon State University facility. However, it is doubtful that Fortran would be practical since it would have added a large number of unnecessary machine steps which would have greatly reduced the signal frequency; thereby causing the frequency range to be outside the scaleable range of the analog computer. The program produced a stable, real time frequency of 1.33 hertz. The flow diagram for the entire digital program is given

in Appendix III.

The data was digitized on the digital computer, stored during the main program computation cycle, and then, after sufficient data had been collected, analyzed by the digital computer. This was done because of noise on the simulated IF input signal, because of the large quantity of data required, and because analog data is hard to analyze. The data consisted of the IF signal amplitude and relative phase. The phase was referenced to the beat signal of the sum of the local oscillator and input signals from their respective inputs. A sense line input from the analog computer was used to start the data taking and storage.

The analog portion of the hybrid computer was used to simulate the diode equivalent circuits, the IF equivalent circuit and the portion of the extended model realization in Figure 9 at the terminals A-A' to or from the diodes or the IF (3). The variable, diode function generator was used to generate Equation (7-1) (3). The analog computing circuit diagram is given in Figure 11 (3). The equations for this diagram are derived in Appendix IV. The output control lines from the digital computer were used to control the track-store summers. The digital portion of the analog computer along with a pushbutton was used to start the data collection in the digital computer and to control an eight channel recorder. The computing circuit diagram for this is shown in Figure 12.

Equations for the scaled signals and the potentiometer coefficients are given in Appendix IV

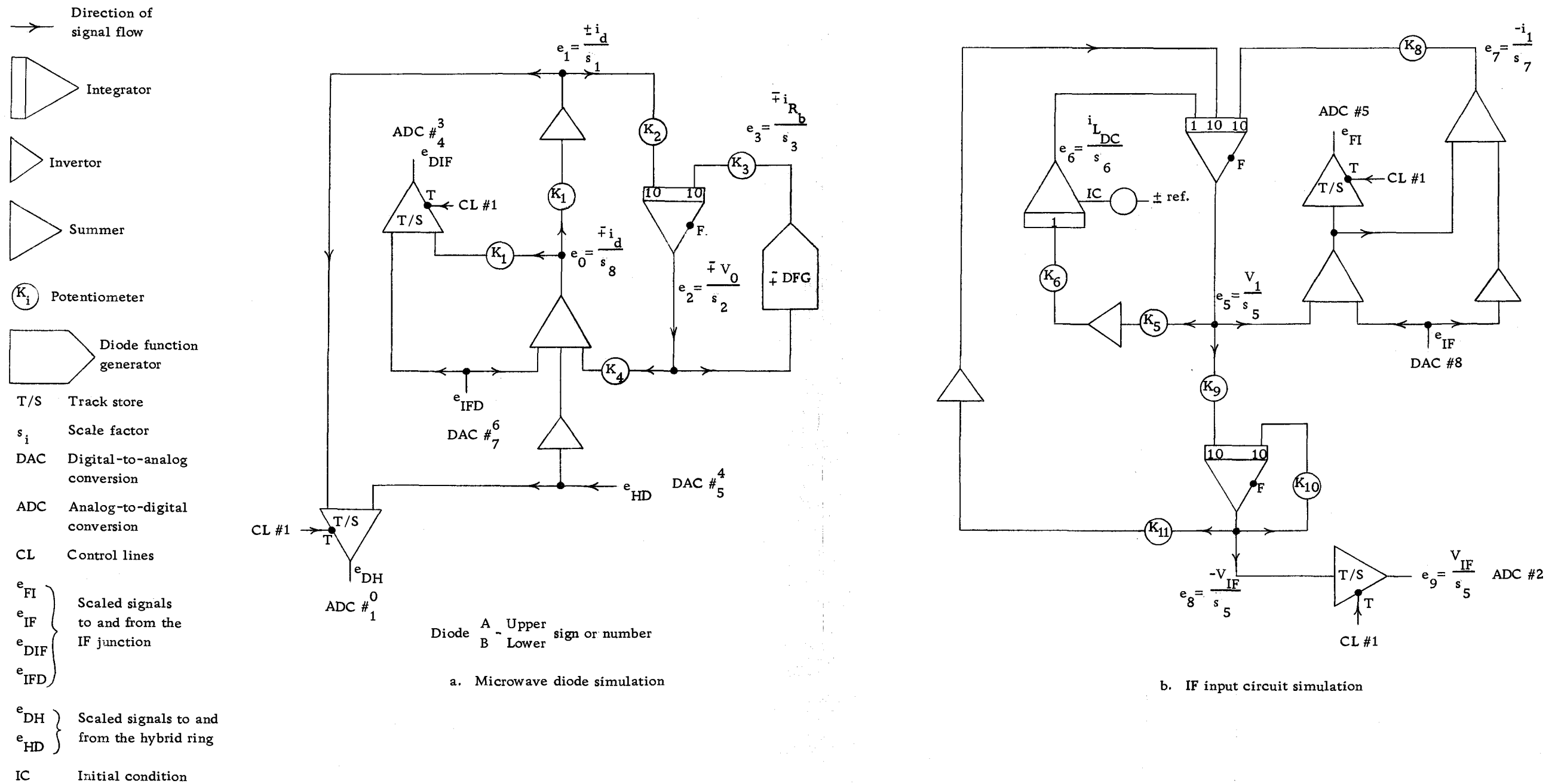
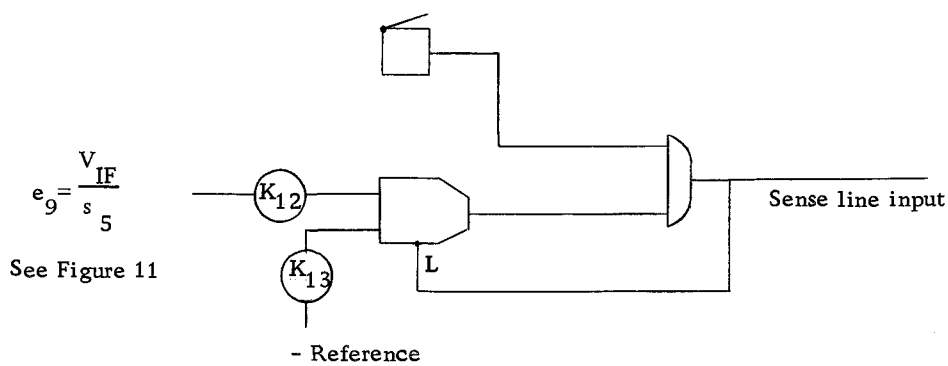


Figure 11. Analog computer circuit diagram for the simulation of the microwave diode and IF input equivalent circuits on the EAI 690 hybrid computer.



Data collection control

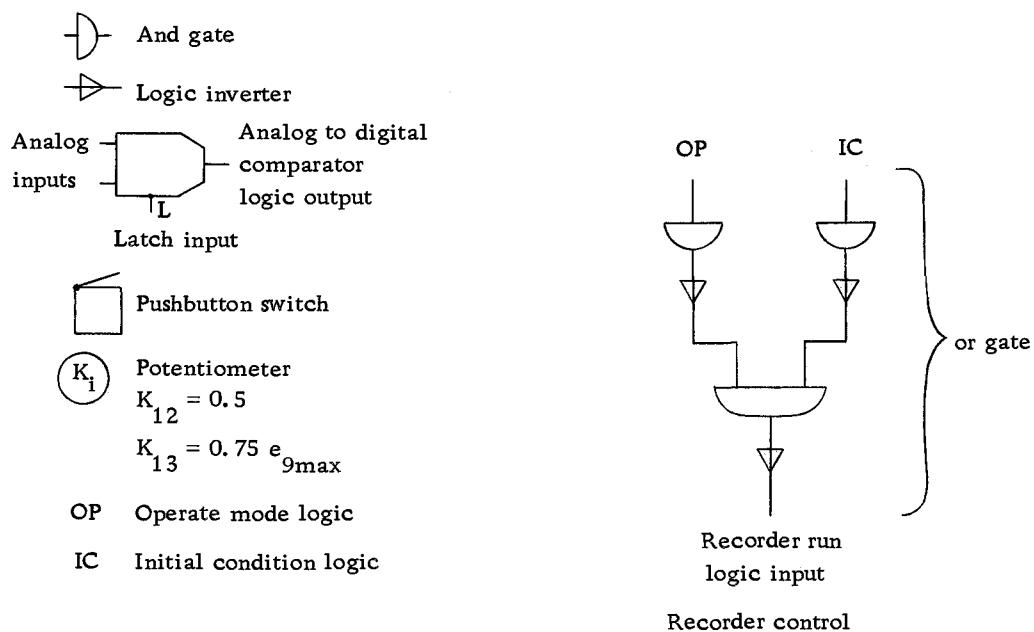


Figure 12. Digital circuit diagram for the analog computer in the simulation of a hybrid-ring, balanced-mixer frequency converter.

In the simulation study, the lengths of lines between the diodes and the hybrid ring or the IF terminal, the IF input impedance, R_{IF} , the characteristic impedance, Z_0 , and/or the local oscillator signal magnitude were varied to find their effects on the IF input signal magnitude. The effects on the IF input signal magnitude of the parameter variations were used to design the hybrid-ring, balanced mixer and to verify the simulation and the simulation model. Designing the balanced mixer consisted of maximizing the IF input signal power for the parameter variations for a given RF input power to the mixer. The effects on the IF input signal magnitude of the parameter variations were measured for $(f_s - f_r)/f_r = \pm 0.005$. It should be noted that, for a CW local oscillator signal, the IF frequency, f_{IF} , is given by

$$f_{IF} = |f_s - f_r| \quad (7-2)$$

The IF input signal voltage was normalized on the analog computer in terms of power at a level of $63.3 \mu\text{w}$. In other words, the maximum allowable scaled analog output of 1.0 for the IF input signal was set to be 5 db down from the RF input power of $200 \mu\text{w}$ for any R_{IF} or Z_0 . The $200 \mu\text{w}$ power level for the RF input power corresponds to a power-normalized amplitude of 0.0633 for the RF input signal. This normalization of the IF input signal was done because, in the balanced-mixer design, the interest is not in the IF input voltage but

in the IF input power, and because the lowest measured insertion loss for the 1N831A mixer diode is 5.5db (9). The power-normalized input signal amplitude of 0.0633 was used; since it is the assumed limit of 0.1 (the local oscillator signal amplitude) that was made for the simplified, balanced-mixer model.

After the design of the hybrid-ring balanced mixer, $(f_s - f_r)/f_r$ was varied from -0.125 to +0.125 in 0.005 steps in order to find the frequency bandwidth of the hybrid-ring balanced mixer. In addition, the effects on the IF input signal of added delays in the received and local oscillator input lines were found for different IF frequencies. This whole simulation was done only for CW input and local oscillator signals. The operating local oscillator frequency was set to be 3.33 Ghz, a middle S-band frequency. Therefore, since the real time frequency was 1.33 hz, it produced a scaling factor of 2.5×10^9 .

Simulation Results

Circuit Design

Initially the extended-model equivalent circuits shown in Figures 9 and 10 were simulated with $L_{IF} = 0$. However, besides the IF signal frequency, it was found that there were too many high frequency signals at the IF input port. These other signals made it impossible to analyze the IF signal frequency. To eliminate these

signals, effective shorts for the second and fourth harmonics of the local oscillator signal frequency were placed at the IF input junction by the use of open stubs. In addition, effective opens for the second and fourth harmonics of the local oscillator signal frequency were placed in the line to the IF input circuit by the use of series shorted stubs. Additional filtering was added to the IF input circuit by adding L_{IF} to the circuit. This reduced the high frequency signals to a level where they were a minor effect.

The open and shorted stubs also produced effective shorts or opens at other frequencies. This is due to the following facts: A quarter wavelength shorted (open) stub produces an effective open (short) at the input for the fundamental frequency and all odd harmonics and an effective short (open) at the input for the even harmonics. A shorted (open) stub, which is designed to produce an effective open (short) for the second harmonic, has an effective open (short) for the second, sixth, tenth, etc. harmonics. Also a shorted (open) stub, which is designed to produce an effective open (short) for the fourth harmonic, has an effective open (short) for the fourth, twelfth, etc. harmonics.

The noise or high frequency signals were due to one or more causes from the following list, in the order of their likelihood;

1. The effective impedance at the IF input junction for harmonics of the fundamental frequency were not low enough to

produce an effective short; thereby causing coupling to the IF input transmission line.

2. The analog computer amplifiers for the IF input signals are saturated by the initial transient signals; thereby feeding abnormal signals back to the balanced mixer.
3. The possibility of the two diode characteristics of the analog computer not being matched; thereby causing an unbalance and coupling to the IF input line.
4. The transient signals are not attenuated as they would be in the actual device; since the extended model was assumed to be lossless.
5. The signals fed to the analog computer from the digital computer and vice versa are digital; thereby causing, by these digital steps, some noise in the analog signals.
6. The accuracy of the digital and analog information was only 13 binary bits which, for the IF input signal, gives an approximate accuracy of 12 parts in 10,000.

In the actual case, the filtering in the IF line by the use of series shorted stubs would not be needed; since there would be a large amount of filtering due to high frequency attenuation in the IF input transmission line and the filtering in the IF amplifier circuitry. However, it is felt that shunt, quarter-wavelength, open stubs at the second and fourth harmonics should be added to the IF junction in addition

to the quarter-wavelength open stub at the fundamental frequency in order to maintain an effective short at this junction for these frequencies; thereby increasing the efficiency of the balanced mixer. The IF junction for the realization of the extended model is thus changed from that of Figure 9 to that of Figure 13. The junctions are analyzed in Appendix II.

Figure 14 shows a typical analog recording of the scaled local oscillator signal, the scaled sum of the local oscillator and the RF input signals referenced to their respective inputs as shown in Figure 9, the scaled, barrier capacitance voltages of diodes A and B, the scaled voltage across C_{IF} , and the scaled IF input voltage across R_{IF} . The starting transient can be noted on e_5 . Before addition of the additional filtering, the transient signals would not die out as fast or not at all. This recording demonstrates that the simulation works and that a beat signal between the local oscillator and receiver input signals is obtained at the IF input port.

The effects on the IF input signal voltage amplitude were found and are shown in Figure 15 as a function of the line lengths between the diodes and the IF terminal or between the diodes and the hybrid ring, while maintaining the other variables constant. These effects on the IF input signal were measured for the conditions given in Figure 15, where the terms are as defined in the symbol table, Appendix I. The effects of the line length between the diodes and the hybrid ring

See Figure 9 for the remainder of the extended model realization

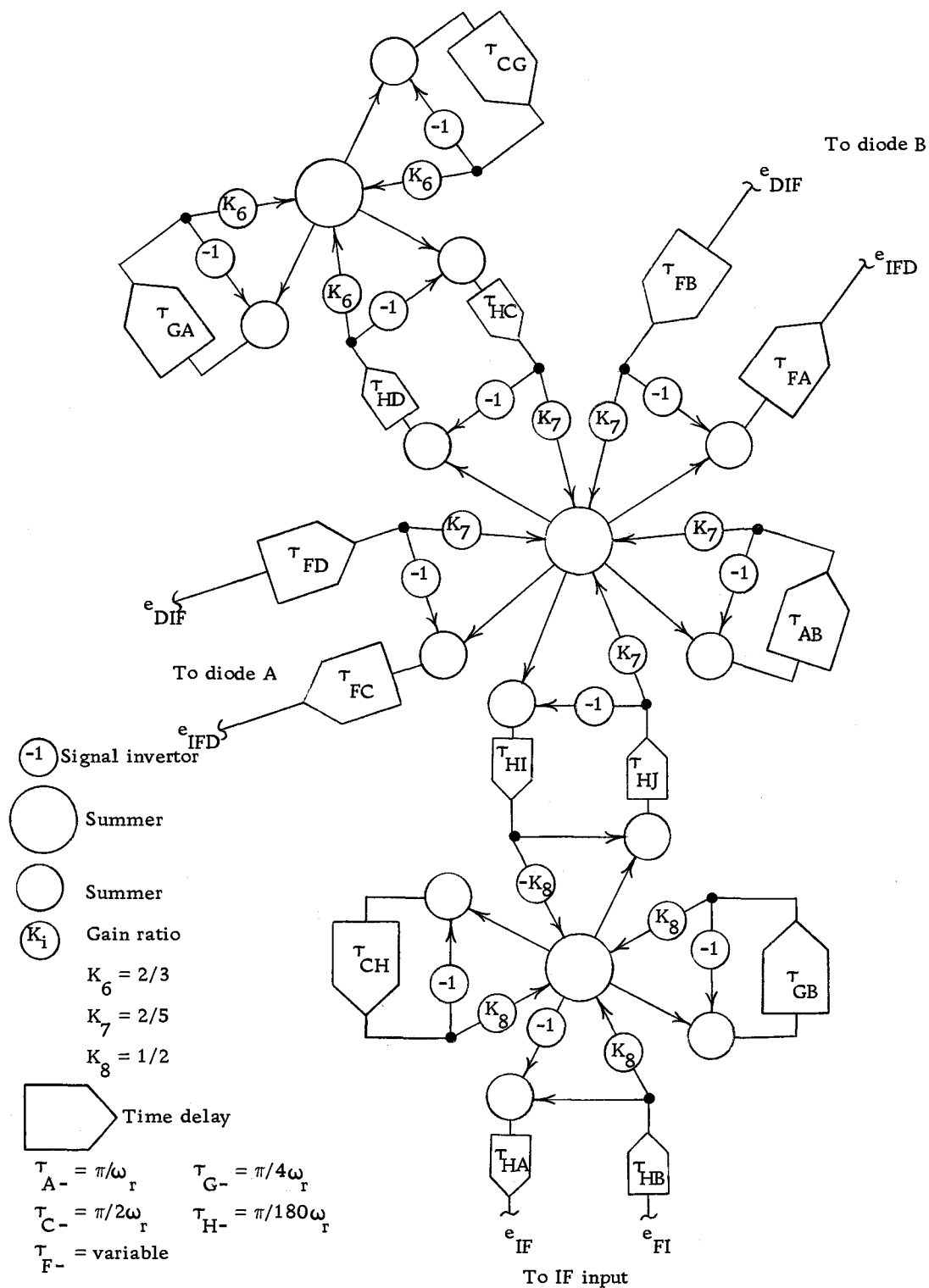


Figure 13. Revised IF junction of the realization of the hybrid-ring, balanced-mixer, extended model.

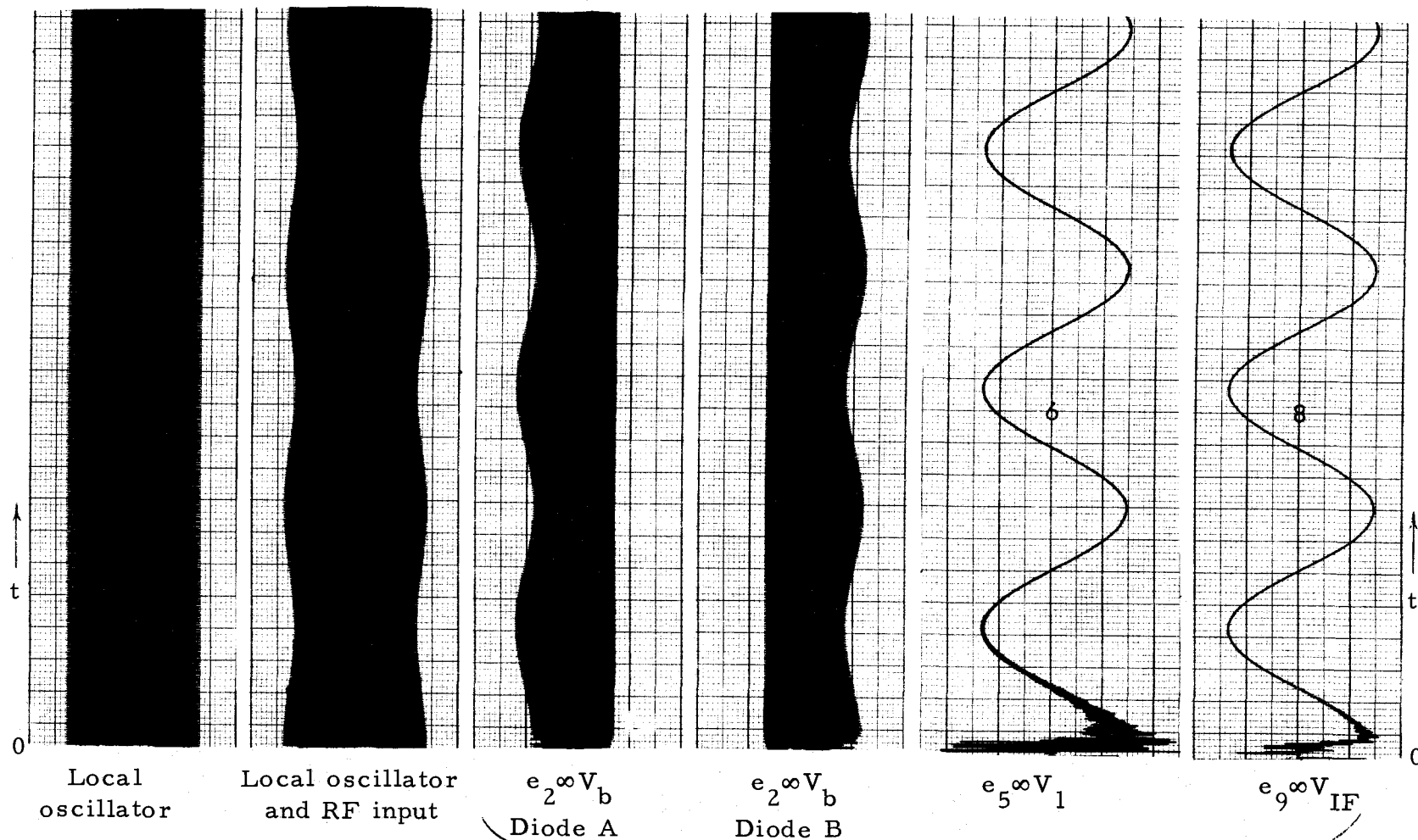
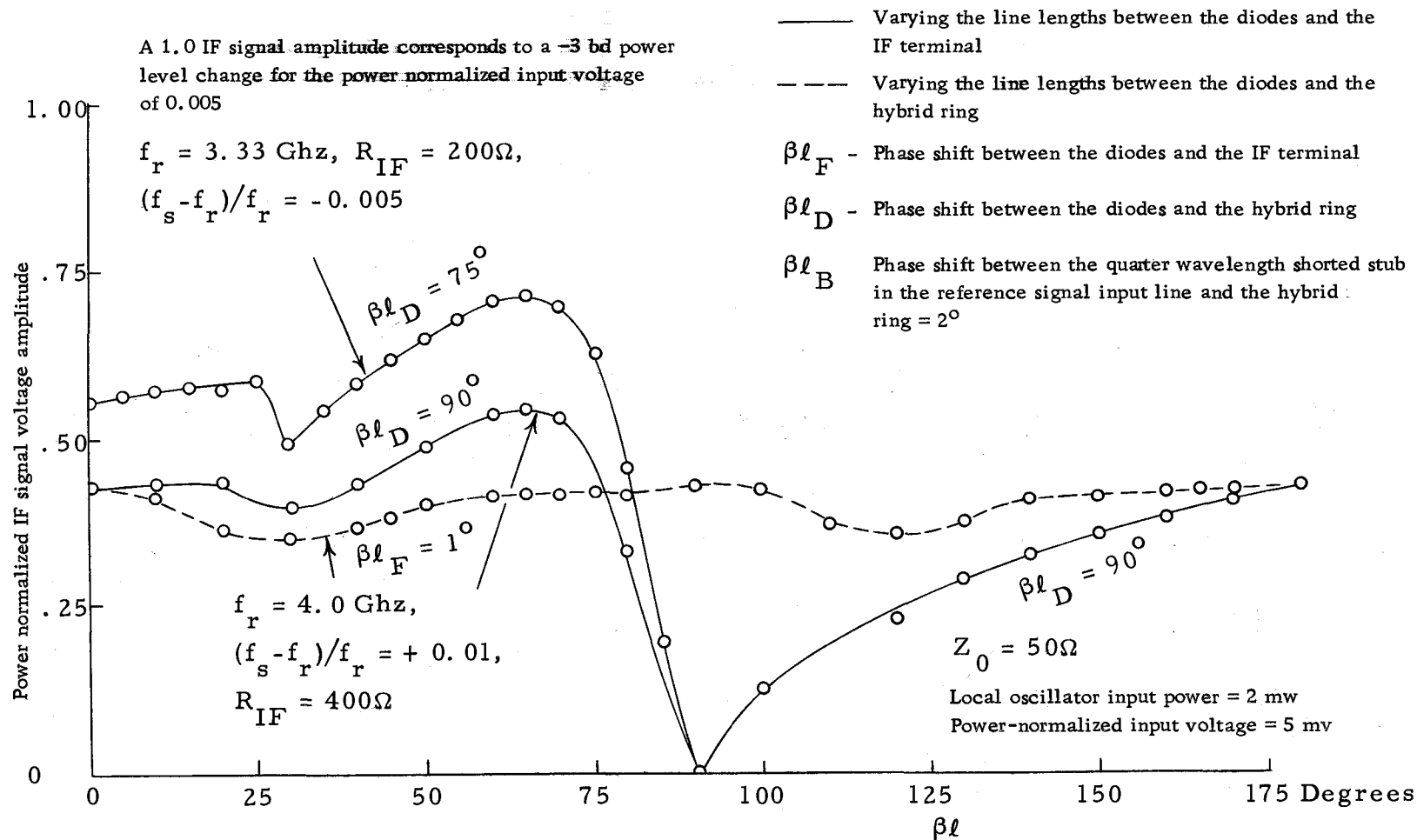


Figure 14. A typical analog recording of various scaled voltages during a simulated balanced-mixer operation.



Line lengths in degrees of phase shift at the local oscillator frequency

Figure 15. The variation of the power-normalized IF signal amplitude as a function of the line lengths between the diodes and the hybrid ring or the IF terminal.

on the IF input signal are shown in Figure 15 to be second order effects as compared to the effects of the line length between the diodes and the IF terminal. Again it should be noted that the IF input signal voltage on the analog computer is normalized in terms of power at a level of $63.3 \mu\text{w}$; so that it is independent of the characteristic impedance, Z_0 , and the IF input impedance, R_{IF} .

Juggling between the two types of measurement of the preceding paragraph for $f_r = 3.33 \text{ GHz}$, $Z_0 = 50 \Omega$, $R_{\text{IF}} = 200 \Omega$, and $\beta l_B = 2^\circ$, the proper line lengths were found that produced a compromise between maximum signal and equal, maximum signal at $(f_s - f_r)/f_r = -0.005$ and 0.005 . This gave line lengths, in units of phase shift at the local oscillator frequency, of 77° between the diodes and the hybrid ring and 63° between the diodes and the IF junction, and gave a power-normalized-average, maximum IF input signal of 0.717 on the analog computer, which is an insertion loss of 5.84 db from the power-normalized, input signal magnitude of 0.005 .

The effects for an increase in the value of the diode barrier capacitance, C_b , were measured at a fixed local oscillator frequency. These effects were found to be a decrease in the maximum, IF input signal and a change of the line lengths to and from the diodes necessary for the maximum IF input signal. An increase in the local oscillator frequency instead of an increase in the capacitance would have given the same effects.

Figure 16 gives the measured effect on the power-normalized, IF input signal as a function of the local oscillator input power. The data was taken for $R_{IF} = 400 \Omega$ and some data was taken for $R_{IF} = 200 \Omega$ with, in both cases, $Z_0 = 50 \Omega$, $f_r = 4 \text{ GHz}$, $\beta l_B = 2^\circ$, $\beta l_P = 75^\circ$, $\beta l_F = 66^\circ$, $(f_s - f_r)/f_r = 0.01$. The power-normalized, RF input signal magnitude was kept at 0.005 until it would have exceeded 0.1 (the local oscillator signal input magnitude) and then it was changed to 0.0025. The IF input signal amplitude data which was taken for the power-normalized, RF input signal magnitude of 0.0025 was multiplied by two before it was plotted in Figure 16. For $R_{IF} = 400 \Omega$, there is essentially negligible effect on the IF input signal magnitude for up to a 5 db decrease in the local oscillator signal input. However, for $R_{IF} = 200 \Omega$, a 2 db decrease gives the same effect as for $R_{IF} = 400 \Omega$ with a 5 db decrease. This will be discussed to a greater extent later in this section during consideration of the validity of the simulation.

For the line length found earlier, $f_r = 3.33 \text{ GHz}$, $(f_s - f_r)/f_r = 0.005$, and a power-normalized RF input signal magnitude of .005, the power-normalized, IF input signal magnitude was measured as a function of the IF input impedance, R_{IF} , and the characteristic impedance, Z_0 . The results are plotted in Figure 17. The results indicate that, for $Z_0 = 50$ or 55Ω and $R_{IF} = 150 \Omega$, the scaled IF input signal on the analog computer was

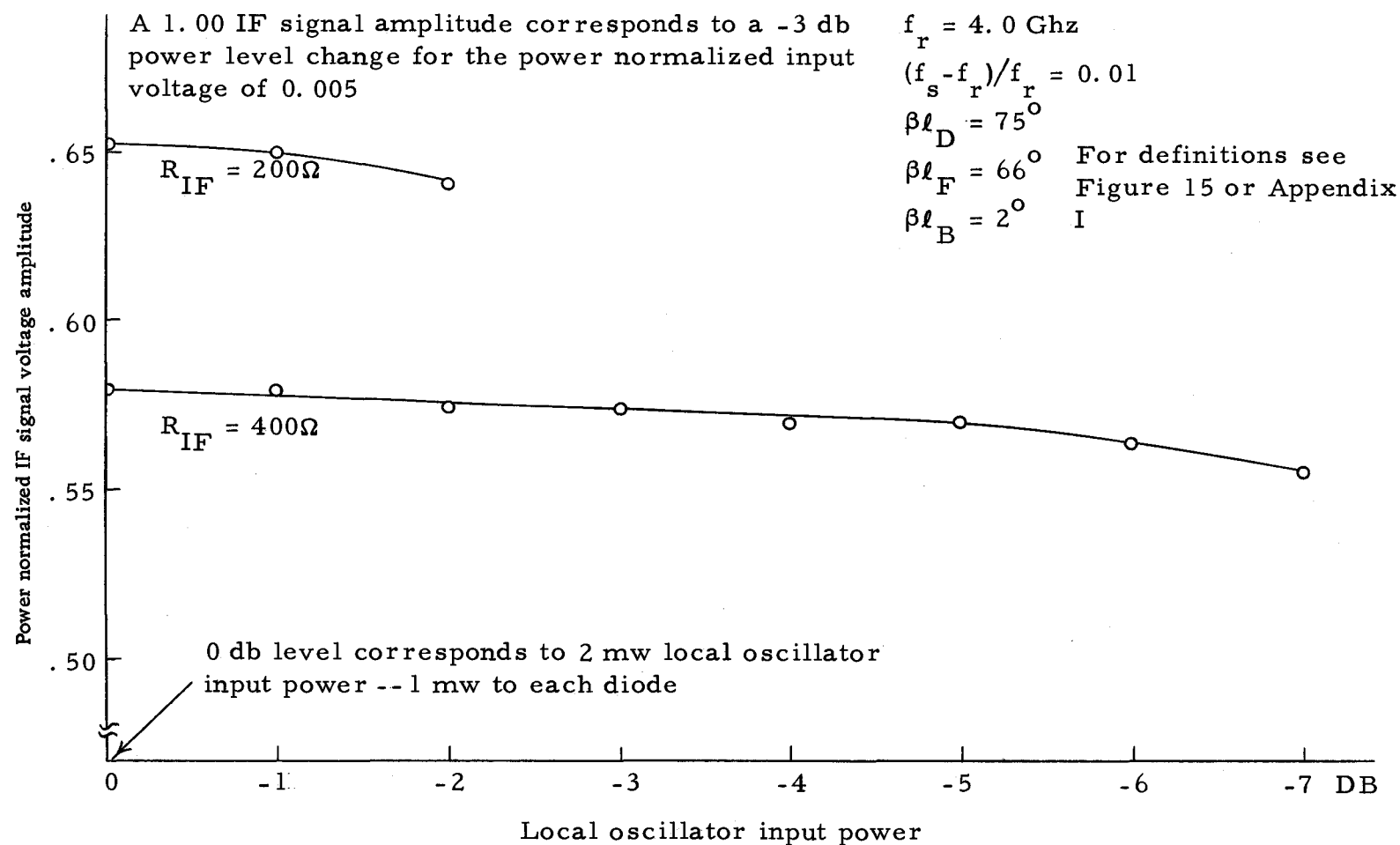


Figure 16. The variation of the power-normalized IF signal amplitude as a function of the local oscillator input power.

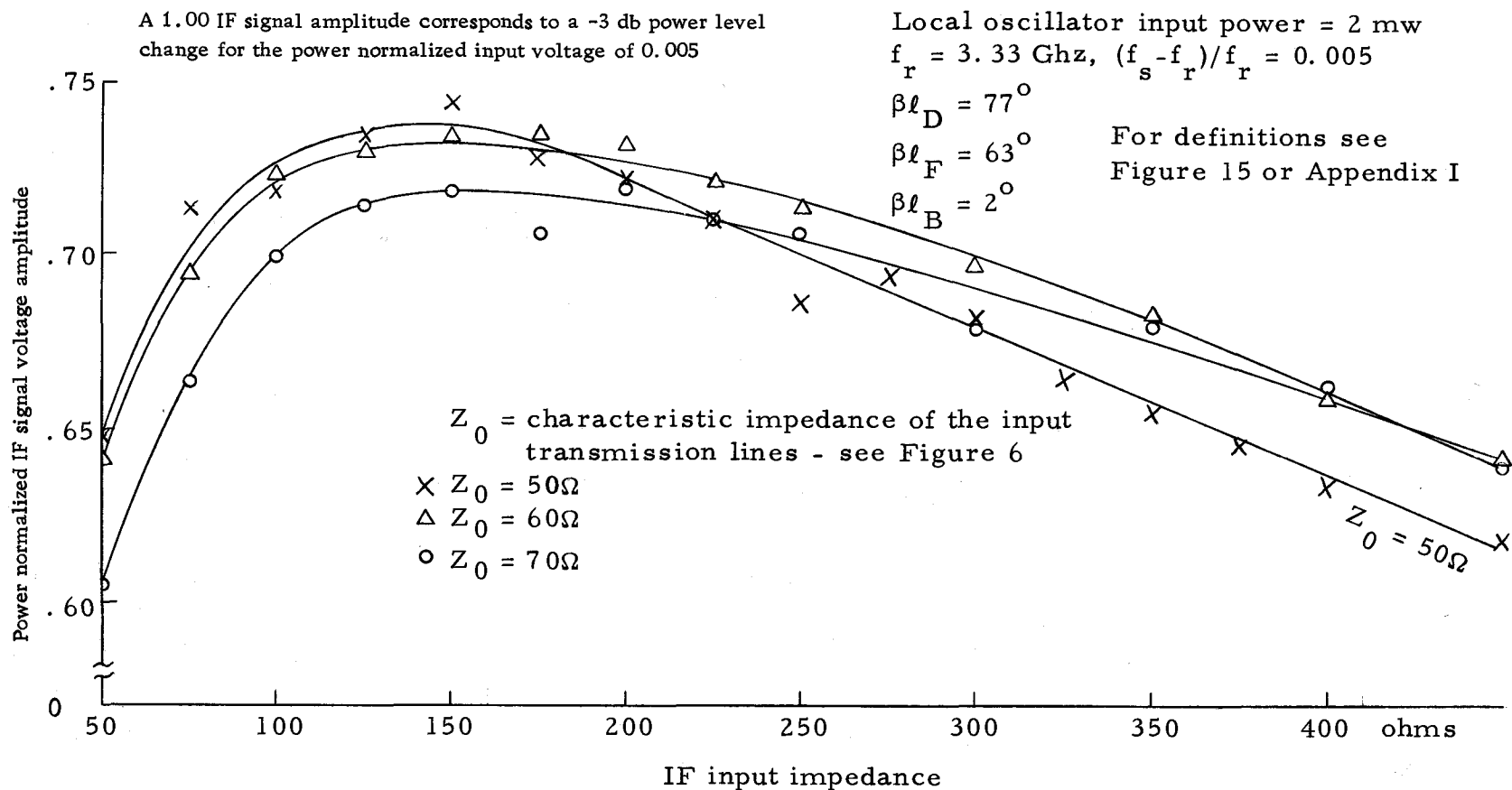


Figure 17. The variation of the power-normalized IF signal amplitude as a function of the IF input impedance and the characteristic impedance of the hybrid-ring circuit.

maximized at 0.738 which is a 5.6 db insertion loss from the RF input signal power.

The circuit for the final design for the center strip of the strip-line, hybrid-ring, balanced-mixer frequency converter is as shown in Figure 18. It uses phase shifts of 77° at the local oscillator frequency between the diodes and the hybrid ring and 63° between the diodes and the IF terminal, an assumed local oscillator input power of $2 \mu\text{w}$, a characteristic impedance of 50Ω for the transmission lines, and an assumed IF input impedance of 200Ω .

IF Signal Characteristics as a Function of the IF Frequency

Using the final design data for the strip-line, hybrid-ring balanced mixer in the extended model, the IF, power-normalized input amplitude and the phase difference between the IF input signal and the beat signal of the sum of the RF input and local oscillator signals from their respective inputs were measured as a function of $(f_s - f_r)/f_r$ from -0.125 to +0.125 in 0.005 steps. The results are shown in Figure 19. The absolute value of the slope of the measured phase difference curve of Figure 19 is plotted in Figure 20. The latter gives an indication of the linearity of the phase difference curves, which will be discussed in the next section.

Also, for slightly different lengths to and from the diodes than for the final design, phase difference measurements were made with

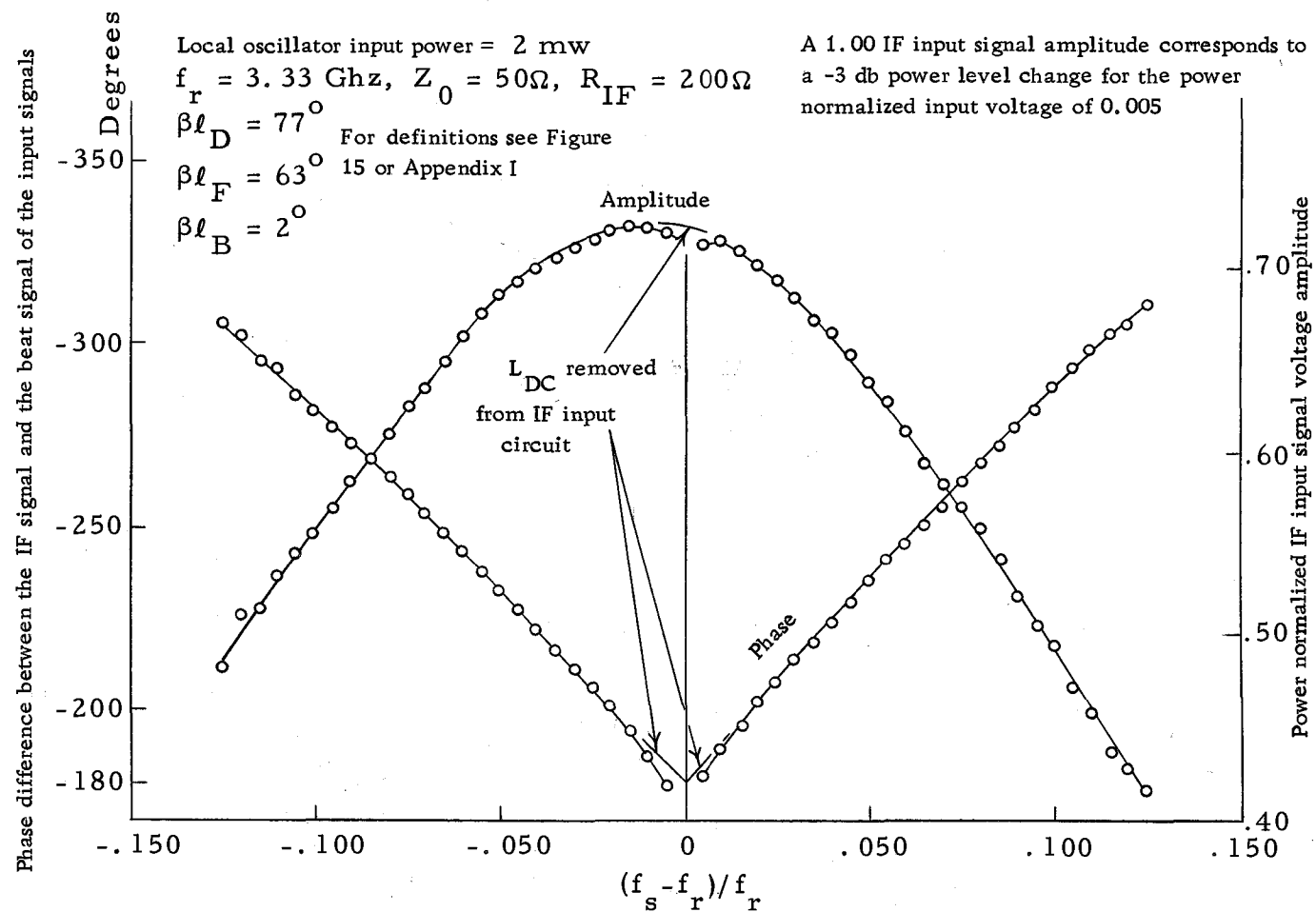


Figure 19. The phase difference between the IF signal and the beat signal of the input signals and the IF signal amplitude as a function of the normalized frequency difference between the input signals.

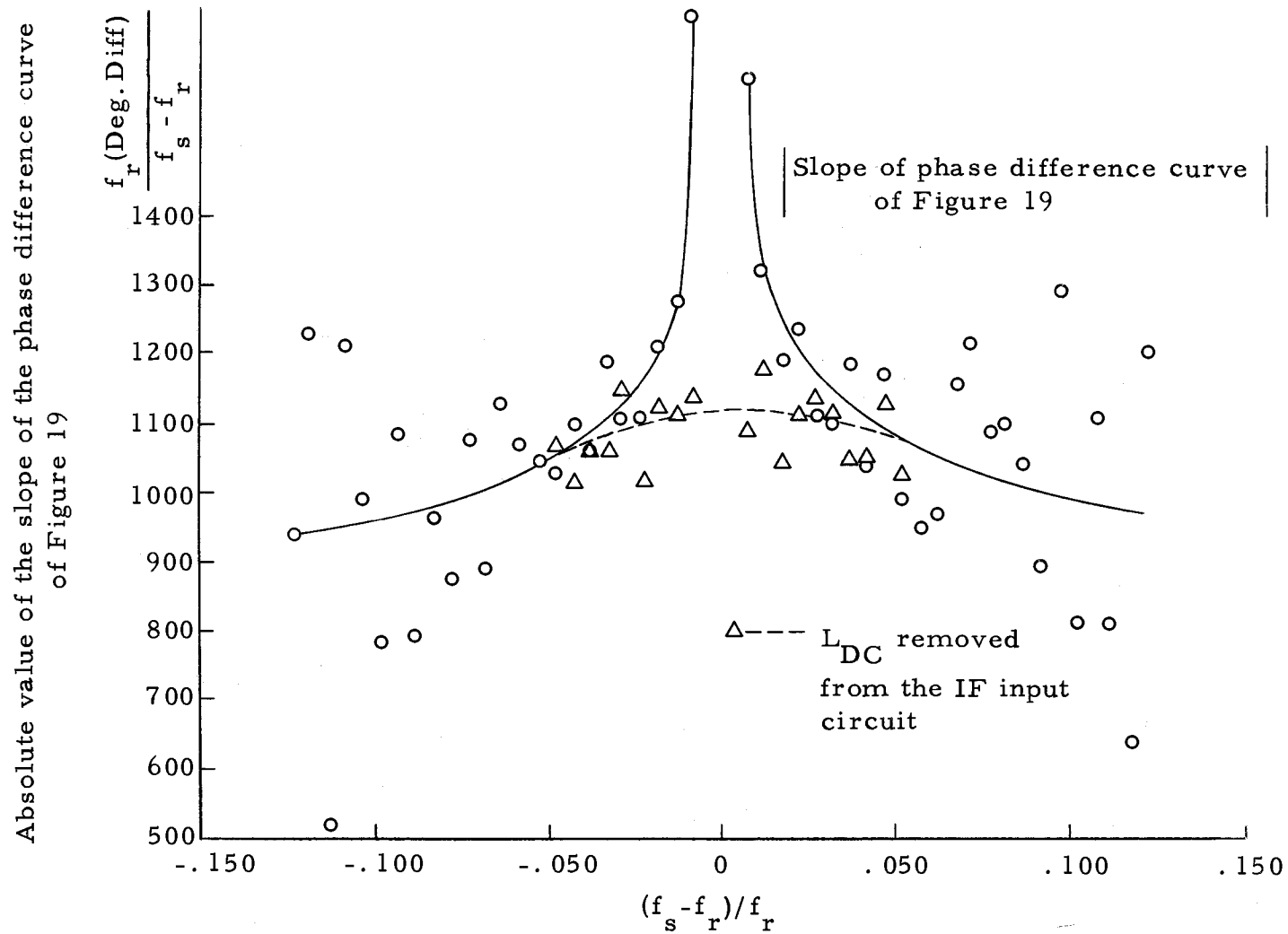


Figure 20. The absolute value of the slope of the phase difference curve of Figure 19 as a function of the normalized frequency difference between the input signals.

no delay in either input line, an additional phase delay of $1,108^\circ$ at the local oscillator frequency in the RF input line, and then with a phase delay of $1,157^\circ$ in the local oscillator input line. These results are plotted in Figure 21 for $(f_s - f_r)/f_r = -0.100$ to 0.100 and will be discussed below.

Validity of the Simulation

In the simulation results, it was indicated by Figure 13 that the IF input impedance for the minimum insertion loss of 5.6 db was 150 ohms. However, the typical measured insertion loss for a balanced mixer is about 6 db and the measured IF impedance is in the range of 300 to 700 ohms (6, 9). These typical measured characteristics are for mixer diodes similar to the 1N831A and for a local oscillator signal power input to the balanced mixer of 1 mw (6, 9). The optimum IF impedance is a decreasing function of the local oscillator power, is a definite function of the RF tuning circuits used, and, by the RF tuning circuits, can be varied over a range greater than 2.5 to 1 (10). Thus, the values found for the IF input impedance and the insertion loss are not unreasonable.

Also in Figure 16, the fact that the IF input impedance for maximum power transfer is a decreasing function with an increase in local oscillator input power would explain the flatness of the curve for 400 ohm, IF input impedance case, and why the IF input signal for the

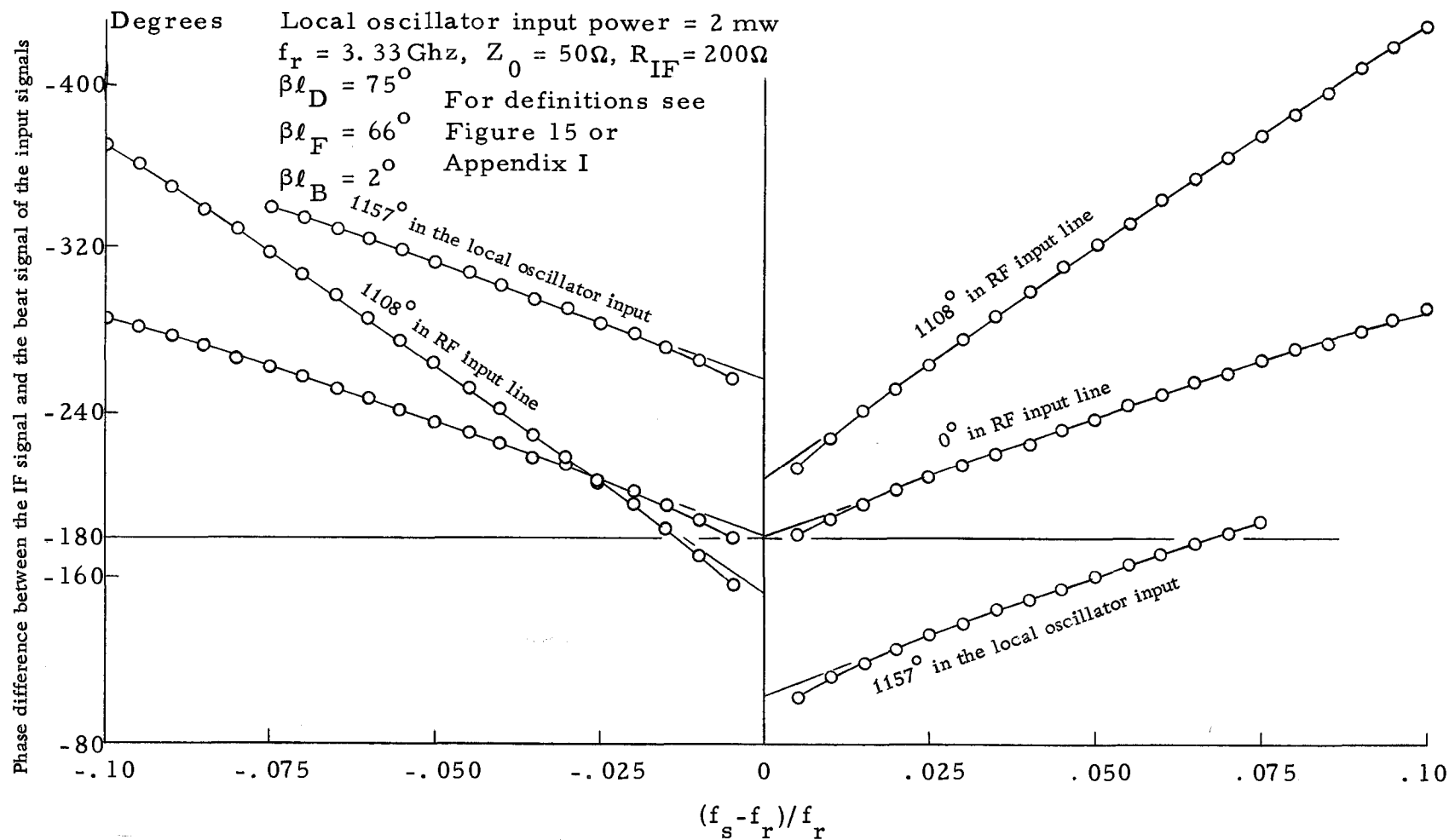


Figure 21. Phase difference between the IF signal and the beat signal of the input signals as a function of the normalized frequency difference between the input signals for various delays in the input lines.

200 ohm IF input impedance case decreases much faster with a decrease in the local oscillator input power. That is, as the local oscillator input power decreases, the IF input impedance for maximum power transfer increases, thus passing the 200 ohm value quickly and approaching or passing the 400 ohm value. Therefore, if the IF input impedance were maintained always at the condition for maximum power transfer, the conversion efficiency would decrease with the local oscillator power faster than the curve for the IF impedance of 400 ohms, but slower than the curve for the 200 ohm case.

For a CW, RF input signal of amplitude B_0 , the IF input voltage given by Equation (3-6) reduces to,

$$V_{IF_i} = \frac{\sqrt{2}}{\pi} B_0 \cos((\omega_s - \omega_0)t + \alpha_{s0} - \alpha_{r0}) \quad (7-3)$$

where the terms are defined in the symbol table, Appendix I. For Equation (3-6), α_{s0} had been assumed linear in ω_s . Therefore, for $\omega_s > \omega_0$, the phase of the IF input signal is $\alpha_{s0} - \alpha_{r0}$, and, for $\omega_s < \omega_0$, it is $\alpha_{r0} - \alpha_{s0}$.

Now in Figures 19 and 21 the linear extrapolations to the $(f_s - f_r)/f_r = 0$ axis give -180° for the phase-difference curves for no phase delay in the input lines. Thus, from Equation (7-3), a length of line causing an $1,108^\circ$ phase delay at the local oscillator frequency added to the RF input line should give an extrapolated intersection on

the zero axis of -208° phase difference when coming from the positive side for $(f_s - f_r)/f_r$ and $-152^\circ (+ 208^\circ)$ for the negative side (see Appendix IV, Interpretation of the IF Input Signal Phase). Also, an $1,157^\circ$ phase delay at the local oscillator frequency added to the local oscillator line should give intersections on the zero axis of -103° for the positive side and $-257^\circ (+ 103^\circ)$ for the negative side according to Equation (7-3). This is exactly what is found in Figure 21 for the measured data. Moreover, for the case for $1,108^\circ$ phase delay in the RF input line, the absolute value of the slope of the phase difference curve should be increased by $1,108^\circ$ over the case for no phase delay in either of the input lines; while no change in slope should be found for the case for $1,157^\circ$ phase delay in the local oscillator line since $\omega_r = \omega_0$ is constant in Equation (7-3). This is also found to be true.

The absolute value of the slope of the phase difference curves in Figures 19 and 21 is around $1,100^\circ$ which would indicate approximately a $1,100^\circ$ phase delay for the RF input signal. However, this phase difference is not only due to the RF input signal, but also due to a phase shift delay at the IF frequency caused by the circuitry. Since the actual RF input signal path averages around 260° , most of the phase change in the phase difference curves is due to the phase shift in the circuitry at the IF frequency.

The phase difference curves in Figures 19 and 21 do not follow a straight line as they approach the $(f_s - f_r)/f_r = 0$ axis due to the IF

input circuitry not giving a pure resistive IF input impedance for low IF frequencies. Likewise, due to the IF input circuitry not giving a pure resistive IF input impedance for high IF frequencies and the non-linear coupling characteristics of the hybrid ring for RF frequencies far from the design frequency, the curves do not follow a straight line for large values of $|f_s - f_r|/f_r$.

The amplitude and phase characteristics shown for the simulated model of the hybrid-ring, balanced-mixer frequency converter for different IF input impedances, characteristic impedances, local oscillator input power and for different delays in the input lines do verify the validity of the simulation and the simulated extended model.

VIII. CALCULATION OF THE BANDWIDTH LIMITATIONS FROM THE SIMULATION RESULTS FOR THE EXTENDED, BALANCED-MIXER MODEL

Using the simulation results, this section will consider the useable operation bandwidth range of the processing system of Figure 5 for a CW input signal, and the bandwidth limitation which is required to meet amplitude and phase requirements for a pulsed input signal. It will not consider the bandwidth limitations on information signals, because the amplitude and phase requirements and the bandwidth limitations on information signals were given in section VI. A mathematical method of obtaining the phase error at the IF input for a pulsed, input signal from the IF input signal characteristics of the balanced mixer as a function of the IF frequency will be given. The bandwidth limitations will be determined first for the processing system which uses a CW local oscillator signal. Then from the simulation results for the balanced mixer with a CW local oscillator some conclusions will be made about the bandwidth for the processing system which uses a pulsed, local oscillator signal.

CW Local Oscillator System

For CW received and CW local oscillator input signals, the IF signal amplitude and phase characteristics of the simulated, hybrid-ring, balanced mixer are shown in Figure 19 for the final design of

the simulated mixer as shown in Figure 18. These characteristics show that, for a CW input signal, any desired IF frequency can be used under the penalty of greater insertion loss. For at most a 2 db increase in the insertion loss from the minimum insertion loss between the received input signal and the IF input signal, the bandwidth limitations on $(f_s - f_r)$ is approximately 17%.

For a pulsed, received input signal and a CW, local oscillator input signal to the balanced mixer, the IF input signal is a sum of the individual frequency components as given by

$$V_{IF_i} = \sum_{m=-q}^{m=q} B_m K_m \cos((\omega_s + m\omega_2 - \omega_r)t + \gamma_{sm} - \gamma_{r0}), \quad (8-1)$$

where the received input signal is given by Equation (3-2), γ_{sm} is α_{sm} (the received signal phase at the input to the balanced mixer for the $(f_s + mf_2)$ frequency component) plus the additional phase shift due the balanced-mixer circuit, γ_{r0} is α_{r0} (the local oscillator signal phase at the input) plus the additional phase shift due to the balanced-mixer circuit, and K_m is the effective amplitude reduction term for the IF input signal from the received input signal at the input signal frequency of $(f_s + mf_2)$. K_m can be found from the amplitude curve in Figure 19, while $\gamma_{sm} - \gamma_{r0}$ can be found directly from the phase difference curve of that figure.

Let f_{IF} , the IF frequency, be as defined in Equation (7-2),
the IF input signal phase be denoted by

$$a_{IF} = \gamma_{s0} - \gamma_{r0}$$

and let the following definitions be made:

$$K_m = C_0 D_m = C_0 (D_{ms} + D_{ma})$$

$$\gamma_{sm} - \gamma_{s0} = a_{IF_m} = \gamma_{mL} + \gamma_{mnL},$$

where

C_0 = constant such that D_m can be taken directly from the IF
input signal amplitude curve of Figure 19.

D_{ms} = the symmetrical part of D_m with m around the frequency
($f_s - f_r$)

D_{ma} = the antisymmetrical part of D_m with m around the fre-
quency ($f_s - f_r$)

γ_{mL} = the linear part of a_{IF_m} for variations of m or frequency
around the frequency ($f_s - f_r$)

γ_{mnL} = the nonlinear part of a_{IF_m} for variations of m or frequency
around the frequency ($f_s - f_r$)

With these definitions, Equation (8-1) becomes, upon separating
it in terms of the IF frequency,

$$V_{IF_i} = C_0 \cos(\omega_{IF} t + a_{IF}) \sum_{m=-q}^{m=q} B_m D_m \cos(m\omega_2 t + a_{IF_m})$$

$$- C_0 \sin(\omega_{IF} t + a_{IF}) \sum_{m=-q}^{m=q} B_m D_m \sin(m\omega_2 t + a_{IF_m})$$

Since B_m is essentially symmetrical in m around $f = f_s$ in normal applications and where γ_{mnL} is small, removal of some zero-sum terms, gives the simplified, IF input voltage for a pulsed, received input signal: (2, 8)

$$\frac{V_{IF_i}}{C_0} \approx \cos(\omega_{IF} t + a_{IF}) \sum_{m=-q}^{m=q} B_m (D_{ms} \cos \beta_m(t) - D_m \gamma_{mnL} \sin \beta_m(t))$$

$$- \sin(\omega_{IF} t + a_{IF}) \sum_{m=-q}^{m=q} B_m (D_{ma} \sin \beta_m(t) + D_m \gamma_{mnL} \cos \beta_m(t))$$

where

$$\beta_m(t) = m\omega_2 t + \gamma_{mL}.$$

The term

$$\sum_{m=-q}^{m=q} B_m D_m \gamma_{mnL} \sin \beta_m(t) = C_m(t)$$

is small compared to the other term multiplying $\cos(\omega_{IF} t + a_{IF})$ in

the input signal. This is true because γ_{mnL} is small and only the antisymmetrical part of $D_m \gamma_{mnL}$ will increase the sum. Therefore $C_m(t)$ will be neglected.

Let the IF input voltage be defined by

$$V_{IF_i} = G(t) \cos(\omega_{IF} t + a_{IF} + a_e(t)), \quad (8-2)$$

where $a_e(t)$ is the phase angle error for the pulse signal and $G(t)$ is the pulse envelope amplitude. Then, assuming $a_e(t)$ to be small, the phase angle error is given inside the pulse envelope by

$$a_e(t) \approx \frac{\sum_{m=-q}^{m=q} B_m (D_{ma} \sin \beta_m(t) + D_m \gamma_{mnL} \cos \beta_m(t))}{\sum_{m=-q}^{m=q} B_m D_{ms} \cos \beta_m(t)} \quad (8-3)$$

and the pulse envelope amplitude by

$$G(t) \approx C_0 \sum_{m=-q}^{m=q} B_m D_{ms} \cos \beta_m(t) \quad (8-4)$$

The error angle, $a_e(t)$, is a function of time. Some of its properties are: when γ_{mnL} is small or antisymmetrical around the IF carrier frequency and D_{ma} is nonzero, the first term in the numerator of Equation (8-3) predominates; when $D_{ma} \approx 0$, the

second term predominates.

The nonlinear portion of the IF signal, phase difference curve as taken from the data of Figures 19 and 20 is plotted in Figure 22 versus $(f-f_r)/f_r$, the normalized frequency difference between the input signals. γ_{mnL} can be found from this curve. The magnitude of the phase change of $a_e(t)$ for variation between different, IF input, pulse amplitude points for a typical, received, input pulse envelope like that of Figure 4 is plotted in Figures 23 and 24 versus $(f-f_r)/f_r$ for different values of $|f_s - f_c|/f_r$. f_c is the frequency which is at the center of the IF signal amplitude distribution of Figure 19. The variation of the pulse position is approximately between the 0.15 points of the maximum pulse amplitude for Figure 23 and between the 0.33 points for Figure 24. The endpoints of the pulse position are given by $\beta_m(t) = \pm \pi$ for Figure 23 and by $\beta_m(t) = \pm 3\pi/4$ for Figure 24. The results will be discussed later in this section.

Since the nonlinearity in the IF input signal phase near $f-f_r = 0$ is due to the IF input circuit of Figure 10c, the removal of the inductance, L_{DC} , should reduce this nonlinearity substantially, while not having much other effect except producing a d. c. voltage across the IF input resistance, R_{IF} . Data was taken for L_{DC} removed and the effects that were found are shown in Figures 19, 20, 22, 23 and 24. The data indicates that indeed the removal of L_{DC} does greatly reduce the nonlinearity of the IF input signal phase near

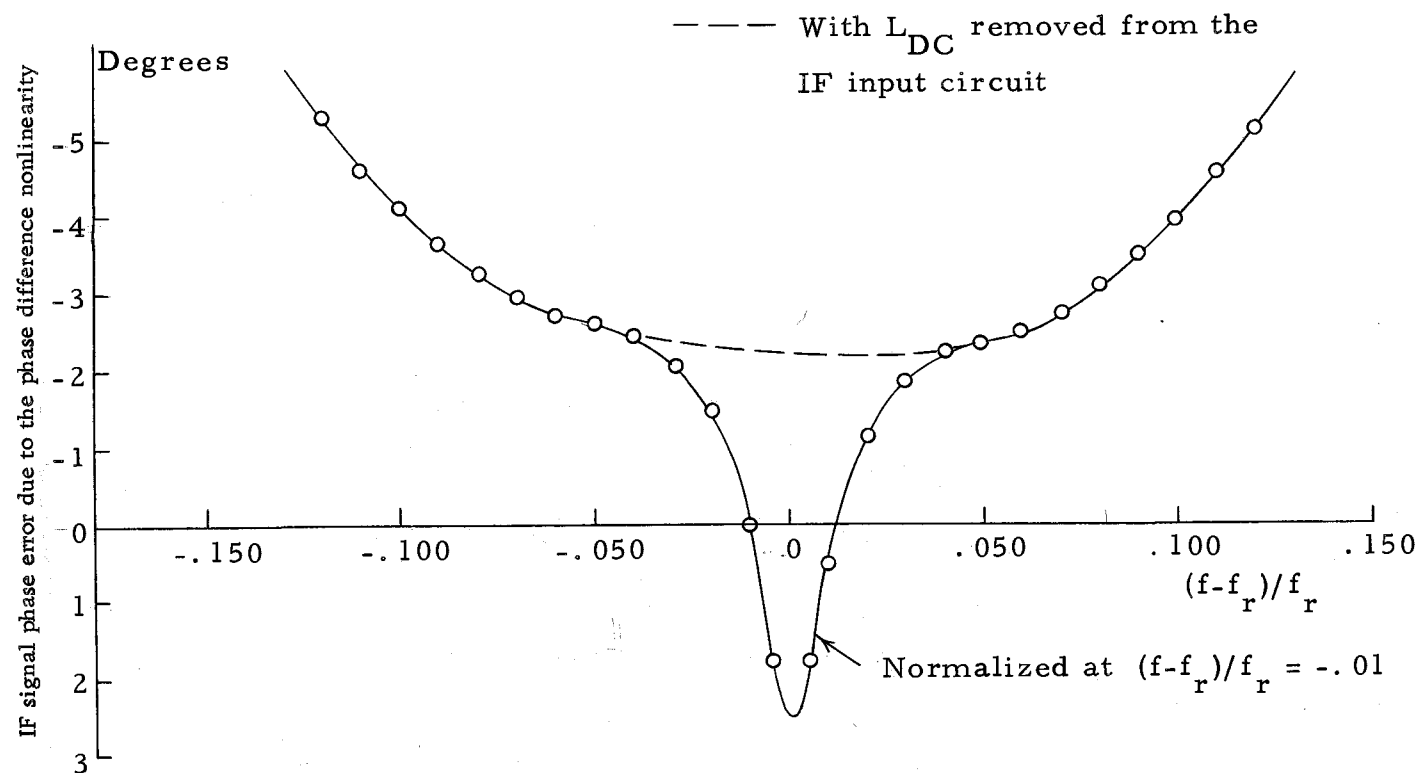


Figure 22. Nonlinear portion of the phase difference curve of Figure 19 as taken from Figure 20 as a function of the normalized frequency difference between the input signals.

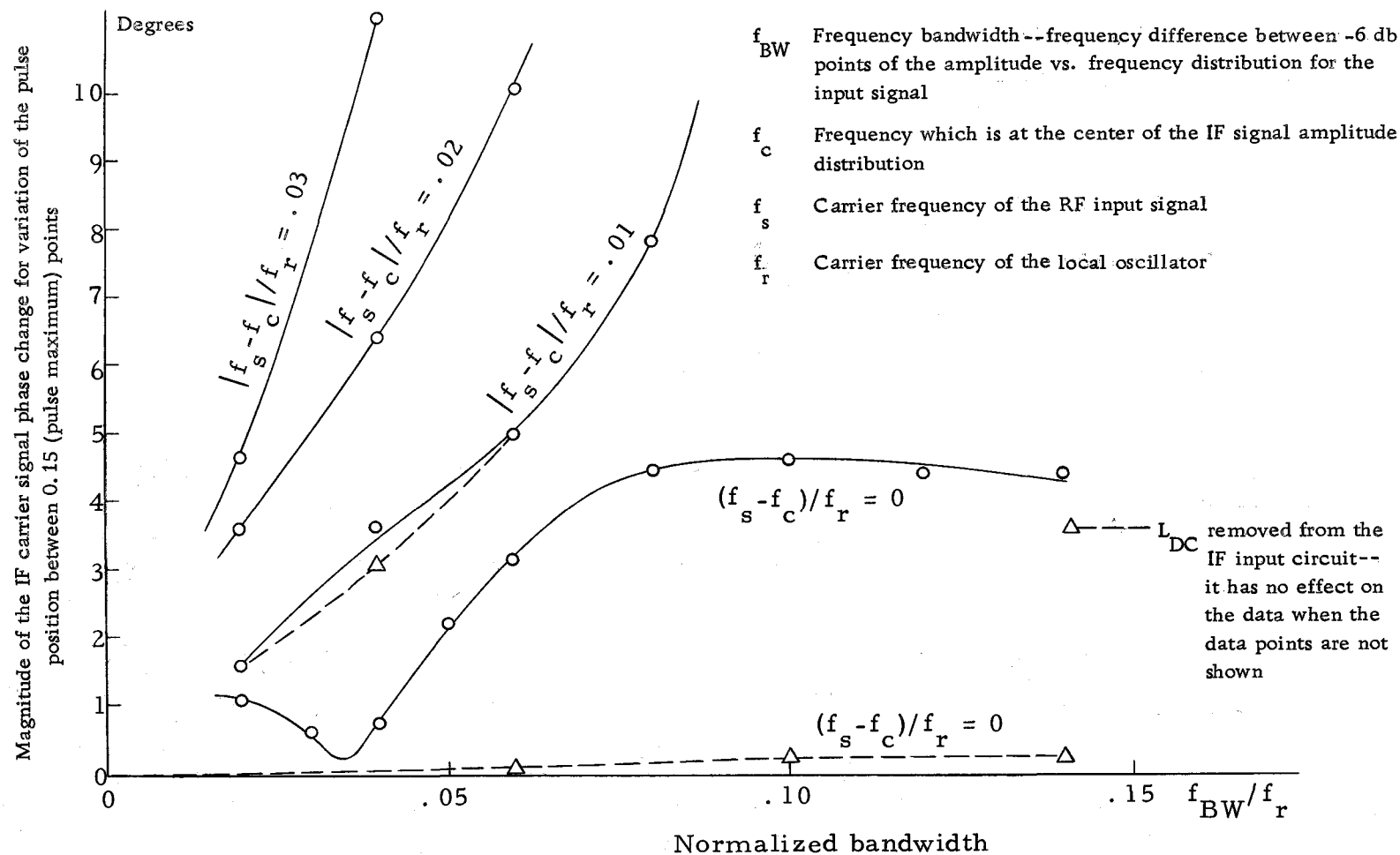


Figure 23. The magnitude of the IF carrier signal phase change for variation of the pulse position between 0.15 (pulse maximum) points versus the normalized bandwidth for various values of the normalized frequency difference between the input signal carrier frequency and the center frequency of the IF input signal amplitude distribution.

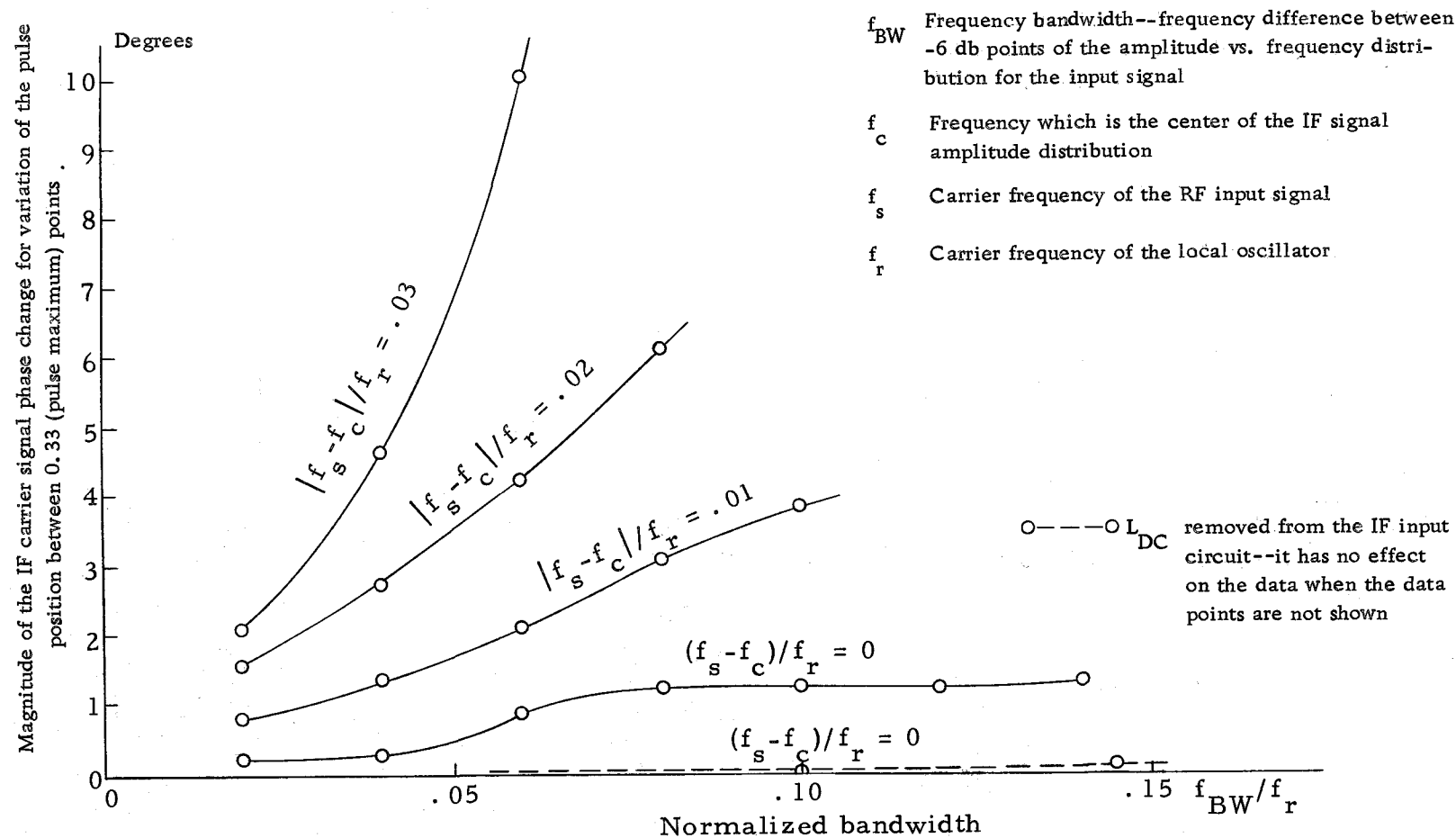


Figure 24. The magnitude of the IF carrier signal phase change for variation of the pulse position between 0.33 (pulse maximum) points versus the normalized bandwidth for various values of the normalized frequency difference between the input signal carrier frequency and the center frequency of the IF input signal amplitude distribution.

$$f - f_r = 0.$$

With L_{DC} removed from the IF input circuit, Figures 23 and 24 indicate that it is possible to maintain the phase error requirements as given in section VI of 1.125° in tracking radar applications for a large input signal bandwidth. This is true only when the IF carrier frequency is very close to the center frequency of the IF signal amplitude distribution. Also, they indicate that the phase error requirement of 11.25° in normal applications would be much easier to maintain for a large input signal bandwidth so far as the restrictions to the closeness of the IF carrier signal frequency to the center frequency of the IF signal amplitude distribution is concerned. However, the data of Figure 19 indicates that the center frequency of the IF signal amplitude distribution, f_c , gives a value for $(f - f_r)/f_r$ of 0.01. Hence, the design of the hybrid-ring balanced mixer of Figure 18 with L_{DC} removed from the IF input circuit would require, for a broadband input signal, a wideband IF. The wideband IF would have to have a passband that extended from the bandwidth of the input signal to d.c. This is not too practical since it includes the very low frequencies. Also, for large bandwidths, the IF signal amplitude distribution of Figure 19 indicates that the pulse width of the pulse would be increased. For instance, for a bandwidth of nine percent, the effective pulse width is increased by five percent.

Two different requirements on the IF circuit and the RF input

signal which will individually result in the meeting of the phase error tolerance of 1.125° for the processing system of Figure 5 are:

1. An IF with a passband from the input signal bandwidth to d. c. which would allow input signal bandwidths of up to nine percent of the local oscillator frequency without increasing the pulsewidth by more than five percent.
2. A more practical IF with a passband that does not extend down to d. c. in which case input signal bandwidths of up to two percent would be allowed.

In either case, a tolerance would need to be placed on $|f_s - f_c|/f_r$ as indicated by Figures 23 and 24.

To maintain a tolerance value for $|f_s - f_c|/f_r$ and therefore the IF phase error requirement, the center frequency, f_c , of the IF, input signal, amplitude distribution should be found by measurement; and, if the input carrier signal frequency, f_s , will always be known, $(f_s - f_r)$ should be set accordingly. If the input carrier frequency is not always known, the local oscillator frequency, f_r , should be adjustable in the processing system so that $(f_s - f_r)$ is always a constant frequency.

The RF input signal bandwidth which meets the phase error tolerance is small for a practical IF which does not have a passband extending down to d. c. The bandwidth is small since the IF signal amplitude distribution of Figure 19 is not centered further away from the

$(f_s - f_r) = 0$ axis. Therefore, in an attempt to move the center frequency of the IF input signal amplitude distribution, it was decided to take data for the balanced mixer when the design frequency of the hybrid ring and of the line lengths to and from the diodes was not the local oscillator frequency. In this new data, if the predominating factor is the frequency dependence of the balanced mixer, the center frequency of the IF signal amplitude distribution should shift with the design frequency. If the predominating factor is the circuitry of the balanced mixer at the IF frequency, the center frequency will hardly shift.

A comparison of the simulation results for the IF signal amplitude versus $(f - f_r)/f_r$, when the design frequency of the hybrid ring and the line lengths to and from the diodes is respectively f_r , the local oscillator frequency, and $1.071 f_r$, is given in Figure 25. It shows that the circuitry of the balanced mixer at the IF frequency is the predominant factor, while some effect of the design frequency is noticeable. This result is somewhat surprising in that most theoretical literature indicates that the line lengths and the terminations at the signal and image frequencies, $f_s = f_r \pm f_{IF}$, and $f_i = f_r \mp f_{IF}$ respectively, have the largest effect on the insertion loss for a constant IF input impedance (6, 10). From these results, it is apparent that the most important design improvement that could be made to the balanced mixer is to reduce the effects of the mixer circuitry at the

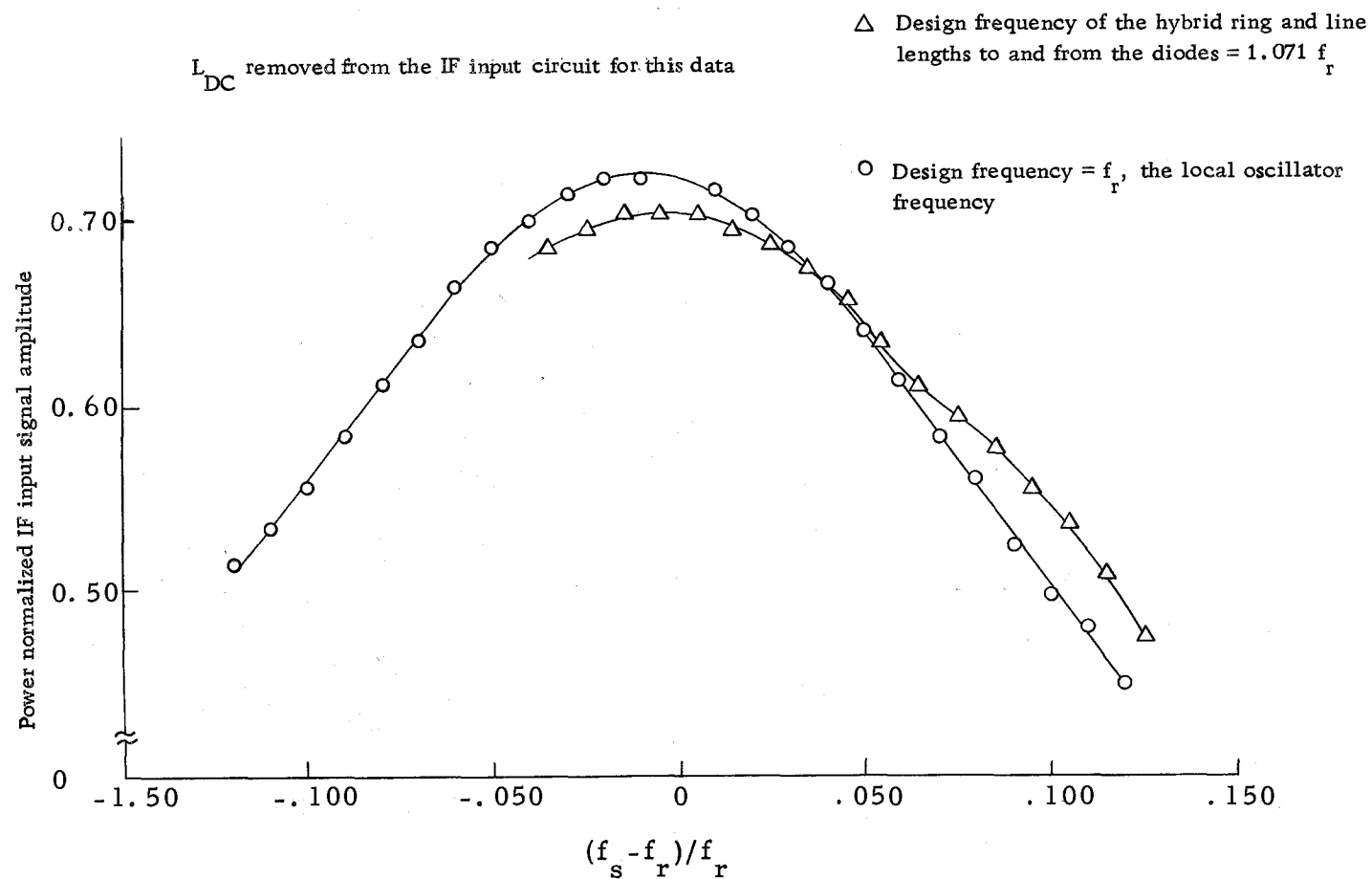


Figure 25. Comparison of the power-normalized IF input signal amplitude as a function of the normalized frequency difference between the input signals for different design frequencies.

IF frequency.

Pulsed Local Oscillator System

For the processing system of Figure 5 with a pulsed local oscillator signal, the carrier frequency for the CW, received input signal is required to be identical to the local oscillator carrier frequency.

Although no data was taken for the simulation of the hybrid-ring balanced mixer with a pulsed local oscillator signal, some bandwidth conclusions can be drawn from the simulation results with a CW local oscillator signal. For the pulsed-local-oscillator signal processing system of Figure 5,, the IF signal frequency is the pulse repetition frequency; thus the mixer circuitry at the IF frequency has a constant effect. However, for the CW-local-oscillator processing system, the IF frequency for each frequency component of the input pulse is different; thus there are different effects for the different components caused by the circuitry. In general the effect of the circuitry is to increase the phase delay and to reduce the amplitude of the IF input signal for an increase in the IF frequency. The magnitude of the phase error as a function of the bandwidth in Figures 23 and 24 is actually worse than it would be for the pulsed-local-oscillator signal processing system. This is true because the effects of the IF input signal phase characteristics had essentially very little effect on the phase error versus bandwidth curve for L_{DC} removed from the IF input

circuit and because the IF input signal amplitude decreases as the IF frequency increases. Also, Figure 25 indicates that the center frequency of the IF input signal amplitude distribution will shift somewhat when the design frequency of the hybrid ring and the line lengths to and from the diodes is shifted away from the local oscillator frequency. Therefore, it should be possible to shift the amplitude distribution so that it is centered around $f - f_r = 0$.

Then Figures 19-25 should give some idea of the bandwidth limitations for the pulsed-local-oscillator processing system. Now the points in the amplitude distribution of Figure 19 at which the input signal pulsewidth is increased by five percent at the IF input gives a bandwidth at the -6 db points for the pulsed signal of $0.09f_r$. For this bandwidth, Figure 24 indicates that, between the 0.33 points of the input pulse, the carrier frequency of the received and the local oscillator signals should be kept within $0.003f_r$ of the frequency for the center of the IF signal amplitude distribution in order to maintain a maximum phase error of 1.125° in tracking radar applications and $0.025f_r$ in order to a maximum phase error of 11.25° for normal communication applications.

In order to maintain this accuracy in $(f_s - f_c)$, the hybrid-ring balanced mixer should be tested with a pulsed, local oscillator signal and a CW input signal of different frequencies to find the IF input signal amplitude distribution versus $(f_s - f_r)$. Upon finding the center

frequency for this amplitude distribution, the local oscillator and input signal carrier frequencies should be adjusted so that the amplitude distribution is centered around $(f_s - f_r) = 0$.

IX. ACCURACY AND LIMITATIONS OF THE SIMPLIFIED, BALANCED-MIXER MODEL

This section will discuss the accuracy and limitations for use of the simplified, balanced-mixer model as indicated by the simulation results for the extended model.

Let us look at the simulation results given in Figures 15, 16, 17 and 19 for the extended, balanced-mixer model as compared to those predicted for the analysis of the simplified model. In Figure 19, it is shown that the IF, input signal amplitude generally decreases as the absolute frequency difference between the local oscillator frequency and the received input frequency increases; however with $q = 0$, Equation (3-6) for the IF input signal shows the amplitude to be constant. Also in Figure 19 with $L_{DC} = 0$, the phase difference varies slightly nonlinearly with the difference frequency while Equation (3-6) with $q=0$ predicts a linear variation. Moreover the analysis for the simplified, balanced-mixer model does not predict the proper amplitude for the IF input amplitude-distribution of Figure 19. This can be explained by the facts that, for the simplified model, the line lengths to and from the diodes were assumed to have negligible effect and the diodes were assumed to be ideal half-wave rectifiers. From Figure 15, it can be seen that the line lengths do have considerable effect on the IF input signal amplitude. The voltage across the barrier capacitance as shown in Figure 14 and the

variation of the IF input signal amplitude with the local oscillator input power as shown in Figure 16 indicate that the diodes are not ideal rectifiers. Moreover for the simplified model, the IF input impedance and the characteristic impedance were found to have no effect on the IF input signal amplitude; however Figure 17 shows that they do have an effect.

In the simulation, the phase dependent term $\cos[(\omega_s - \omega_0)t + \gamma]$ in Equation (3-6) was found to be accurately represented. Therefore, except for the IF input signal amplitude, a representative analysis of the balanced mixer can be made using the simplified model.

From the bandwidth limitations, which were found in the preceding section from the simulation results, it can be seen that, for a pulsed input signal, a representative analysis can be made from the simplified, balanced-mixer model for only a narrow bandwidth. Restrictions must be placed on the frequency difference between the local oscillator and received, input, carrier signals. However it can be seen that a representative analysis of the balanced mixer can be made from the simplified model when the CW input frequency is within a ten percent bandwidth of the local oscillator frequency.

The simplified, balanced mixer should be considered to be an adequate model with the following restrictions.

1. The input carrier signal frequency should be within ten percent bandwidth of the local oscillator frequency.

2. The actual IF input signal is only proportional to the IF signal found for the model.
3. The model alone should not be used for a pulsed input signal when the phase information is important.

X. SUMMARY AND CONCLUSION

This thesis has presented a signal-processed antenna and receiver system that utilizes a phase and amplitude detection system to obtain a phase-dependent amplitude factor in the processed, output signal. A method of phase manipulation, which uses a reference antenna displaced from a one-dimensional array to adjust the phase of the array signal at the receiver, was given. This method of phase manipulation can be used to greatly improve the antenna array pattern beamwidth or sidelobe level. Then the limitations of the method of phase manipulation and of the processing system for a simplified, balanced-mixer model were given. This included bandwidth of pulsed input signals, the bandwidth for information carried on these signals, and signal phase-error limitations for different applications. A simulation of the lossless, strip-line, hybrid-ring, balanced-mixer frequency converter utilizing an extended model was made on a hybrid computer. One of the greatest benefits that has resulted from this study is the indication that microwave devices can be simulated using the hybrid computer. Since a microwave device can be simulated in scaled real time while using the hybrid computer, this simulation provides an intuitive understanding of the device and methods of design improvements.

The basic conclusions of this thesis are, for the signal-processed

antenna system:

1. By using amplitude and phase detection, a phase-dependent amplitude term is introduced in the effective electric field pattern of an antenna array after amplitude detection.
2. A method of phase manipulation can be used to make the phase-dependent amplitude term depend on the characteristics of the antenna array, and the displacement distance of a reference antenna from the array and a pattern control phase shift. The method of phase manipulation uses the processed signal from a reference antenna displaced from the one-dimensional antenna array to adjust the phase of the array signal to the main processor.
3. The phase-manipulated term in the effective pattern can then be used to improve the pattern over that for the normal pattern for simple amplitude detection. The pattern improvements consist of sidelobe reductions as great as 5.3 db or, with the original sidelobe level, beamwidth reductions as great as a factor of two.
4. The reproduction restrictions on the bandwidth for information signals carried on the receiver input signal are similar to other detection systems.
5. The bandwidth limitation on pulsed input signals required to hold normal beam-pointing angle accuracies depends on

the characteristics of the signal processor. These characteristics are CW or pulsed local oscillator, bandpass or lowpass IF and the IF input signal amplitude distribution for the frequency difference between the input carrier and the local oscillator carrier frequencies. Typical input signal bandwidths that can meet the beam-pointing accuracies are: (a) two percent of the local oscillator carrier frequency for a processor with a CW local oscillator signal and a bandpass IF (b) nine percent for a processor with a CW local oscillator signal and a lowpass IF (c) nine percent or larger for a processor with a pulsed local oscillator signal and a bandpass IF.

6. A CW input signal frequency must be kept within a 17% bandwidth range of the local oscillator frequency for the processor with a CW local oscillator signal and must be identical to the local oscillator carrier frequency for the processor with a pulsed local oscillator signal.

The basic conclusions for the balanced-mixer models are:

1. A simplified model of the balanced mixer should only be used to give a representative analysis of balanced-mixer frequency conversion. Restrictions that must be placed on its use are: (a) The input carrier signal frequency should be within a ten percent bandwidth of the local oscillator

frequency. (b) The actual IF input signal is only proportional to the IF signal found for the model. (c) The model alone should not be used for a pulsed input signal when the phase information is important.

2. An extended mathematical model of the balanced mixer can be simulated accurately on the hybrid computer. The actual correlation of the mathematical model to the balanced mixer depends on the degree of refinement of the mathematical model. Most refinements of the mathematical model can be simulated on a hybrid computer with the limitation of the computer capacity.

BIBLIOGRAPHY

1. Altman, Jerome L. Microwave circuits. New York, Van Nostrand, 1964. 462 p.
2. Berkowitz, Raymond S. Modern radar. New York, Wiley, 1965. 660 p.
3. James, M. L., G. M. Smith and J. C. Wolford. Analog computer simulation of engineering systems. Scranton, International, 1966. 246 p.
4. Kraus, John D. Antennas. New York, McGraw-Hill, 1950. 553 p.
5. Ksienski, A. A. and M. E. Pedinoff. Multiple target response of data-processing antennas. IRE Transactions on Antennas and Propagation 10:112-126. 1962.
6. Pound, Robert V. Microwave mixers. New York, McGraw-Hill, 1958. 381 p.
7. Reed, J. and G. J. Wheeler. A method of analysis of symmetrical four-port networks. IRE Transactions on Microwave Theory and Techniques 4:246-252. 1956.
8. Skolnik, Merrill L. Introduction to radar systems. New York, McGraw-Hill, 1962. 648 p.
9. Sylvania Electric Products. Semiconductor Division. Microwave diode product guide. 1st rev. Woburn, Mass., n.d. 29 p.
10. Torrey, Henry C. and Charles A. Whitmer. Crystal rectifiers. New York, McGraw-Hill, 1948. 441 p.
11. Williamson, James Allen. Short-pulsed operation of the balanced detector. Master's thesis. Corvallis, Oregon State University, 1967. 69 numb. leaves.

APPENDICES

APPENDIX I

List of Symbols

A_u	= weighting factor of the u^{th} element of the array at the receiver
B_m	= amplitude of the processor input signal component for the frequency, $f_s + mf_2$
c	= velocity of light
C_b	= microwave diode barrier capacitance--see Figure 10a
C_{IF}	= a capacitance of the IF input circuit--see Figure 10c
CW	= continuous wave
d	= spacing between antenna elements of the array
f	= frequency
f_0	= design frequency of the hybrid-ring balanced mixer
f_1	= pulse repetition frequency for the local oscillator signal and the IF frequency for the processor
f_2	= pulse repetition frequency for the received signal
f_c	= frequency which is at the center of the IF input signal amplitude versus $(f_s - f_r)/f_r$ distribution
f_I	= frequency of the information signal
f_r	= carrier frequency of the local oscillator signal
f_s	= carrier frequency of the received signal
$g(\theta, \phi)$	= antenna element electric field pattern
H_i	= amplitude of the local oscillator signal component for the frequency $f_r + if_1$

- $h(\omega)$ = total loss factor for the transmission line and free space
 IF = intermediate frequency amplifier
 k = $2\pi/\lambda = \omega/c$ = propagation constant of free space
 k_s = k for $\omega = \omega_s$
 ℓ_0 = median length of the transmission lines from the antenna elements of the array to the receiver
 $\ell_0 + u\ell_1$ = length of the transmission line from the u^{th} antenna element to the receiver
 ℓ_1 = incremental effective transmission line length change between adjacent elements of the antenna array
 L_e = effective length of an antenna element
 L_{DC} = an inductance of the IF input circuit--see Figure 10c
 L_{IF} = an inductance of the IF input circuit--see Figure 10c
 L. O. = local oscillator
 n = number of antenna elements in the array
 R = distance from the center of the antenna array to the effective source
 R_b = microwave diode barrier resistance--see Figure 10a
 R_{IF} = IF input impedance--see Figure 10c
 R_s = microwave diode ohmic spreading resistance--see Figure 10a
 t_0 = time of diode turnoff for the balanced mixer
 T_1 = pulse repetition period for the local oscillator signal
 T_2 = pulse repetition period for the received signal
 t_d = pulsewidth between half-voltage points of the received signal

- v = phase velocity in the transmission line
 V_0 = amplitude of the signal at the effective source
 V_m = amplitude of the signal component for the frequency, $f_s + mf_2$, at the effective source
 Z_0 = characteristic impedance of the transmission line
 α_e = error angle in γ
 α_{em} = maximum error angle in γ
 α_{r0} = pulsed local oscillator signal phase at the processor for the frequency, $f_r + if_1$
 α_{s0} = median phase of the received carrier signal at the receiver
 $= \gamma_0(\omega_s) - \gamma_1(\omega_s) - \beta_s \ell_0 - k_s R$
 α_{sm} = median phase of the received signal component for the frequency, $f_s + mf_2$
 $= \gamma_0(\omega_s + m\omega_2) - \gamma_1(\omega_s + m\omega_2) - (\omega_s + m\omega_2)((R/C) + (\beta_s \ell_0 / \omega_s))$
 for β , $\gamma_0(\omega)$, and $\gamma_1(\omega)$ linear in ω
 β = $2\pi/\lambda_g = \omega/v$ = propagation constant of the transmission line
 β_0 = β for $\omega = \omega_0$
 $\beta_0^{\ell_B}$ = phase shift between the quarter wavelength shorted stub in the local oscillator signal input line and the hybrid ring of the balanced mixer of Figure 6
 $\beta_0^{\ell_D}$ = phase shift between the diodes and the hybrid ring of the balanced mixer of Figure 6
 $\beta_0^{\ell_F}$ = phase shift between the diodes and the hybrid ring of the balanced mixer of Figure 6
 β_s = β for $\omega = \omega_s$
 γ = phase difference of the received and the local oscillator input signal = $\alpha_{s0} - \alpha_{r0}$

- $\gamma_0(\omega)$ = phase of the signal at the effective source
 $\gamma_1(\omega)$ = phase shift of an antenna element
 δf_{IF} = bandwidth of IF amplifier of Figure 5
 θ = angle defined by Figure 2
 θ_e = error angle between θ and θ_m for the source
 θ_m = antenna beam pointing angle
 λ = wave length in free space
 λ_g = wave length in the transmission line
 τ = time delay
 ϕ = angle defined by Figure 2
 ϕ_0 = pattern control phase shift
 $\psi_0(\theta) = k_s d \sin \theta - \beta_s \ell_1$
 ψ_e = error in $\psi_0(\theta)$
 ψ_{em} = maximum ψ_e
 ψ_{BW} = pattern beamwidth in ψ_0
 $\psi_m = (\omega_s + m\omega_2)\psi_0/\omega_s$ for β linear in ω
 Ω = ohms of resistance
 ω = $2\pi f$ = circular frequency
 ω_r = carrier circular frequency of the local oscillator signal
 ω_s = carrier circular frequency of the received signal

APPENDIX II

Scattering Coefficients of Microwave JunctionsParallel Junctions of Lines of Unequal Characteristic Impedance

Assuming a parallel junction of $n + 1$ transmission lines, where n -lines have identical characteristic impedances, then the voltages at the individual terminals of the junctions are

$$V_0 = (Z_{00})^{1/2}(a_0 + b_0)$$

$$V_i = (Z_{01})^{1/2}(a_i + b_i) \quad \text{for } i = 1 \text{ to } n$$

where the a 's and b 's are respectively power-normalized incident and reflected wave coefficients (1). By power-normalized it is meant that, for a single traveling wave, the power is given by $aa^*/2$ or $bb^*/2$. Since the voltages at a parallel junction are all equal, the following equations hold true:

$$\left(\frac{Z_{00}}{Z_{01}}\right)^{1/2}(a_0 + b_0) = a_i + b_i \quad i = 1 \text{ to } n \quad (\text{A2-1})$$

The scattering matrix relationship between the incident and reflected waves is given by

$$\underline{b} = \underline{S}\underline{a}$$

or,

$$\begin{aligned}
 b_0 &= s_{00}a_0 + s_{01}a_1 + s_{02}a_2 + \dots + s_{0n}a_n \\
 b_1 &= s_{10}a_0 + s_{11}a_1 + \dots + s_{1n}a_n \\
 &\vdots \\
 b_n &= s_{n0}a_0 + s_{n1}a_1 + \dots + s_{nn}a_n
 \end{aligned} \tag{A2-2}$$

Some of the properties of scattering matrices for passive, lossless networks are $\underline{S} = \underline{S}_t$, and $\underline{S}^* = \underline{S}^{-1}$ where \underline{S}_t is the transposed matrix of \underline{S} , \underline{S}^* is the complex conjugate matrix of \underline{S} and \underline{S}^{-1} is the inverse matrix of \underline{S} (1). Therefore we have $s_{ij} = s_{ji}$. Since all the arms have identical characteristic impedances except the 0th arm, we then have

$$\begin{aligned}
 s_{0i} &= s_{i0} \quad i = 1 \text{ to } n \\
 s_{ij} &= s_{ji} \quad i = 1 \text{ to } n, \quad j = 1 \text{ to } n, \quad i \neq j \\
 s_{11} &= s_{ii} \quad i = 1 \text{ to } n
 \end{aligned}$$

The reflection coefficient for the i^{th} line can be determined from the relationship,

$$s_{ii} = r_{ii} = \frac{Z_{Li} - Z_{0i}}{Z_{Li} + Z_{0i}} \tag{A2-3}$$

where Z_{0i} is the characteristic impedance of the i^{th} line and Z_{Li}

is the load impedance seen by the i^{th} line. For $i = 0$, $Z_{L0} = Z_{01}/n$ so that Equation (A2-3) becomes

$$s_{00} = \frac{\frac{Z_{01}}{n} - Z_{00}}{\frac{Z_{01}}{n} + Z_{00}} = - \left(\frac{\frac{nZ_{00}}{Z_{01}} - 1}{\frac{nZ_{00}}{Z_{01}} + 1} \right)$$

For $i = 1$ to n ,

$$Z_{Li} = \frac{1}{\frac{(n-1)}{Z_{01}} + \frac{1}{Z_{00}}}$$

so that Equation (A2-3) becomes upon multiplying numerator and denominator by $(n-1)/Z_{01} + 1/Z_{00}$

$$s_{ii} = \frac{1 - (n-1 + \frac{Z_{01}}{Z_{00}})}{1 + (n-1 + \frac{Z_{01}}{Z_{00}})} = - \frac{(n-2) \frac{Z_{00}}{Z_{01}} - 1}{\frac{nZ_{00}}{Z_{01}} + 1} \quad i = 1 \text{ to } n$$

Let there only be signal incident in arm 0, $a_0 = 1$, and let all other arms be matched, $a_i = 0$ $i = 1$ to n . Then from Equations (A2-1) and (A2-2) and for the preceding conditions and results,

$$s_{0i} = s_{i0} = \frac{b_i}{a_0} = \left(\frac{Z_{00}}{Z_{01}}\right)^{1/2} \left(\frac{a_0 + b_0}{a_0}\right) = \left(\frac{Z_{00}}{Z_{01}}\right)^{1/2} (1 + s_{00})$$

$$= \frac{2\left(\frac{Z_{00}}{Z_{01}}\right)^{1/2}}{1 + n\left(\frac{Z_{00}}{Z_{01}}\right)^{1/2}} \quad \text{for } i = 1 \text{ to } n$$

and

$$s_{00} = \left(\frac{Z_{01}}{Z_{00}}\right)^{1/2} s_{0i} - 1 \quad \text{for } i = 1 \text{ to } n$$

Now for a signal incident only in the i^{th} line, $a_i = 1$ $i = 1$ to n , and all other lines matched, $a_j = 0$ $j = 0$ to n $i \neq j$, then from Equations (A2-1) and (A2-2), and for the preceding conditions and results,

$$s_{ji} = s_{ij} = \frac{b_i}{a_i} = \frac{a_i + b_i}{a_i} = 1 + s_{ii}$$

$$\begin{aligned} & \frac{2Z_{00}}{Z_{01}} \quad \text{for } i \neq j \text{ } i \text{ and } j = 1 \text{ to } n \\ & = \frac{\frac{Z_{01}}{Z_{00}}}{1 + n\frac{Z_{00}}{Z_{01}}} = \left(\frac{Z_{00}}{Z_{0i}}\right)^{1/2} s_{i0} \end{aligned}$$

and

$$s_{ii} = s_{ij} - 1$$

$$s_{00} = \frac{s_{i0}^2}{s_{ij}} - 1 \quad \text{for } i \neq j \text{ } i \text{ and } j = 1 \text{ to } n$$

Let

$$s_{ij} = T_{aa}$$

$$s_{i0} = T_{ai}$$

and

$$Q_k = T_{ai} a_0 + \sum_{i=1}^n T_{aa} a_i \quad (A2-4)$$

With these relationships, Equations (A2-2) become

$$b_0 = -a_0 + \frac{T_{ai}}{T_{aa}} Q_k$$

$$b_j = -a_j + Q_k \quad j = 1 \text{ to } n \quad (A2-5)$$

Thus at a parallel junction of $n + 1$ lines with n lines having identical characteristic impedances, as in Figures 9 and 13, Q_k represents the center or common summer and the reflected waves are given by Equations (A2-5).

Parallel Junctions of Equal Characteristic Impedance Lines

For the case of a parallel junction of $n + 1$ equal characteristic impedance, transmission lines, the results can be taken directly from Equations (A2-4) and (A2-5) since then $T_{ai} = T_{aa}$. Therefore the results are

$$Q_k = \sum_{i=0}^n T_{aa} a_i \quad \text{common summer}$$

$$T_{aa} = \frac{2}{1+n}$$

$$b_j = -a_j + Q_k \quad j = 0 \text{ to } n, \quad \text{reflected wave coefficients}$$

Shorted Line at a Parallel Junction

This can be considered to be a special case at the parallel junction. Since a short gives a reflection coefficient of -1 at the end of the line, this reflection coefficient can be transferred to the junction. For a short at the end of the m^{th} line, the length of delay the incident wave travels from the junction to its return to the junction is a constant, but it can be made a continuous effective length by moving the reflection coefficient in the middle of the delay to the junction. Doing this results in, say for the equations for equal characteristic impedance,

$$Q_k = \sum_{i=0}^n (1-2\delta_{im}) T_{aa} a_i \quad \text{common summer}$$

$$T_{aa} = \frac{2}{1+n}$$

$$b_j = (2\delta_{im} - 1)a_j + Q_k \quad j = 0 \text{ to } n, \quad \text{reflected wave coefficients}$$

where

$$\delta_{im} = 1 \quad \text{for } i = m \quad \text{and} \quad \delta_{ij} = 0 \quad \text{for } i \neq m.$$

Series Junction of Equal Characteristic Impedance Lines

For a junction with n series lines and the two normal input and output lines with all having equal characteristic impedances, then the voltages and currents at the junctions are,

$$\begin{aligned}
 & \left. \begin{aligned} V_0^i &= (Z_0)^{1/2} (a_0^i + b_0^i) \\ i_0^i &= \frac{(a_0^i - b_0^i)}{(Z_0)^{1/2}} \end{aligned} \right\} \text{input line} \\
 & \left. \begin{aligned} V_0^0 &= (Z_0)^{1/2} (a_0^0 + b_0^0) \\ i_0^0 &= \frac{(a_0^0 - b_0^0)}{(Z_0)^{1/2}} \end{aligned} \right\} \text{output line} \quad (\text{A2-6}) \\
 & \left. \begin{aligned} V_j &= (Z_0)^{1/2} (a_j + b_j) \\ i_j &= \frac{(a_j - b_j)}{(Z_0)^{1/2}} \end{aligned} \right\} j = 1 \text{ to } n
 \end{aligned}$$

Since at a series junction the currents are of equal magnitude and in the same direction, but since the current notation is for currents into the junction, the following equations hold:

$$b_0^i + a_0^i = a_0^0 + b_0^0 + \sum_{j=1}^n (a_j + b_j)$$

$$b_0^i - a_0^i = a_0^0 - b_0^0 \quad (A2-7)$$

$$b_0^i - a_0^i = a_j - b_j \quad j = 1 \text{ to } n$$

Adding all the equations of (A2-7) and solving for b_{0i} gives,

$$b_0^i = \frac{na_0^i}{n+2} + \frac{2a_0^0}{n+2} + \sum_{j=1}^n \frac{2a_j}{n+2}$$

Let,

$$R_k = \frac{2}{n+2} (a_0^0 - a_0^i + \sum_{j=1}^n a_j) \quad (A2-8)$$

Then solving for the reflected waves in terms of the incident signals gives,

$$b_0^i = a_0^i + R_k$$

$$b_0^0 = a_0^0 - R_k \quad (A2-9)$$

$$b_j = a_j - R_k \quad j = 1 \text{ to } n$$

Thus for a series junction in Figures 9 and 13, the common summer is determined by Equation (A2-8) and the reflected wave coefficients by Equations (A2-9).

Shorted Line at a Series Junction

The same type of manipulation of the position of the reflection coefficient for the shorted line can be done in this case as it was for the case for the shorted line at a parallel junction. Then for the m^{th} series line being shorted in the previous case for a series junction, Equations (A2-8) and (A2-9) become

$$R_k = \frac{2}{n+2} (a_0^0 - a_0^i + \sum_{j=1}^n (1-2\delta_{jm})a_j)$$

$$b_0^0 = a_0^0 - R_k$$

$$b_0^i = a_0^i + R_k$$

$$b_j = (1-2\delta_{jm})a_j - R_k \quad j = 1 \text{ to } n$$

Microwave Diode Series Junction

In this case for a series junction with $n = 1$, and due to the fact that the analog simulation uses current and voltage, let us solve for the reflected wave coefficients from Equations (A2-7) while utilizing the voltage definition of Equations (A2-6) for the diode. Doing this, except with the diode voltage notation given in Figure 10b, gives

$$b_0^0 = a_0^i - \frac{(\pm V_d)}{2(Z_0)^{1/2}}$$

$$b_0^i = a_0^0 + \frac{(\pm V_d)}{2(Z_0)^{1/2}}$$

and solving for the diode current gives,

$$\pm i_d = \frac{a_0^i - b_0^i}{(Z_0)^{1/2}} = \frac{b_0^0 - a_0^0}{(Z_0)^{1/2}}$$

where the upper sign is for the case of the diode polarity at the junction being identical to that shown in Figure 10b.

APPENDIX III

EAI 690 Hybrid Computer Characteristics

The characteristics listed below are for the Electronic Associates Inc. 690 hybrid computer in the Engineering Simulation Laboratory at Oregon State University at the time of the simulation study of the balanced mixer.

The digital part of this hybrid computer has a cycle time of 1.65 microseconds and has 8,192 words of memory. Each word consists of 15 binary bits plus a sign bit. In addition, there are 10 digital-to-analog channels and 10 analog-to-digital channels of 13 binary bits plus the sign bit. The basic computer operation uses octal numbers. The analog portion of the computer has 11 integrators or summers, 6 limit summers, 2 track-store summers, 3 multipliers, 2 variable diode function generators, 4 inverters, 24 potentiometers, and many digital functions such as and-gates, flip-flops, monostable pulse generators, differentiators, analog-to-digital comparators, relays, counters, integrator and summer controls, sense line inputs to the digital computer, operation control line outputs from the digital computer, and other computer controls. The simulation study used all the analog portion of the hybrid computer except the multipliers and some digital functions, all the memory of the digital portion, nine of the digital-to-analog channels and six analog-to-digital channels.

Flow Diagram of the Digital Program for the Simulation
of the Hybrid-Ring, Balanced Mixer

The flow diagram for the digital part of the simulation of the extended model realization of the hybrid-ring, balanced mixer of Figures 9, 10 and 13 is given in this part of the Appendix. The program uses the power-normalized traveling wave coefficients. The digital program simulates directly the signals for the partial realizations of the extended model of Figures 9 and 13 with the exception of the portions of the figures marked A-A'. The digital computer is also used to collect data and, after completion of the balanced-mixer simulation, to analyze it. The data consists of the phase difference between the received input signal and the local oscillator signal (phase of the beat signal of the sum of the two signals) and also consists of the scaled IF input signal. The data is stored consecutively in pairs of two for each data acquisition point. The distance between the data acquisition points in integer degrees of the local oscillator signal is determined by the digital computer. The distance depends on the number of memory spaces available for data storage and is set by the digital computer so that at least 240° of the IF input signal is obtained in the data. The analog computer data collection control is arranged so that only one positive peak and one negative peak is obtained in the data for the

IF input signal (see Figure 12). Before the flow diagram is given, a list of the symbols used in the flow diagram will be provided.

List of Flow Diagram Symbols

AA(K), AB(K), BA(J), BB(J), CA(L), CB(L), CC(L), CD(L), CE(L), CF(L), CG(L), CH(L), DA(N), DB(N), DC(N), DD(N), EA(M), EB(M), FA(I), FB(I), FC(I), FD(I), GA(II), GB(II), RA(JJ)

= Delayed signals of Figures 9 and/or 13 with the notation corresponding to the delay subscripts of these figures

ADC 1 = Analog to digital channel No. 1 output

ALPHA = Fractional part of a degree for the received signal phase

COUNT = (No. of storage spaces for data acquisition points -- 2 memory spaces per data point)

DAC 2 = Digital to analog channel No. 2 input

DAT = $s_0 * \text{SCALED} * (\text{IF input voltage})$ = scaled, power-normalized IF input signal

DATA(MI) = Data consisting of the degrees of phase difference between the received input signal and the local oscillator signal (phase of the beat signal of the sum of the two signals) with a storage cycle of two memory spaces

DATA(MI+1) = Data consisting of the scaled IF input signal with a storage cycle of two memory spaces

FDGINC = degree increment of the IF input signal between data points

FFREG = $(f_s - f_r) / f_r$ -- increments of 0.005

FREGCT = IF frequency control count

FREGN = No. of IF frequencies to be checked - must be even

HA, HB, HC, HD, HI, HJ = Delayed signals of Figure 13 which are delays one cycle of the real time operating program - notations corresponds to the delay subscripts of Figure 13

I, J, K, L, M, N, II, JJ = Integer variables of the delays

IMAX = No. of degrees delay for FA, FB, FC, and FD

ITIMEO = (Degree increment of the local oscillator signal between data acquisition points)

ITIME = -(Count. of degrees of the local oscillator signal to next data acquisition point)

JJMAX = No. of degrees delay for RA

JMAX = No. of degrees delay for BA, and BB

KI, KM = Integer variables for the received input signal

KK = Integer variable for local oscillator signal - each increment corresponds to one degree

MI = Data location integer variable

NMAX = No. of degrees delay for DA, DB, DC and DD

Real time operating program = part of the digital program that simulates all the balanced-mixer operations at one instant of time -- each cycle of the real time operating program corresponds to one degree of the local oscillator signal

REC = Scaled, power-normalized, received input signal

RECAM = Scaled, power-normalized amplitude of the received input signal

RECOUT= Scaled, power-normalized output of the received input port

REF(KK)= Local oscillator signal waveform - sine wave

REFDR = Scaled, power-normalized, local oscillator signal level

REFIN = Scaled, power-normalized, local oscillator input signal

REFOUT= Scaled, power-normalized output of the local oscillator port

RIF = IF input impedance

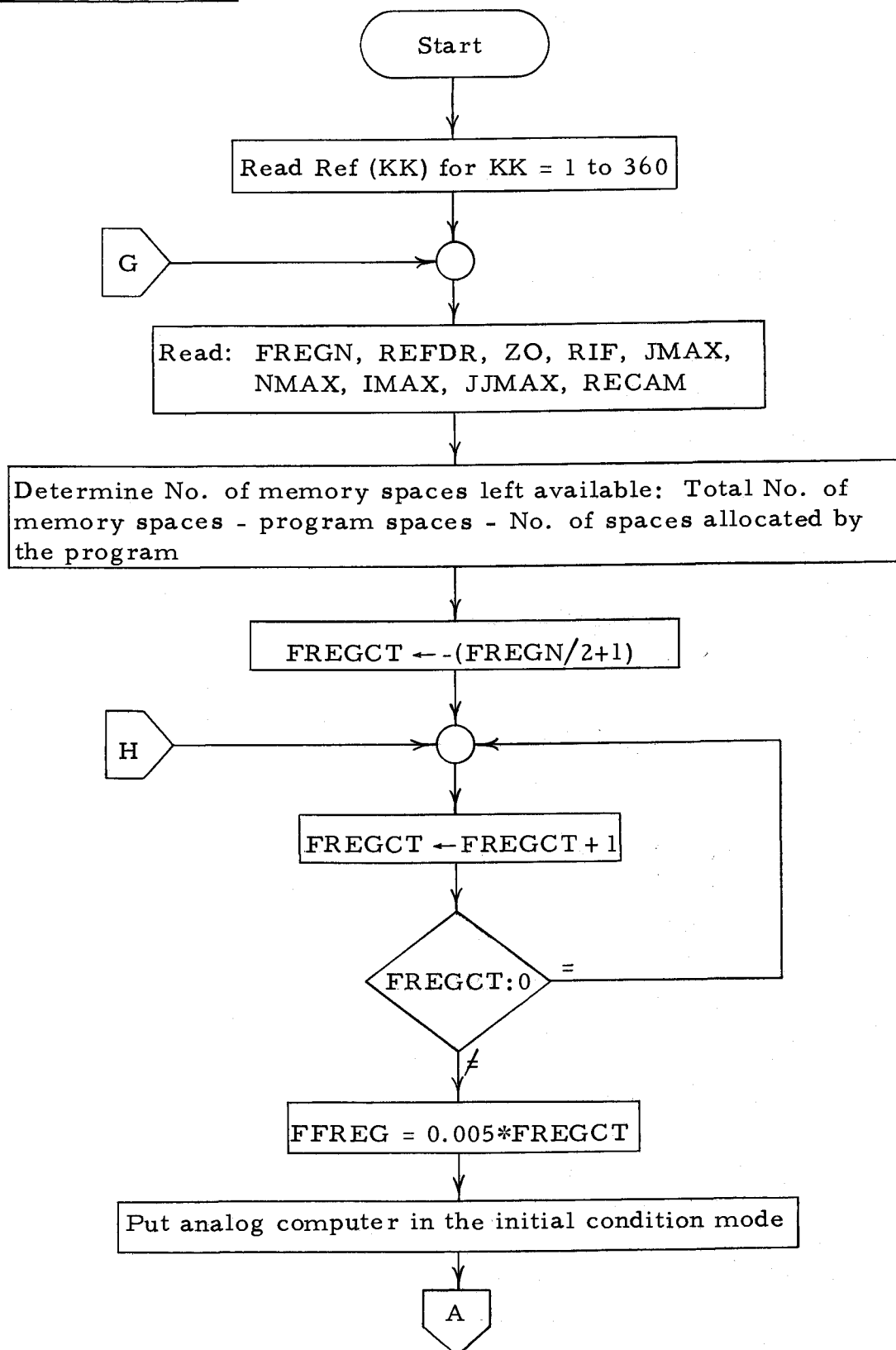
s_0 = 0.1 = Scale factor for the real time-operating-program, digital input and output signals except those simulating IF signals - see Appendix IV, Determination of Constants for the IF Input Circuit Simulation

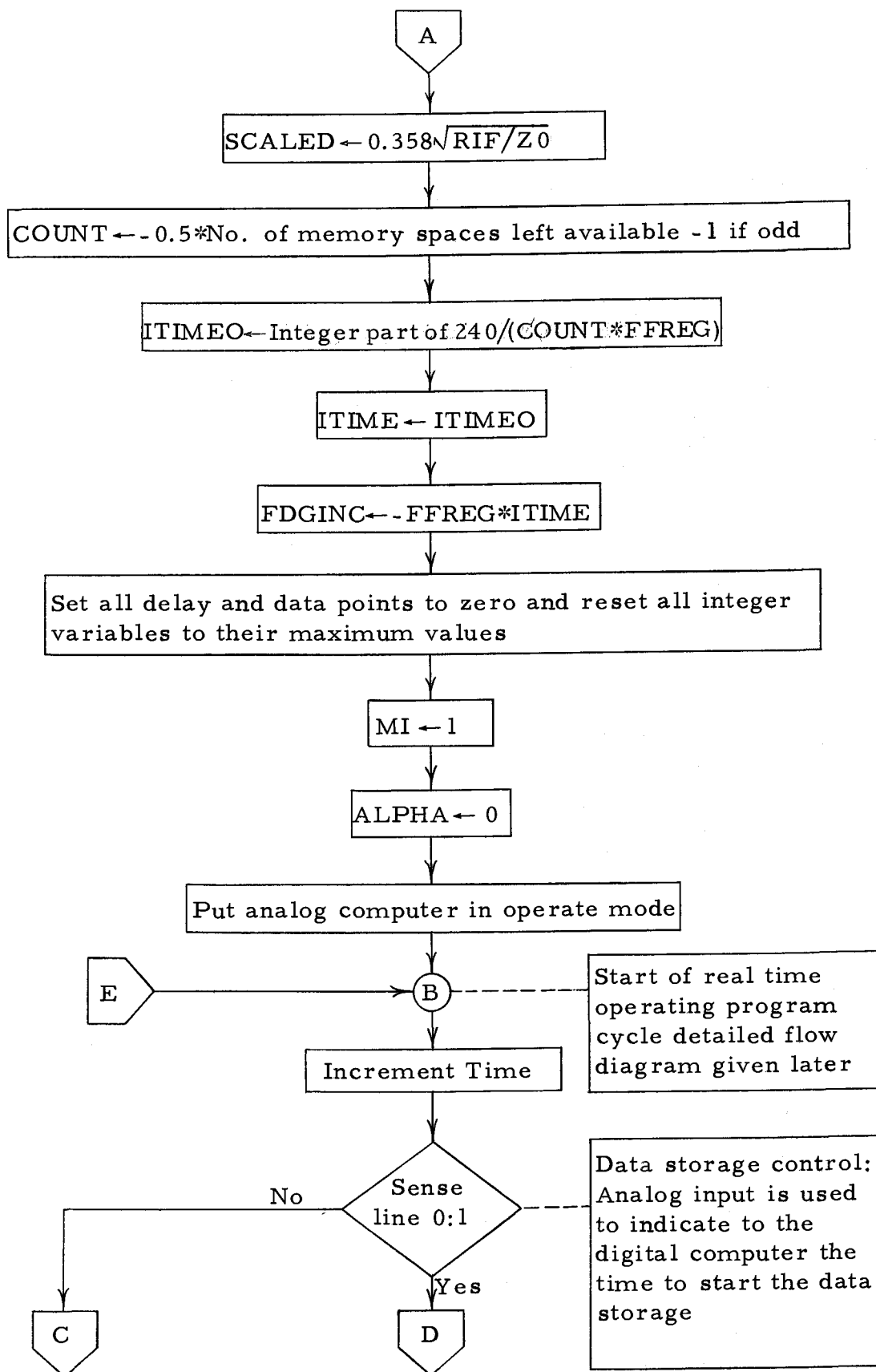
SCALED = Scale factor --part of the scale factor for the real-time-operating-program, digital input and output signals which are simulating signals of the IF input circuit -- see Appendix IV, Determination of Constants for the IF Input Circuit Simulation

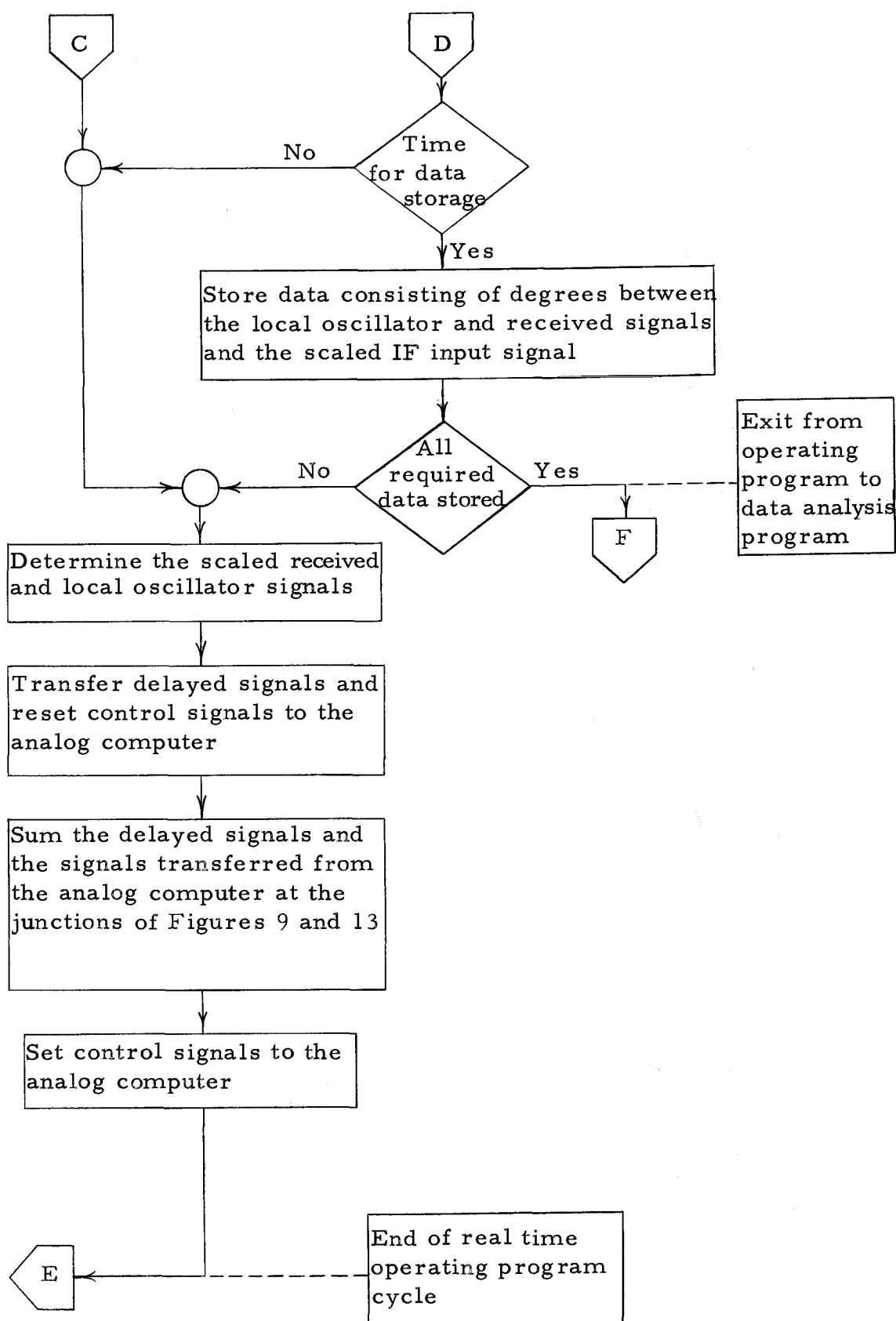
TAA, TAI = Scattering coefficients, values of which are given in Figure 9

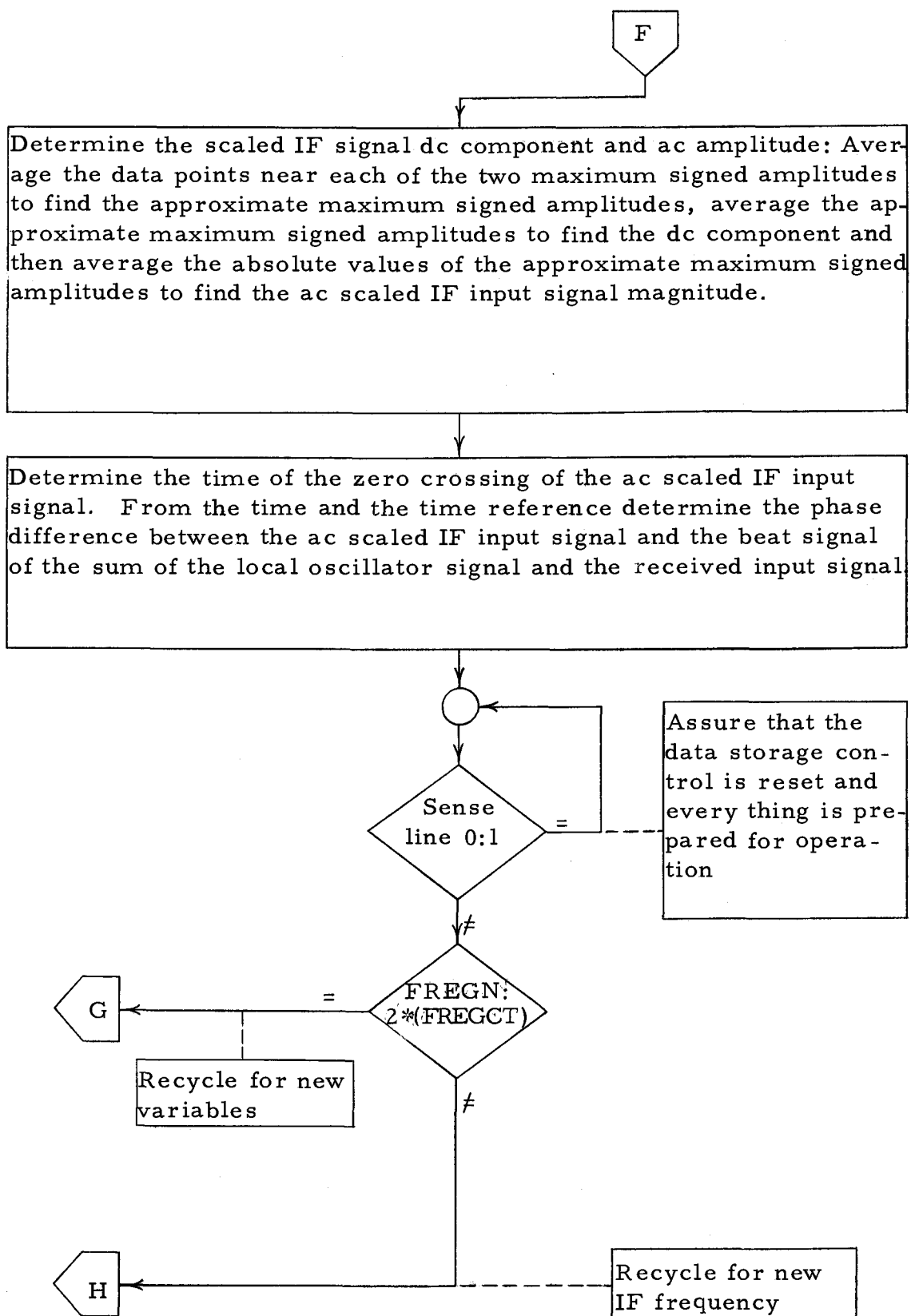
XA, XB, XC, XD, XE = Dummy variables

Z0 = Characteristic impedance of the transmission line

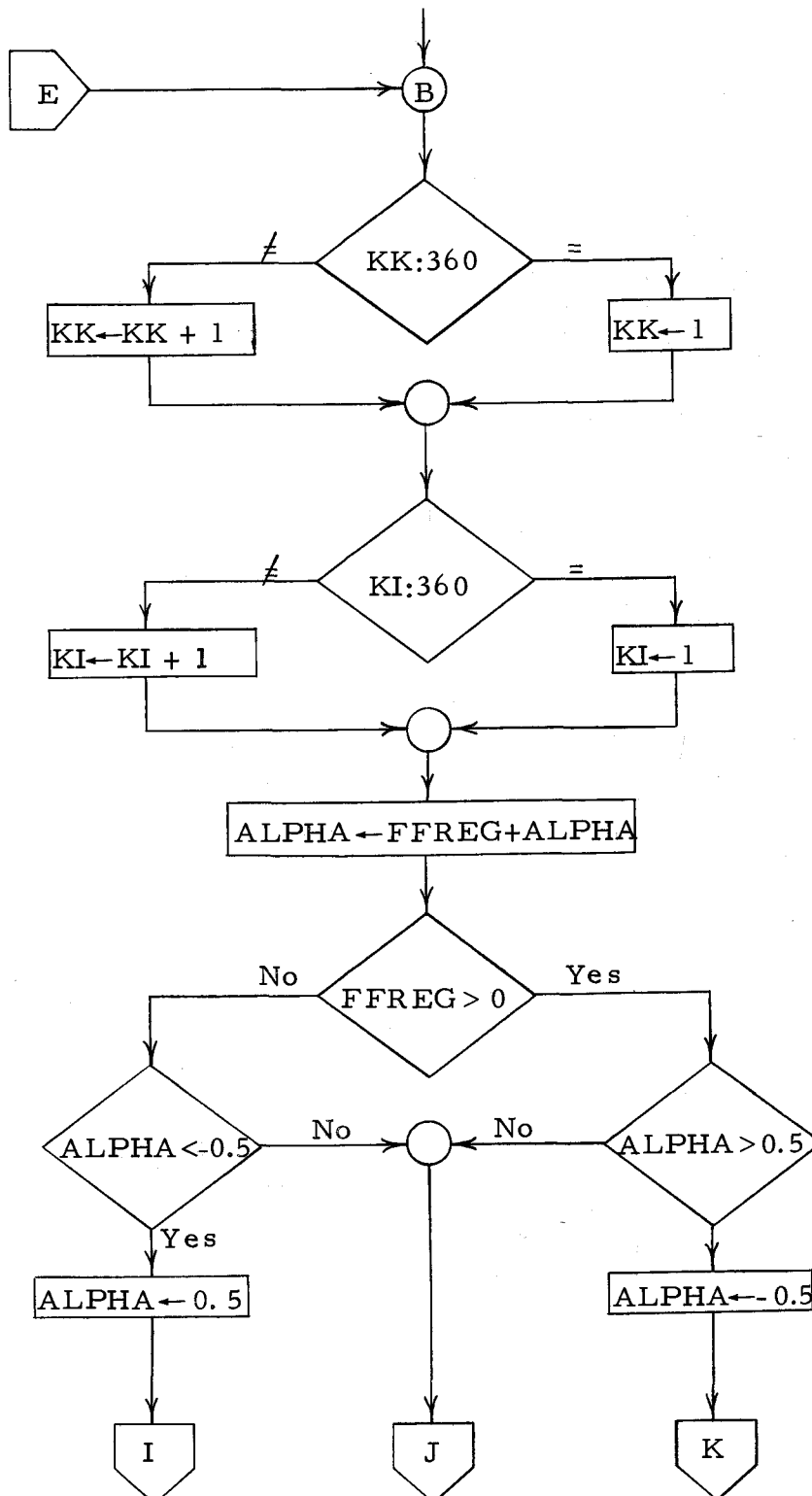
The Flow Diagram

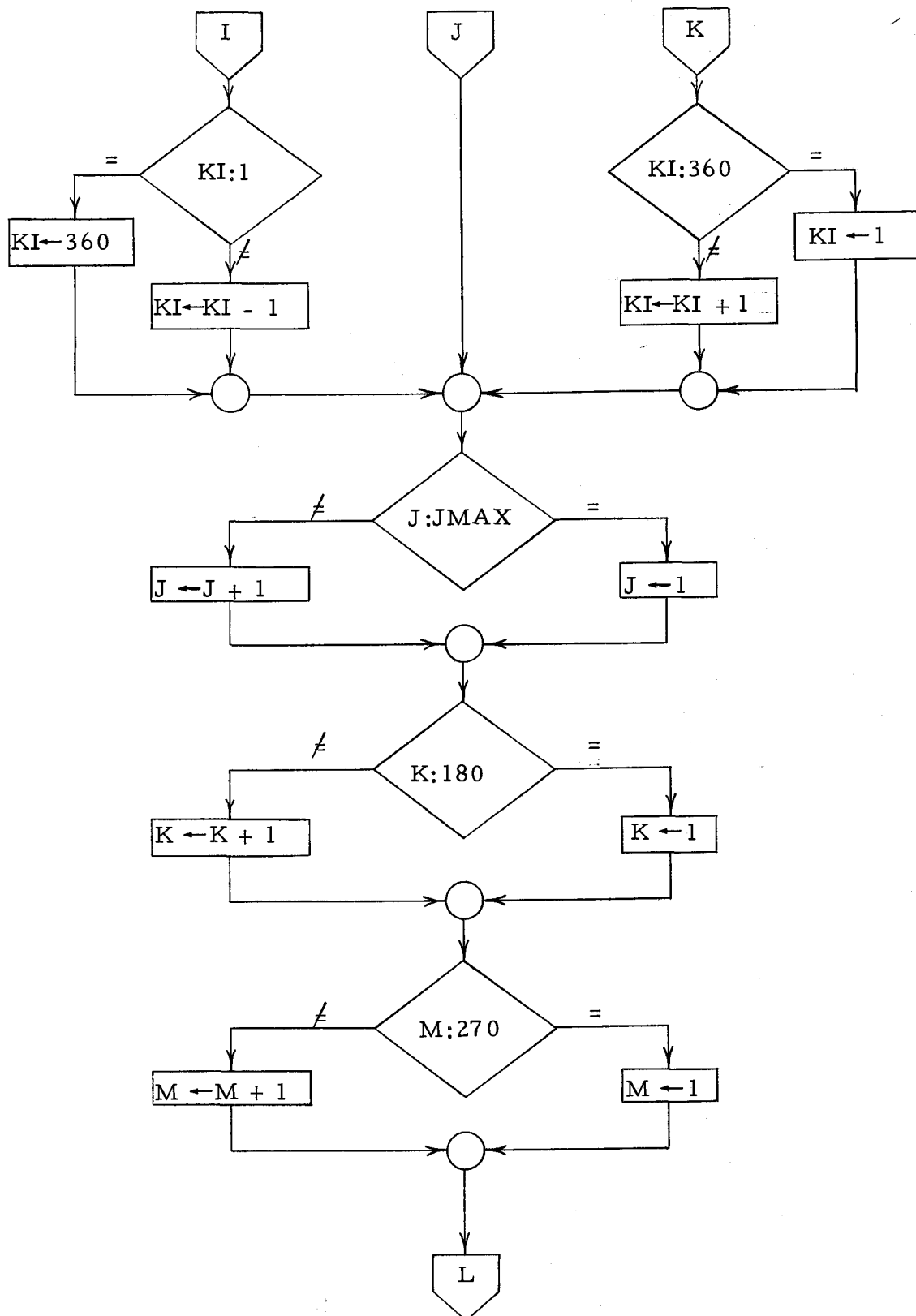


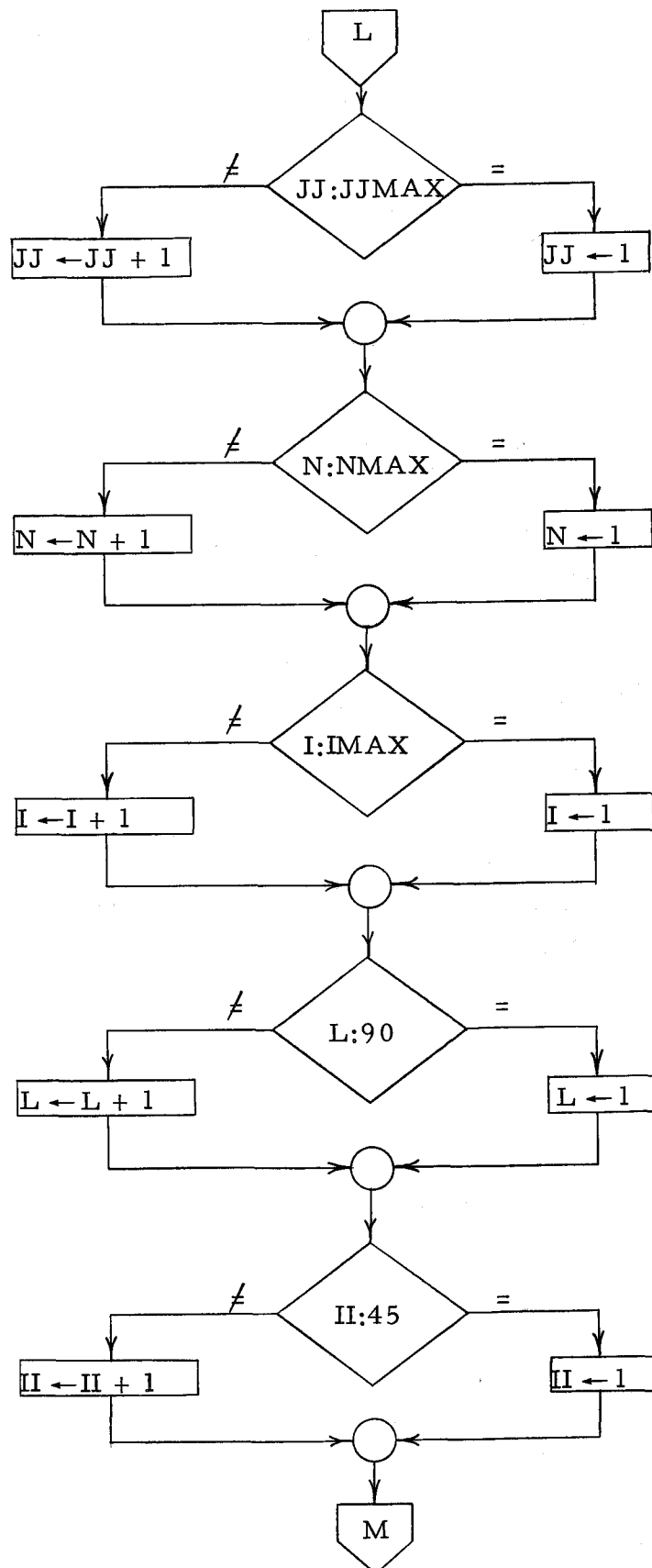


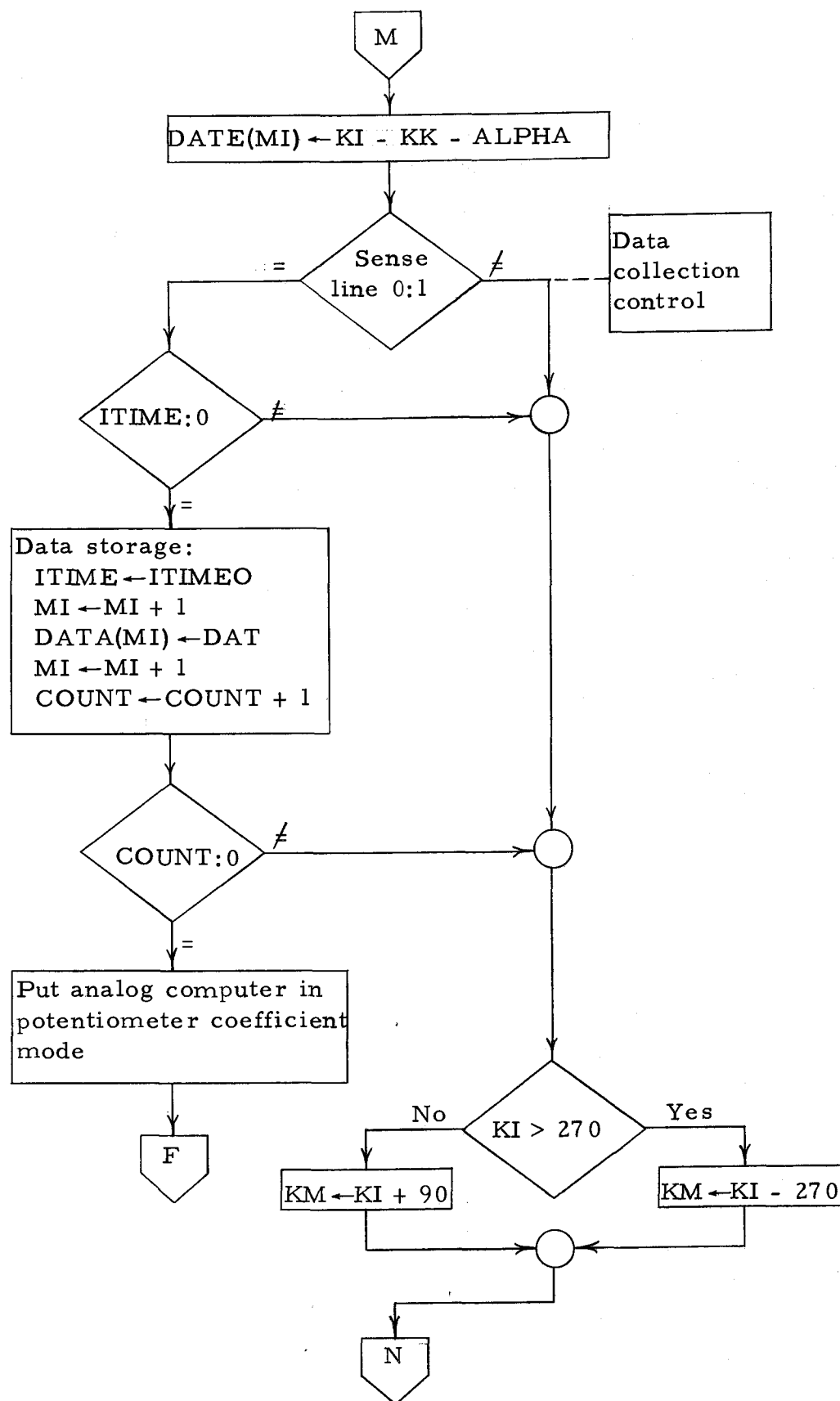


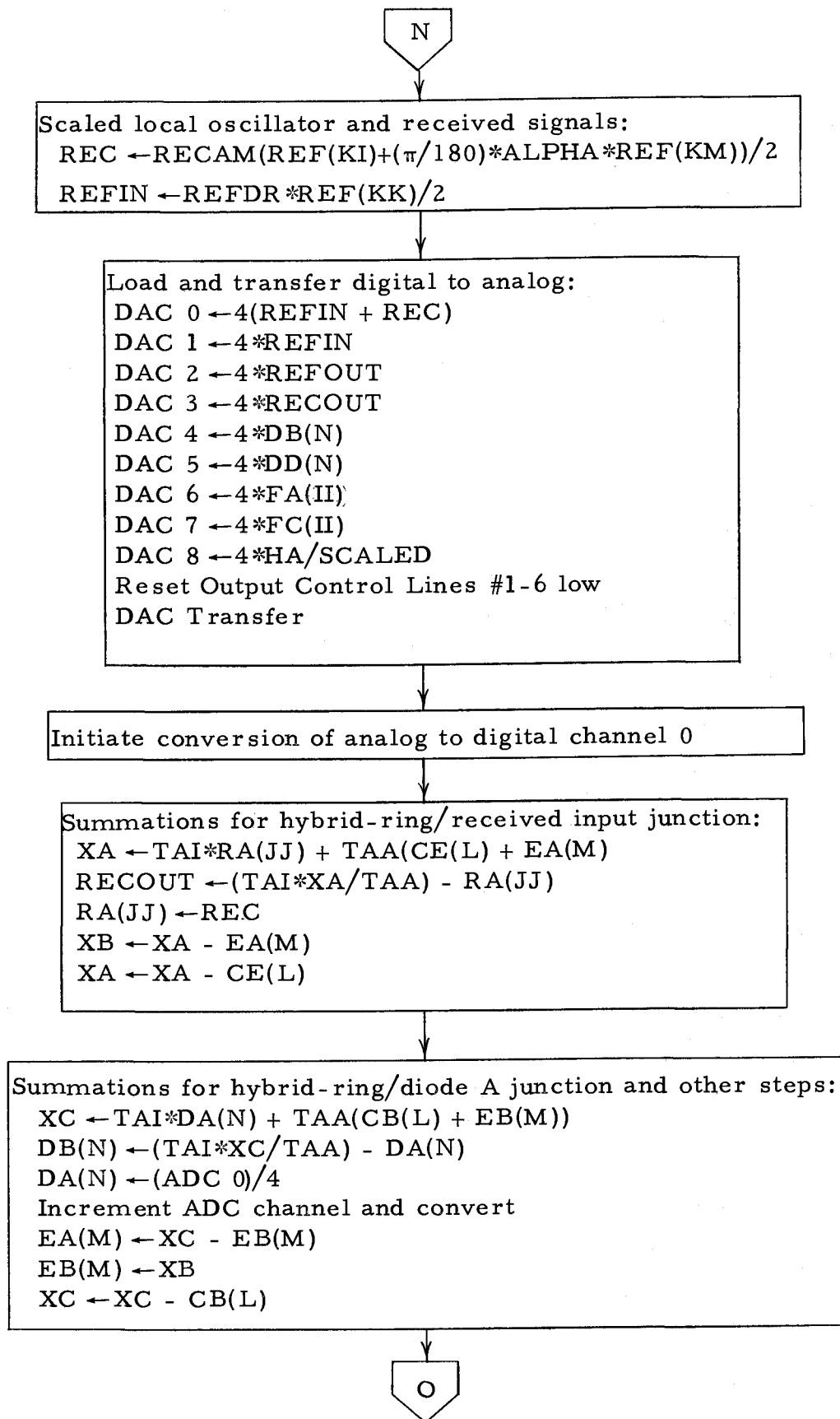
Detailed Flow Diagram for the Real Time Operating Program













Summations for hybrid-ring/diode B junction and other steps:

$$XB \leftarrow TAI * DC(N) + TAA(CD(L) + CF(L))$$

$$DD(N) \leftarrow (TAI * XB / TAA) - DC(N)$$

$$DC(N) \leftarrow (ADC\ 1) / 4$$

Increment ADC channel and convert

$$CE(L) \leftarrow XB - CF(L)$$

$$CF(L) \leftarrow XA$$

$$XB \leftarrow XB - CD(L)$$

Summations for IF terminal junctions, Figure 13 and other steps:

$$XD \leftarrow 2(CG(L) + GA(II) + HD) / 3$$

$$CG(L) \leftarrow XD - CG(L)$$

$$GA(II) \leftarrow XD - GA(II)$$

$$XD \leftarrow XD - HD$$

$$DAT \leftarrow ADC\ 2$$

Increment ADC channel and convert

$$XA \leftarrow 0.4 (HJ + HC + FB(I) + AB(K) + FD(I))$$

$$FA(I) \leftarrow XA - FB(I)$$

$$AB(K) \leftarrow XA - AB(K)$$

$$FC(I) \leftarrow XA - FD(I)$$

$$HD \leftarrow XA - HC$$

$$HC \leftarrow XD$$

$$XE \leftarrow XA - HJ$$

$$FB(I) \leftarrow (ADC\ 3) / 4$$

Increment ADC channel and convert

$$XD \leftarrow 0.5 (HI - HB + GB(II) + CH(L))$$

$$GB(II) \leftarrow XD - GB(II)$$

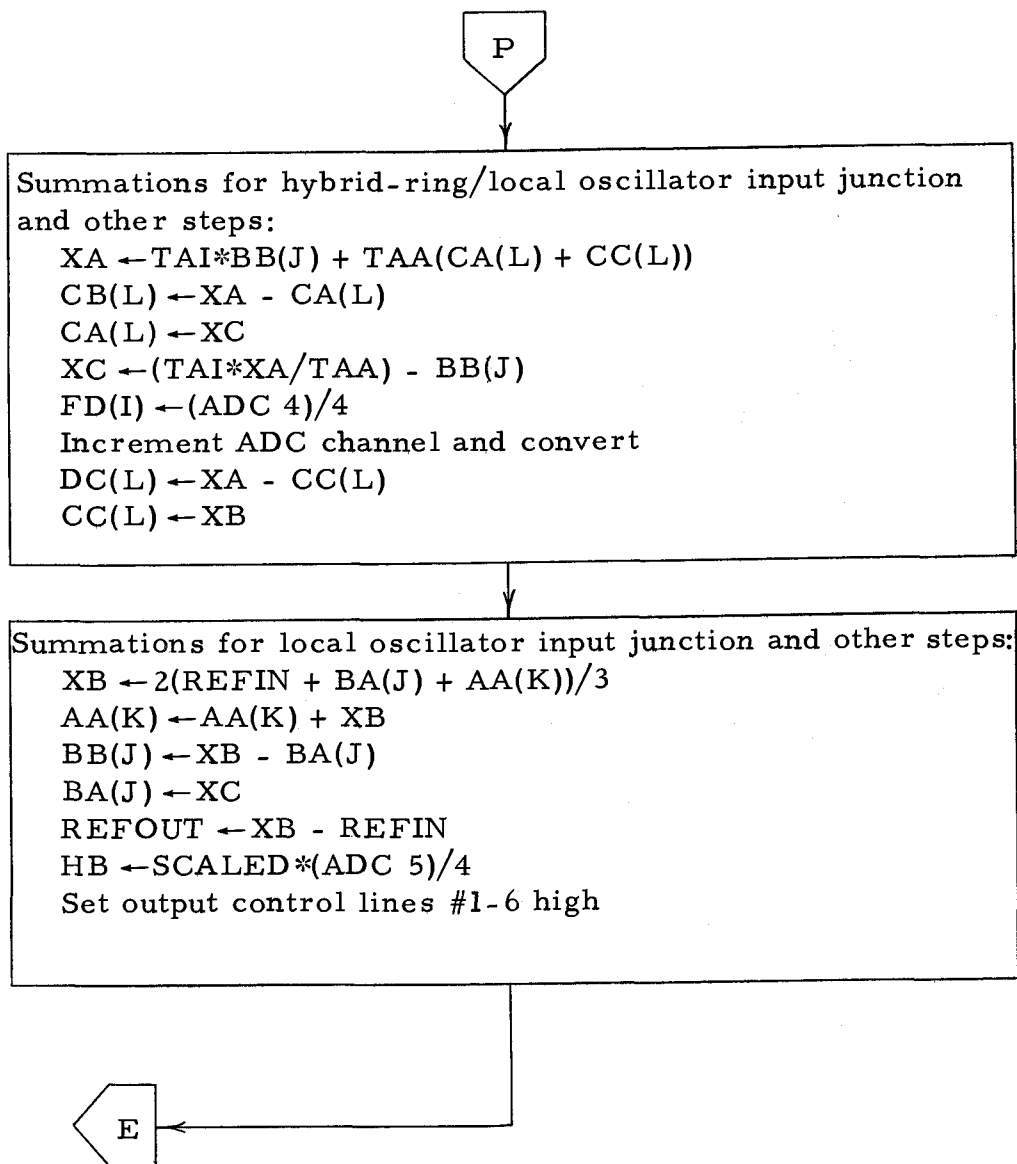
$$CH(L) \leftarrow XD - CH(L)$$

$$HA \leftarrow XD + HB$$

$$HJ \leftarrow HI - XD$$

$$HI \leftarrow XE$$





APPENDIX IV

Determination of Constants for the Microwave Diode Simulation

The basic equations for the microwave diode equivalent circuit as shown in Figure 10a are

$$V_d = i_d R_s + V_b \quad (A4-1)$$

$$V_b = \frac{1}{C_b} \int i_{C_b} dt = \frac{1}{C_b} \int (i_d - i_{R_b}) dt \quad (A4-2)$$

$$i_{R_b} = 5.2(10^{-6})(e^{21.6V_b} - 1) \quad (A4-3)$$

The equations for the reflected wave coefficients at the microwave diode junction are from Appendix II

$$b_0^o = a_0^i - \frac{\pm V_d}{2(Z_0)^{1/2}} \quad (A4-4)$$

$$b_0^i = a_0^o + \frac{\pm V_d}{2(Z_0)^{1/2}} \quad (A4-5)$$

$$\pm i_d = \frac{a_0^i - b_0^i}{(Z_0)^{1/2}} = \frac{b_0^o - a_0^o}{(Z_0)^{1/2}} \quad (A4-6)$$

where the input arm (i) was assumed to be from the hybrid-ring to the diode and where the upper sign was for diode A of Figure 6.

Let us solve for i_d from Equations (A4-4) and (A4-5)

$$\pm i_d = \frac{a_0^i - a_0^o}{(Z_0)^{1/2}} - \frac{\pm V_d}{2(Z_0)}$$

Substituting for V_d in this equation and solving for i_d again

$$\pm i_d = \frac{2(Z_0)^{1/2}}{2Z_0 + R_s} \left[a_0^i - a_0^o \mp \frac{V_b}{2(Z_0)^{1/2}} \right] \quad (\text{A4-7})$$

Let us use the normal notation in analog simulation where $1/D$ means integration with respect to time and $1/aD$ means integration in scaled real time or $t' = at$ (3). For the analog amplifier output voltages of Figure 11a, let us define

$$e_0 = \frac{\mp i_d}{s_8}, \quad e_1 = \frac{\pm i_d}{s_1}, \quad e_{IFD} = \frac{-a_0^o}{s_0}, \quad e_{DIF} = \frac{b_0^o}{s_0}$$

$$e_2 = \frac{\mp V_b}{s_2}, \quad e_3 = \frac{\mp i_{R_b}}{s_3}, \quad e_{DH} = \frac{-a_0^i}{s_0}, \quad e_{HD} = \frac{b_0^i}{s_0}$$

where the s_i are scale factors. All analog amplifier functions as well as the digital-to-analog conversion have a sign inversion between the input and output signals.

Solving for e_0 and e_1 from Equation (A4-7), it is found :

that

$$e_0 = - \left(\frac{s_0^2 (Z_0)^{1/2}}{(2Z_0 + R_s) s_8} \right) \left[-e_{DH} + e_{IFD} + \left(\frac{s_2}{s_0^2 (Z_0)^{1/2}} \right) e_2 \right]$$

$$e_1 = - \frac{s_8}{s_1} e_0$$

From Equation (A4-6) it can be seen that solving for e_{DIF} and e_{DH} gives

$$e_{DIF} = - \left[e_{IFD} + \frac{s_8 (Z_0)^{1/2}}{s_0} e_0 \right]$$

$$e_{DH} = - \left[e_{HD} + \frac{s_1 (Z_0)^{1/2}}{s_0} e_1 \right]$$

Making the analog substitutions in Equations (A4-2) and (A4-3), we find

$$e_2 = - \frac{1}{D} \left(\frac{s_1 e_1 + s_3 e_3}{a C_b s_2} \right)$$

$$e_3 = \pm \frac{5.2(10^{-6})}{s_3} (e^{\pm 21.6 e_2 / s_2 - 1})$$

Now the equations for the analog computing diagram of Figure 11a are

$$\begin{aligned}
e_0 &= - (e_{IFD} - e_{HD} + K_4 e_2) \\
e_1 &= - K_1 e_0 \\
e_{DIF} &= - (K_1 e_0 + e_{IFD}) \\
e_{DH} &= - (e_{HD} + e_1) \\
e_2 &= - \frac{1}{D} (100K_2 e_1 + 100k_3 e_3)
\end{aligned} \tag{A4-8}$$

These equations produced the best operation without any saturation of the amplifiers. Also for the variable diode function generators it was found that the best operation was given by

$$e_3 = \mp 1.3(10^{-4})(e^{\mp 21.6e_2} - 1) \tag{A4-9}$$

where the top sign is again for diode A. Since for reverse bias of the diode, e_3 would be small. Therefore it was neglected and the diode current through R_b was reproduced for forward bias by the diode function generator. A diode function generator will only produce an output for one voltage polarity.

Equating identical equations, we find

$$K_4 = \left(\frac{s_2}{s_0^2(Z_0)^{1/2}} \right)$$

$$s_8 = s_0 \left(\frac{2(Z_0)^{1/2}}{2Z_0 + R_s} \right)$$

$$K_1 = \frac{s_8}{s_1}$$

$$K_1 = \frac{s_8 (Z_0)^{1/2}}{s_0}$$

$$s_1 = \frac{s_0}{(Z_0)^{1/2}}$$

$$K_2 = \frac{s_3}{100aC_b s_2}$$

$$s_3 = 4(10^{-2})$$

$$s_2 = 1$$

From these equations and since $s_0 = 1/10$ for the digital program, we find for the potentiometer values

$$K_1 = \frac{2Z_0}{2Z_0 + R_s}$$

$$K_2 = \frac{1}{1000(Z_0)^{1/2} aC_b}$$

$$K_3 = \frac{4(10^{-4})}{aC_b}$$

$$K_4 = \frac{5}{(Z_0)^{1/2}}$$

For the scaled frequency of 3.33 Ghz, $a = 2.5(10^{+9})$. The value of C_b used was $C_b = 0.25(10^{-12})$.

Determination of Constants for the IF Input Circuit Simulation

The basic equations for the IF input circuit as shown in Figure 10c are with assignment of analog variables and use of analog notation

$$V_1 = \frac{1}{D} \left(\frac{i_{C_{IF}}}{aC_{IF}} \right) = s_5 e_5$$

$$i_{C_{IF}} = i_1 = i_{L_{DC}} - \frac{V_{IF}}{R_{IF}}$$

$$i_{L_{DC}} = \frac{1}{D} \left(\frac{V_1}{aL_{DC}} \right) + i_{L_{DC}} \Big|_{t=0}$$

$$V_{IF} = \frac{1}{D} \left(\frac{R_{IF}(V_1 - V_{IF})}{aL_{IF}} \right) = s_5 e_9 = -s_5 e_8$$

The relationship between the incident and reflected wave coefficients and i_1 and V_1 is using analog notation (1)

$$i_1 = - \frac{(b_{IF} - a_{IF})}{(Z_0)^{1/2}} = -s_7 e_7$$

$$b_{IF} = \frac{V_1}{(Z_0)^{1/2}} - a_{IF} = (s_0 \text{ Scale D}) e_{FI}$$

where $a_{IF} = - (s_0 \text{ Scale } D) e_{IF}$, $s_0 \text{ Scale } D$ is the scaling factor used on the digital computer for output and input of the signals to the IF input circuit and $s_0 = 1/10$ is the scaling factor for all the other wave coefficient outputs and inputs on the digital computer.

Rearranging all these equations in terms of their analog variables, we find

$$e_5 = -\frac{1}{D} \left(\frac{s_7 e_7}{s_5 a_{C_{IF}}} + \frac{s_6 e_6}{s_5 a_{C_{IF}}} - \frac{e_8}{a_{R_{IF}} C_{IF}} \right)$$

$$e_6 = \frac{1}{D} \left(\frac{s_5 e_5}{s_6 a_{L_{DC}}} \right) + e_6 \Big|_{t=0}$$

$$e_7 = + \left(\frac{s_0 \text{ Scale } D}{s_7 (Z_0)^{1/2}} \right) (e_{FI} + e_{IF}) = - \left(\frac{s_0 \text{ Scale } D}{s_7 (Z_0)^{1/2}} \right) (-e_{FI} - e_{IF})$$

$$e_8 = -e_9 = -\frac{1}{D} \left(\frac{R_{IF} e_5}{a_{L_{IF}}} + \frac{R_{IF} e_8}{a_{L_{IF}}} \right)$$

$$-e_{FI} = - \left(e_{IF} + \frac{s_5 e_5}{(Z_0)^{1/2} s_0 \text{ Scale } D} \right)$$

Now since V_{IF} should be power-normalized in terms of Z_0 and R_{IF} in order to determine easily the insertion loss between the received input signal and the IF input signal, let

$$\frac{a_{\text{rec max}}}{1.78} = \frac{s_5 e_9 \text{ max}}{(R_{IF})^{1/2}}$$

where $e_{9_{\max}} = 1$, $a_{\text{rec}_{\max}} = 0.00633 = 0.1a_{\text{LO}}$ and where a_{rec} and a_{LO} are the power-normalized wave coefficients for the received input signal and the local oscillator signal respectively. The 1.78 factor assumes a minimum insertion loss of 5 db. Therefore

$$s_5 = (R_{\text{IF}})^{1/2} (0.358)(10^{-2})$$

The equations for the analog computer circuit diagram of Figure 11b are

$$e_5 = -\frac{1}{D}(10e_6 + 100K_8e_7 - 100K_{11}e_8)$$

$$e_6 = \frac{1}{D}(K_5K_6e_5) - K_7(\pm e_{\text{ref}})$$

$$e_7 = -(-e_{\text{IF}} - e_{\text{FI}})$$

$$e_8 = -\frac{1}{D}(100K_9e_5 + 100K_{10}e_8)$$

$$e_9 = -e_8$$

$$e_{\text{FI}} = -(-1)(e_{\text{IF}} + e_5)$$

These equations produced the best analog operation without saturation of the amplifiers for L_{IF} , C_{IF} , and L_{DC} as given in section VII.

Equating the identical equations, we find for the scale factors and the potentiometer values

$$s_6 = 10s_5 aC_{IF}$$

$$s_7 = \frac{s_0 \text{Scale D}}{(Z_0)^{1/2}} = \frac{s_5}{(Z_0)} = \frac{0.00358(R_{IF})^{1/2}}{Z_0}$$

$$\text{Scale D} = \frac{s_5}{s_0(Z_0)^{1/2}} = 0.0358\left(\frac{Z_0}{R_{IF}}\right)^{1/2}$$

$$K_8 = \frac{s_7}{100s_5 aC_{IF}} = \frac{1}{100Z_0 aC_{IF}}$$

$$K_{11} = \frac{1}{100aR_{IF}C_{IF}}$$

$$K_5 K_6 = \frac{s_5}{s_6 aL_{DC}} = \frac{1}{10a^2 L_{DC} C_{IF}}$$

$$\pm K_7 e_{\text{ref}} = e_6 \Big|_{t=0} = \text{any desired initial condition--usually steady state value}$$

$$K_9 = K_{10} = \frac{R_{IF}}{100aL_{IF}}$$

Interpretation of the IF Input Signal Phase

The form of the IF input signal voltage of Equation (7-3) is

$$\cos((\omega_s - \omega_0)t + a_{s0} - a_{r0}) = \cos(\omega_{IF}t + a_{IF})$$

Thus, for $\omega_s \geq \omega_0$, the phase shift of the IF input signal, a_{IF} , is $a_{s0} - a_{r0}$ and, for $\omega_s \leq \omega_0$, the phase shift is $a_{r0} - a_{s0}$.

Since a_{s0} and a_{r0} had been assumed linear in ω , let

$$a_{s0} - a_{r0} = -(\omega_s \tau_1 - \omega_r \tau_2) = -(\omega_s - \omega_r) \tau_1 - \omega_r (\tau_1 - \tau_2)$$

where τ_1 and τ_2 are time delays. Also, let

$$\omega_r (\tau_1 - \tau_2) = a_c$$

where a_c is a constant phase for the specific delays. Then, for

$$\omega_s \geq \omega_0$$

$$a_{IF} = -(\omega_s - \omega_r) \tau_1 - a_c \quad (A4-10)$$

and for $\omega_s \leq \omega_0$

$$a_{IF} = +(\omega_s - \omega_r) \tau_1 + a_c \quad (A4-11)$$

Subtracting an arbitrary 360° from the case for $\omega_s \leq \omega_0$, we obtain

$$a_{IF} = +(\omega_s - \omega_r) \tau_1 + a_c - 360^\circ \quad (A4-12)$$

Except for the phase reference points for the local oscillator signal and the received input signal, Equations (A4-10) and (A4-12) are those used for the phase difference curves plotted in this thesis. The intersections on the $(f_s - f_r)/f_r = 0$ axis are $-a_c$ for $(f_s - f_r)/f_r \geq 0$ and when $(f_s - f_r)/f_r \leq 0$, $+(a_c - 360^\circ)$ by Equation (A4-12) or $+a_c$ by Equation (A4-11).